RADIATION RESEARCH **166**, 652–689 (2006)
0033-7587/06 $15.00

EXTENDED ABSTRACTS

Proceedings of the 7th International Workshop: Microbeam Probes of Cellular Radiation Response

Columbia University, New York, New York, March 15–17, 2006

SCIENTIFIC PROGRAM COMMITTEE

Leslie Braby, *Texas A&M*
David Brenner, *Columbia University* (Workshop Organizer)
Roberto Cherubini, *INFN, Legnaro, Italy*
Thomas Cremer, *Ludwig-Maximilians-Universität, Munich, Germany*
Marco Durante, *INFN, Napoli, Italy*
Charles Geard, *Columbia University*
Katsumi Kobayashi, *KEK, Tsukuba, Japan*
John Miller, *Washington State University*
Kevin Prise, *Gray Cancer Institute, London, England*
Gisela Taucher-Scholz, *GSI, Darmstadt, Germany*

The extended abstracts that follow present a summary of the Proceedings of the 7th International Workshop: Microbeam Probes of Cellular Radiation Response, held at Columbia University's Kellogg Center in New York City on March 15–17, 2006. These International Workshops on Microbeam Probes of Cellular Radiation Response have been held regularly since 1993 (*1–5*). Since the first workshop, there has been a rapid growth (see Fig. 1) in the number of centers developing microbeams for radiobiological research, and worldwide there are currently about 30 microbeams in operation or under development.

Single-cell/single-particle microbeam systems can deliver beams of different ionizing radiations with a spatial resolution of a few micrometers down to a few tenths of a micrometer. Microbeams can be used to address

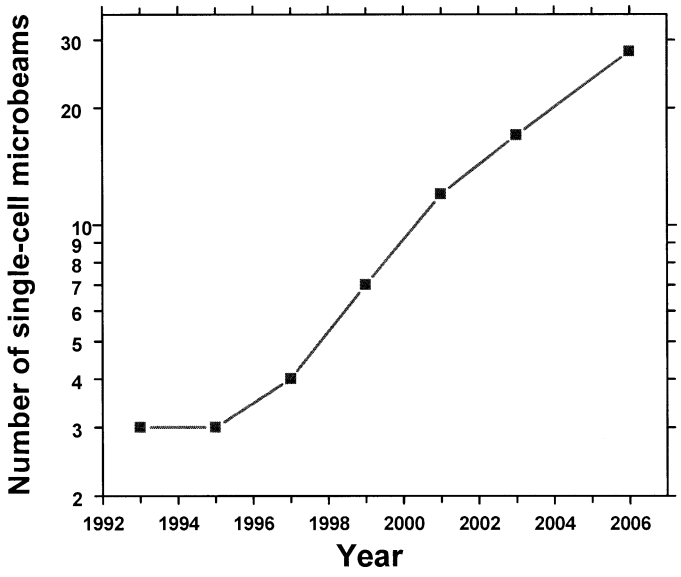

FIG 1. Number of single-cell microbeams, operational or under development, reported at past international microbeam workshops.

questions relating to the effects of low doses of radiation (a single radiation track traversing a cell or group of cells), to probe subcellular targets (e.g. nucleus or cytoplasm), and to address questions regarding the propagation of information about DNA damage (for example, the radiation-induced bystander effect). Much of the recent research using microbeams has been to study low-dose effects and ''non-targeted'' responses such as bystander effects, genomic instability and adaptive responses.

This Workshop provided a forum to assess the current state of microbeam technology and current biological applications and to discuss future directions for development, both technological and biological. Over 100 participants reviewed the current state of microbeam research worldwide and reported on new technological developments in the fields of both physics and biology.

The 8th International Workshop: Microbeam Probes of Cellular Radiation Response will be held in 2 years in Japan.

Acknowledgments

Support for this workshop was provided by National Institutes of Health grant P41 EB002033-10 and U.S. Department of Energy Low Dose Radiation Program grant DE-FG02-06ER64217.

References

1. B. D. Michael, M. Folkard and K. M. Prise, Meeting report: Microbeam probes of cellular radiation response, 4th L. H. Gray Workshop, 8–10 July 1993. *Int. J. Radiat. Biol.* **65**, 503–508 (1994).
2. Proceedings of the 4th International Workshop: Microbeam Probes of Cellular Radiation Response. *Radiat. Res.* **153**, 220–238 (2000).
3. Proceedings of the 5th International Workshop: Microbeam Probes of Cellular Radiation Response. *Radiat. Res.* **158**, 365–385 (2002).
4. D. J. Brenner and E. J. Hall, Microbeams: A potent mix of physics and biology. Summary of the 5th International Workshop on Microbeam Probes of Cellular Radiation Response. *Radiat. Prot. Dosim.* **99**, 283–286 (2002).
5. Proceedings of the 6th International Workshop/12th L. H. Gray workshop: Microbeam probes of cellular radiation response. *Radiat. Res.* **161**, 87–119 (2004).

SESSION 1: MICROBEAM SOURCE DEVELOPMENT

Chair: Melvyn Folkard

The Munich Microprobe SNAKE, a Single-Ion Cell Irradiation Facility

C. Greubel,[a] V. Hable,[a] G. Dollinger,[a] A. Hauptner,[b] R. Krücken,[b] H. Strickfaden,[c] S. Dietzel,[c] T. Cremer,[c] G. A. Drexler,[d] M. Deutsch[d] and A. A. Friedl[d]

[a]Applied Physics and Metrology, LRT2, Bundeswehr University, Neubiberg, Germany; [b]Physics Department E12, Technical University of Munich, Garching, Germany; and [c]Biology Department II and [d]Radiobiological Institute, University of Munich, Munich, Germany

The ion microprobe SNAKE [Superconducting Nanoscope for Applied Nuclear (Kernphysikalische) Experiments] at the Munich 14 MV tandem accelerator provides focused ion beams with spot sizes in the submicrometer range (*1*). It is used for high-resolution material analysis like hydrogen microscopy or material modification as well as radiobiological experiments. Due to the available ion species and energies, SNAKE is an ideal instrument to use for cell irradiation. The stopping power and thus the damage can be chosen from about 2 keV/μm by irradiating with 25 MeV protons up to several MeV/μm for 100 MeV sulfur ions. An upgrade of SNAKE to a single-ion cell irradiation facility was completed 2 years ago and successfully tested and is now routinely used for radiobiological experiments.

A narrow ion beam prepared by a micro slit system is focused by the superconducting multipole lens of SNAKE. The beam is transported under vacuum conditions through a flexible coupling to a beam exit nozzle. There the horizontal beam enters the atmosphere by passing a 1-mm bore covered with a 7.5-μm Kapton foil. The cell sample to be irradiated is grown onto a thin foil in a specially prepared container positioned in the focal plane of the ion beam. The experiments are done with single, counted ions. These are prepared by a fast switchable electrostatic deflection system and a detector counting ions that have passed through the cell sample (*2*). In this setup, arbitrary point patterns with an accuracy of 0.55 μm in the *X* direction and 0.40 μm in *Y* direction (both FWHM) can be applied (*3*).

To observe and align the cells, an inverted microscope was mounted at the beam exit nozzle. By using transmitted light illumination with phase contrast, the cell sample can be visualized without staining techniques that might disturb biological processes. Using the microscope as an inherent position reference, in a first attempt, chosen cell nuclei could be irradiated with an accuracy of about 2 μm. The accuracy is mainly limited by the available mechanical positioning system and the low-power objective and might be improved to 1 μm. Special microstructured cell carrier foils allow us to easily locate the irradiated cells during retrospective microscopy.

Acknowledgments

Radiobiological experiments at SNAKE are supported by grant Str.Sch.4450 of the Bundesamt für Strahlenschutz and grant 02S8264 of the Bundesministerium für Bildung und Foschung to AAF, by Eurodyna grants of the European Science Foundation to AAF, TC and GD, and by the Maier Leibnitz Laboratorium of the TU Munich and the University of Munich. We thank the technical staff of the Munich tandem accelerator.

References

1. G. Dollinger, A. Datzmann, A. Hauptner, R. Hertenberger, H-J. Körner, P. Reichart and B. Volckaerts, The Munich ion microprobe: Characteristics and prospects. *Nucl. Instrum. Methods Phys. Res. B* **210**, 6–13 (2003).
2. A. Hauptner, S. Dietzel, G. A. Drexler, P. Reichart, R. Krücken, T. Cremer, A. A. Friedl and G. Dollinger, Microirradiation of cells with energetic heavy ions. *Radiat. Environ. Biophys.* **42**, 237–245 (2004).
3. G. Dollinger, V. Hable, A. Hauptner, R. Krücken, P. Reichart, A. A. Friedl, G. Drexler, T. Cremer and S. Dietzel, Microirradiation of cells with energetic heavy ions. *Nucl. Instrum. Methods Phys. Res. B* **231**, 195–201 (2005).

A Scanning Focused Vertical Ion Nanobeam: A New UK Facility for Cell Irradiation and Analysis

K. J. Kirkby,[a] G. W. Grime,[a] R. P. Webb,[a] N. F. Kirkby,[b] M. Folkard,[c] K. Prise[c] and B. Vojnovic[c]

[a]Surrey Ion Beam Centre, Advanced Technology Institute, School of Electronics and Physical Sciences, University of Surrey, Guildford GU2 7XH, United Kingdom; [b]Fluids & Systems Research Centre, School of Engineering, University of Surrey, Guildford GU2 7XH, United Kingdom; and [c]The University of Oxford, Gray Cancer Institute, Mount Vernon Hospital, Northwood HA6 2JR, United Kingdom

Introduction

The Gray Cancer Institute (GCI) has been actively involved in the development and application of ion and focused X-ray microbeams for radiobiological research since the early 1990s. The Surrey Ion Beam Centre (IBC) is a UK national center for research using ion beams and has been actively involved in the development of ion beam analysis techniques since the late 1970s. In 2002 this expertise was strengthened when Dr. Geoffrey Grime joined the IBC from the University of Oxford and brought with him a wealth of experience in the design of focused scanning ion microbeam systems.

In this report we describe an ambitious new collaborative research program between Surrey and GCI that seeks to build a vertical focused scanning nanoirradiation and analysis facility. This radically new technology will be used to challenge and characterize living biological materials, with clear applications in cancer treatment, understanding the risks associated with occupational and environmental exposure to radiation and probing the internal working of cells and how cells respond to external and internal stimuli such as stress, toxins, drugs, nutrition and radiation.

The specific objectives of this project are to:

1. Develop and build a horizontal nanobeam system to act as a test bed for the development of a vertical nanobeam.
2. Design, build, commission and use a vertical focused scanning ion nanobeam for applications such as studies of radiation biology and DNA damage and repair, using a range of ions from hydrogen to argon.
3. Within the same facility, develop *in vitro* elemental ion beam analysis of living cells.
4. Using data from nanobeam studies, develop further a comprehensive mechanistic mathematical model of the response of cells and tissues to ionizing radiation for the design and optimization of individualized radiotherapy treatment schedules (*1*).

The funding is now in place from the Wolfson Foundation, UK Research Councils and the EU to begin this ambitious research program.

Vertical Beam Line

The new vertical nanobeam will use the state of the art 2 MV High Voltage tandetron accelerator which was installed at the University of Surrey in 2001. In addition to protons and helium ions, this machine is also capable of supplying heavy-ion beams (e.g. oxygen, fluorine, carbon, neon, argon, xenon and gold). Instead of relying on collimation, the beam will be focused by means of a quadrupole triplet so that it can target areas of <10 nm (*in vacuo*). The system will be designed so that it can run in either single-ion or full-current modes.

1. The full-current mode will be used for ion beam analysis, where a

beam spot of typically ~100 nm will be employed to give a capability for trace element mapping.
2. The single-ion mode will allow the ions to be precisely positioned and targeted with a spatial resolution of <10 nm.
3. Single ions will also be used to target cells outside the vacuum system, i.e., where they are maintained in appropriate physiological conditions. Here a reduced spatial resolution will be available, limited by the inevitable ''beam scattering''.

The ability to scan and maintain focus will enable the number of cells irradiated per second to be greatly increased. We estimate that, when fully developed, the facility will be capable of irradiating ~100,000 cells per hour. Complementary imaging techniques will of course need to be developed, but the intention is to operate under conditions in which the beam positioning is not the limiting factor in achieving high-throughput targeting accuracy. Ultimately three-dimensional and functional (i.e. molecular) imaging methods will be necessary to fully use the performance achievable with this type of nanobeam.

The Cell Irradiation ''End-Station''

The development of an end-station to support, find and align cells at the correct location for irradiation will build on the experience of the GCI Group, who have already established robust methods in their facility (*2*). The GCI group is also in the final stages of commissioning a second X-ray microprobe that takes full advantage of recent developments in the performance of desktop computers and electronic imaging hardware, and we anticipate implementing similar state-of-the-art capability on the new facility at Surrey. Particular attention will be given to environmental control and to enabling off-line (trans-illuminating) cell imaging.

Models and Applications

We anticipate many research applications for this new facility. For instance, precise data can be acquired concerning cell death and DNA damage and repair that can be used to inform and validate mathematical models. Such models can be used to optimize radiotherapy planning using both conventional photons as well as eventually light ions. Experimental data on normal tissue and tumor cell response may eventually be incorporated with imaging systems to maximize both tumor killing and normal tissue sparing.

Concluding Comments

A new vertical nanobeam is to be built at the Ion Beam Centre at the University of Surrey in a new collaborative venture with GCI. The beam will be focused and scanned into an end-station system capable of both internal *in vacuo* and externalized operation. Detectors for ion beam analysis will be present as well as microscopy and imaging for precise positioning of the ions in both full-current and single-ion modes. The system is primarily designed to irradiate and analyze biological samples, but other exciting applications are also possible.

Acknowledgments

The authors would like to thank the Wolfson Foundation, the UK Engineering and Physical Sciences Research Council and the European Union (Marie Curie Research Training Network Cellion MCRTN-CT-2003-503923) for their support of this work.

References

1. N. F. Kirkby, D. B. F. Faraday, S. C. Short, M. Woodcock, M. C. Joiner and N. G. Burnet, Mathematical modelling to develop a novel radiotherapy schedule for high-grade brain tumours, based on phase distribution of low-dose hypersensitivity in human glioma cell lines. *Radiother. Oncol.* **64** (Suppl. 1), 57 (2002). [abstract]
2. M. Folkard, B. Vojnovic, S. Gilchrist, K. M. Prise and B. D. Michael, The design and application of ion microbeams for irradiating living cells and tissues. *Nucl. Instrum. Methods Phys. Res. B* **210**, 302–307 (2003).

Development of the Lund Single Ion Hit Facility at the New Submicrometer Beam Line

N. Arteaga-Marrero, J. Pallon, V. Auzelyte, M. Elfman, P. Kristiansson, K. Malmqvist, C. Nilsson and M. Wegdén

Division of Nuclear Physics, Department of Physics, Lund Institute of Technology, Lund University, SE-221 00 Lund, Sweden

The CELLION project is directed toward the studies on cellular response to targeted single ions. The final aim of the project is to study low-dose radiation effects. Several institutions in Europe are dedicated to this objective, and a few of them are already operational. The new submicrometer beam line at the Lund Nuclear Probe is being used to create a Single Ion Hit Facility. The system is presently under construction, and this abstract describes the system operation.

Single Ion Hit Facility

Lund Nuclear Probe is using a 3 MeV single-ended Pelletron electrostatic accelerator. The submicrometer beam is focused using a two-stage system with a doublet at each stage (*1*). The first stage focuses the beam in an intermediate chamber; the real image obtained at the first stage is used as a virtual object for the second stage.

The development of a Single Ion Hit Facility is done in several steps. The irradiation chamber at the submicrometer beam line is adapted for biological experiments using an extended beam pipe. The extensible pipe brings the beam closer to the sample to minimize the air gap in between. The beam current is limited by slits. A fast beam deflecting system (*2*), which has an activation speed of 200 ns, combined with an after-target silicon-particle detector prevents secondary hits, i.e., limits the dose applied.

The beam is extracted to the atmospheric environment using a 200-nm Si_3N_4 vacuum window. Occasional damage of the vacuum system can occur by the breakage of the vacuum window. Therefore, a new vacuum guard has been installed recently to avoid this situation.

Cell Recognition Program

Cells must be positioned vertically; thus special irradiation dishes and a sample holder have been designed. A microscope connected to a CCD camera with home developed software is used to locate the cells. The recognition is made online, and a picture taken by a microscope is used as the input parameter for the recognition program. The program is made in IDL language and provides coordinates of the center of the cell. Since the procedure is not completely optimized, and nonstained cells are used, the main purpose is to locate the cell without distinguishing between the cytoplasm and the nucleus. Cells can be located with an accuracy better than 1 μm. Using V79 Chinese hamster cells, the recognition procedure can be done in less than 1 min for a picture size of 768 × 576 pixels with approximately 95% efficiency.

Acknowledgments

This work is supported by Marie Curie Research Training Network, Contract MRTN-CT-2003-503923 and Crafoordska Stiftelsen 20041003.

References

1. A. Shariff, V. Auzelyte, M. Elfman, P. Kristiansson, K. Malmqvist, C. Nilsson, J. Pallon and M. Wegdén, The Lund Nuclear Microprobe sub-micron set-up. Part I: Ion optics calculation. *Nucl. Instrum. Methods Phys. Res. B* **231**, 1–6 (2006).
2. V. Auzelyte, M. Elfman, P. Kristiansson, K. Malmqvist, L. Wallman, C. Nilsson, J. Pallon, A. Shariff and M. Wegdén, The beam blanking

system for microlithography at Lund Nuclear Microprobe. *Nucl. Instrum. Methods Phys. Res. B* **219–220**, 485–489 (2004).

Status of the Stand-Alone Microbeam at Columbia University

G. Garty, G. J. Ross, A. W. Bigelow, G. Schettino, G. Randers-Pehrson and D. J. Brenner

Columbia University, Radiological Research Accelerator Facility, Irvington, New York 10533

Columbia University's Radiological Research Accelerator Facility (RARAF) currently offers its users access to a few-micrometer-diameter single-cell/single-particle microbeam irradiator, based on a recently installed 5 MV HVE Singletron particle accelerator and an electrostatic quadrupole triplet. Currently, intensive development work is being performed on upgrading the electrostatic lens to achieve a submicrometer microbeam. During this development work, we foresee long periods in which this microbeam will be unavailable for biology. To continue providing this essential service to our users, we have developed a second microbeam irradiator that can be operated either directly from the accelerator or using an isotopic source (*1, 2*).

So far the ''Stand-Alone Microbeam'' (SAM) has only been tested with an accelerator-based beam, although it has been designed around operation with a custom-made polonium α-particle emitter. The source is made in-house by electroplating a 200-nm-thick layer of pure ^{210}Po onto the tip of a 1-mm-diameter rod obtaining a 240.5 MBq (6.5 mCi) source of monochromatic α particles (40 keV FWHM) (*1*). At this stage we have succeeded in efficiently plating several test sources ranging in activity between 1000 Bq (30 nCi) and 4000 kBq (100 μCi). We are currently in the process of making the 240 MBq source necessary for the SAM.

The SAM is based on a compound magnetic lens consisting of two permanent magnet quadrupole triplets in Russian symmetry. Simulations indicate that, using the source described above, a beam flux of ~1 particle/second onto a 10-μm-diameter spot is achievable (*1*). When using an accelerator, a smaller spot size is achievable at up to 1000 particles/second.

The use of permanent magnet quadrupoles (*3*) simplifies the SAM operation and stability, making use of the fact that this is a fixed-energy beam that requires no daily tuning, The magnets are tuned once to an optimal beam spot, and as long as the incident particles have the same magnetic rigidity, they will be focused to the same spot size. The lack of large coils in the design allows for a smaller pole-face gap for the magnet, resulting in better focusing properties. Each quadrupole consists of four movable permanent magnets in a shaped iron yoke (*3*). The quadrupole strength as well as some steering can be adjusted by individually inserting or retracting the magnets. The use of permanent magnets also eliminates the need for costly power supplies and bulky cooling equipment while also significantly simplifying SAM operation. In addition, our simulations have shown that the spherical aberrations in a magnetic triplet are about three times lower than in an equivalent electrostatic quadrupole triplet (*1*).

For tuning purposes, the RARAF accelerator was used to generate a 1-mm collimated beam, mimicking the α particles generated by an isotopic source. The optimal focusing of the first triplet was found by iteratively adjusting the strength of each quadrupole while monitoring the beam image formed on a CCD chip placed at its focal plane (*4*). The optimal spot size was seen to be 50 μm × 150 μm, in good agreement with simulations. Next the second triplet was brought into Russian symmetry with the first, and both quadrupoles were then adjusted while maintaining Russian symmetry. The final spot size measured at the SAM image plane using the knife edge technique was seen to be 20 μm × 20 μm, twice as large as the expected value (*4*). This can be attributed to a residual octapole moment of ~1% that has not yet been canceled out or to a slight misalignment of the triplets with respect to each other.

Once fully optimized, the SAM will provide a useful secondary microbeam facility at RARAF and will enable biology to be performed in parallel with developments on the electrostatic microbeam. Based on our experience, a similar facility can be reproduced in any large radiobiology laboratory, although the tuning and alignment procedures are faster when an accelerator is available.

References

1. G. Garty, G. J. Ross, A. W. Bigelow, G. Randers-Pehrson and D. J. Brenner, A microbeam irradiator without an accelerator. *Nucl. Instrum. Methods Phys. Res. B* **241**, 392–396 (2005).
2. G. J. Ross, G. Garty, G. Randers-Pehrson and D. J. Brenner, A single-particle/single-cell microbeam based on an isotopic alpha source. *Nucl. Instrum. Methods Phys. Res. B* **231**, 207–211 (2005).
3. S. C. Gottschalk, D. H. Dowell and D. C. Quimby, Permanent magnet systems for free-electron lasers. *Nucl. Instrum. Methods Phys. Res. A* **507**, 181–185 (2003).
4. G. Garty, G. J. Ross, A. W. Bigelow, G. Schettino, G. Randers-Pehrson and D. J. Brenner, Testing the stand-alone microbeam at Columbia University. *Radiat. Prot. Dosim.*, in press.

SESSION 2: PHOTON/ELECTRON MICROBEAMS

Chair: Marianne Sowa

A Novel, High-Brightness Electrodeless Z-Pinch Soft X-Ray Source for Microbeam Applications

S. F. Horne,[a] M. M. Besen,[a] R. D'Agostino,[a] D. K. Smith,[a] P. A. Blackborow[a] and A. Aquila[b]

[a]Energetiq Technology, Inc. and [b]Center for X-ray Optics, Lawrence Berkeley National Laboratory, Berkeley, California 94720

Soft X-ray light, in the so-called water window between the carbon and oxygen absorption edges at 2.3 nm and 4.4 nm, is a candidate for microbeam studies into the effects of ionizing radiation on biological cells. At these wavelengths, due to the relatively high soft X-ray transmission of water, radiation can penetrate depths of 10 μm or more in typical samples. Soft X-ray light can be focused readily into a small spot using nano-fabricated Fresnel zone plate lenses. This approach has enabled soft X-ray microscopy and tomography of biological samples with resolution in the 20-nm range (*1*). Soft X-ray light for microbeam studies and microscopy can readily be found at the synchrotron light sources of the national laboratories. However, this limits the availability of soft X rays to those researchers who are able to obtain beam time and are able to bring their experiments to the synchrotrons. Here we describe a compact source of soft X-ray light based on a novel plasma approach that would enable soft X-ray microbeam experiments to be carried out in any typical biological research laboratory.

Soft X-ray light may be produced in a plasma by heating a target material to a high temperature such that it emits at characteristic wavelengths in the spectral region of interest. The target material may be heated by a pulsed laser, the so-called laser-produced plasma, or in a z-pinched discharge, the so-called discharge-produced plasma.

Laser-produced plasmas have been used to produce soft X rays using Mylar tape (*2*) or a stream of liquid nitrogen as the target materials (*3*). The Mylar tape approach produces significant debris from the target that can contaminate the optical system. The liquid nitrogen stream target approach suffers from poor stability and reliability. Both approaches produce soft X rays at a high cost per photon, given the high cost of the required pulsed lasers.

Traditional z-pinch discharge plasma sources designed for soft X-ray applications use electrodes to conduct the high current pulse into the plasma. The contact of these electrodes with the high-temperature plasma required for soft X-ray production can cause electrode erosion, electrode ''spitting'' and even melting. These can be sources of contaminating de-

bris for any optical system connected to the source. Discharge sources, however, intrinsically have a lower cost per soft X-ray photon produced since they avoid the need for the high-cost pulsed laser.

We will present a novel approach to the z-pinch discharge plasma where the current pulse is induced into the discharge rather than conducted. The inductive coupling creates magnetic fields that position the resulting electrodeless z-pinch plasma away from the source walls, thereby allowing relatively straightforward approaches to source cooling. We have results from a commercially available electrodeless z-pinch soft X-ray source that delivers 10^{16} photons per second into 2π steradians at 2.88 nm using nitrogen as the soft X-ray emitting gas. The plasma size is shown to be smaller than 1 mm in diameter. In related work at 13.5 nm using xenon as the target gas, we showed how the emitting source size can be reduced for specific applications.[1] We have designed an experimental microbeam apparatus that would use Fresnel zone plate lenses to focus the light from the soft X-ray source to a spot of 100 nm diameter or smaller, with controllable dose in the range of 1 Gy per second for radiation studies. Such a small beam would allow microbeam probing of subcellular structures.

References

1. W. Chao, B. D. Harteneck, J. A. Liddle, E. H. Anderson and D. T. Attwood, Soft x-ray microscopy at a spatial resolution better than 15 nm. *Nature* **435**, 1210–1213 (2005).
2. A. G. Michette, S. J. Pfauntsch, A. K. Powell, T. Graf, D. Losinski, C. D. McFaul, G. J. Hirst and W. Shaikh, Progress with the King's College laboratory scanning x-ray microscope. In *RAL Central Laser Facility Annual Report 2001–2002,* pp. 152–153. Rutherford Appleton Laboratory, Chilton, UK, 2001.
3. P. A. C. Jansson, U. Vogt and H. M. Hertz, Liquid-nitrogen-jet laser-plasma source for compact soft x-ray microscopy, *Rev. Sci. Instrum.* **76**, 043503-1–5 (2005).

Femtosecond Near Infrared Laser Microbeam Technique for Submicrometer Point Source for High-Resolution Cell DNA Damage, Signaling and Repair Studies

S. W. Botchway,[a] J. V. Harper,[b] E. Leatherbarrow,[b] A. W. Parker[a] and P. O'Neill[b]

[a]*Rutherford Appleton Laboratory, CCLRC, Chilton, Didcot, Oxfordshire OX11 0QX, United Kingdom; and* [b]*Medical Research Council, Harwell, OX11 0RD, United Kingdom*

The use of microbeam techniques to induce submicrometer localized energy deposition within regions of a cell nucleus is imperative to extend our understanding of cell function, in particular DNA damage and repair mechanisms (*1, 2*). Near infrared (NIR) multiphoton absorption occurs primarily within the 3D femtoliter volume of a highly focused Gaussian beam. This phenomenon provides a novel optical microbeam tool for both complex ionizing and UV-radiation-type cell damage such as double-stand breaks (DSBs) and base damage (*3*). We have used the NIR laser microbeam probe to investigate the 3D formation of these lesions, DNA DSB repair, and recruitment of repair proteins to the submicrometer size site of damage in viable cells.

Experimental Technique

1. NIR laser microbeam

The laser source consists of a solid-state titanium sapphire (Ti:Sa) laser (Mira, Coherent lasers Ltd.), that is tunable from 700–980 nm (horizontally polarized) with a pulse width of 180 fs and can be passively mode locked at a 73–78 MHz repetition rate. The total maximum power output is 1.4 W when pumped with the 8W Verdi (Coherent Laser Ltd.) operating at 532 nm in a CW mode. The laser wavelength may be extended using an optical parametric oscillator (OPO, APE Germany) to give wavelengths of 550–650 nm mode locked at 75 MHz with 200-fs pulses. Output from either the Ti:Sa or OPO laser is expanded through a telescope and directed to the back of an inverted microscope (TE2000 Nikon Ltd.) equipped with a computer-controlled *XYZ* stage with resolution of ~100 nm (Marzhauser, Wetzlar, Germany) and a CCD camera (Q-imaging) coupled to custom-written software using LabVIEW™ programming language. The laser beam was passed through an *XY* galvanometer mirror (GSL Lumonics) for translating the microbeam to the coordinates of interest. The exit beam was imaged in the back focal plane of the microscope objective using a scan lens. A hot dichroic mirror (Comar, 660IK) placed just before the microscope objective was used to reflect the NIR laser beam and to transmit any required fluorescence. The microscope was also fitted with a filter (Comar, BG39) to remove the laser light. A CCD camera was attached to the microscope to visualize the cells prior to and during sample irradiation.

The microscope setup also has the ability to perform fluorescence lifetime image mapping (FLIM) and fluorescence lifetime measurements using an *XY* coordinate scanning of the galvanometer and the microscope stage. Time-correlated single photon counting (TCSPC) is performed using an SPC 700 Becker & Hickl system. The image resolution is better than 700 nm, and excited state lifetimes down to less than 1 ns can be obtained. The combination of an online real-time biophysical damage analysis provided by the NIR laser microbeam technique is unique in our microbeam studies. The lasers and optical system are mounted on an anti-vibration damper optical bread board for stability.

2. Sample preparation and cell culture

CHO (Chinese hamster ovary cells) and V79-4 cells (Chinese hamster lung fibroblasts) were cultured in the presence of minimal essential medium (MEM) supplemented with 10% fetal calf serum (Sigma Biochemicals), 1% penicillin and 1% L-glutamine on a specially designed No. 1 cover slip base. The cells were grown for 40–60 h in a humidified 95% air/5% CO_2 incubator at 310 K to allow the cells to adhere. Hoechst dye (No. 33258) was added to the culture medium 10 min prior to laser beam irradiation, and the cells were cooled on ice. Cells were then irradiated with the NIR 710–800-nm laser beam at 283 K (to reduce damage repair or 310 K by either raster scanning a predefined pattern using computer-controlled stage or *x,y* galvanometer mirrors. After irradiation, the cells were washed and fixed in 3% paraformaldehyde at 277 K and stored at 277 K until stained for immunofluorescence, or treated for the comet assay for whole cell DNA strand break determination. The samples for immunofluorescence staining were incubated in anti-phospho-γ-H2AX, anti-phospho-ATM or anti-RAD51 primary antibody solution overnight at 277 K (*4*). Cells were then washed and incubated with FITC- and/or Cy5-labeled secondary antibodies for 1 h at room temperature, and images were recorded using a Radiance 2000 or MRC 600 laser scanning confocal microscopy (BioRad, UK). *Z*-plane images were taken using a 60× oil immersion objective, NA 1.4.

3. Single-cell targeting and irradiation

V79-4 cells were plated as described above except into square dishes. The square cell culture dishes were mounted on a sample holder and placed onto the temperature-controlled microscope stage and allowed to reach the required temperature prior to irradiations. The cell holder *X, Y, Z* coordinates as well as every position within a cell to be irradiated are recorded and logged. These precise positions can then be revisited for future analysis and laser microbeam irradiation.

Results and Discussion

The NIR 180-fs pulse light distribution through the cells is different from using UV light (*3*). DNA DSBs are induced in the irradiated cells

[1] S. F. Horne, M. M. Besen, D. K. Smith and P. A. Blackborow, A novel, high-brightness electrodeless Z-pinchTM EUv Source. Presented at the Fourth International Extreme Ultraviolet Lithography (EUVL) Symposium, November 2005, San Diego, California.

as demonstrated by the neutral comet assay. During the microbeam irradiation, the Hoechst dye that is intercalated into the nuclear DNA absorbs two photons of 730 nm followed by transfer of energy to the DNA, or alternatively the cellular DNA directly absorbs three photons simultaneously in the 3D focal femtoliter volume produced at the focus of the high NA microscope objective. For this latter process to occur, the peak intensities needed are of the order of 10^{-19} J cm^{-2}. It is therefore clear that a CW light source will require in excess of 100 mW at the sample, which is highly detrimental to mammalian cells. However, the use of ultrashort pulses (<1 ps) at high repetition rate (>50 MHz) and average powers of less than 10 mW will lead to the necessary high (GW cm^{-2}) peak intensities required to cause the multiphoton absorption process. Using a UV photon would cause absorption in a cone of localized irradiation throughout the light path, thereby increasing collateral damage.

When two or more proteins involved in DNA DSB repair were detected immunohistochemically after NIR laser irradiation of the cells, colocalization of the resulting foci due to the repair proteins assembling at the sites of the DSBs was observed within the femtoliter irradiation volume. Furthermore, real-time observation of GFP-tagged RAD51 and immunostaining of 53BP1 repair proteins detected by immunohistochemistry provided time scales of the signaling responses of these proteins to the induction of DNA damage. Preliminary repair studies after postirradiation incubation of the cells at 310 K prior to staining showed loss of intensity of the focus tracks with increasing time of incubation for cell repair. The cell repair mechanisms are therefore still occurring after laser microbeam irradiation. The data indicate a very complex type of cellular damage that is similar to damage produced by ionizing radiation. Thus the new microbeam method is capable of mimicking the effects of ionizing radiation on a spatial resolution, better than that currently achievable in 3D, of less than 1 μm.

Conclusions

The new NIR laser microbeam allows localized submicrometer cellular damage induction. The use of NIR light leads to reduced collateral cell damage since there is little absorption of the NIR light by other cellular components. Preliminary results show repair of the induced damage with time. This work paves the way for studies of repair in individual cells to be made using controlled ionizing radiation damage produced in defined sites. Typical UV-radiation-induced DNA damage such as CPDs and 6-4 photoproducts has also been produced efficiently and has been observed in mammalian cells after induction by the NIR microbeam. Unlike the masking methods for localized irradiation of whole cell cultures, the current multiphoton microbeam technique can specifically target a single cell and its subnuclear structures such as nucleoli, nuclear membrane or other fluorescently tagged cellular entities within a femtoliter volume with negligible effect of the whole cell and its surroundings.

References

1. K. Konig, I. Riemann, P. Fischer and K. J. Halbhuber, Intracellular nanosurgery with near infrared femtosecond laser pulses. *Cell Mol. Biol.* **45**, 195–201 (1999).
2. K. M. Prise, O. V. Belyakov, M. Folkard, A. Ozols, G. Schettino, B. Vojnovic and B. D. Michael, Investigating the cellular effects of isolated radiation tracks using microbeam techniques. *Adv Space Res.* **30**, 871–876 (2002).
3. V. Shafirovich, A. Dourandin, N. P. Luneva, C. Singh, F. Kirigin and N. E. Geacintov, Multiphoton near-infrared femtosecond laser pulse-induced DNA damage with and without the photosensitizer proflavine. *Photochem. Photobiol.* **69**, 265–227 (1999).
4. K. König, Multiphoton microscopy in the life sciences. *J. Microsc.* **200**, 83–104 (2000).
5. R. A. Meldrum, S. W. Botchway, C. W. Wharton and G. J. Hirst, Nanoscale spatial induction of ultraviolet photoproducts in cellular DNA by three-photon near-infrared absorption. *EMBO Rep.* **4**, 1144–1149 (2003).

Development of a Carbon Nanotube-Based Low-LET Multi-pixel Microbeam Array

S. Chang,[a] J. Zhang,[a] D. Bordelon,[b] E. Schreiber,[a] A. Cox[a] and O. Zhou[b,c]

[a]Department of Radiation Oncology, [b]Curriculum in Applied and Materials Sciences, and [c]Department of Physics and Astronomy, University of North Carolina at Chapel Hill, Chapel Hill, North Carolina

Introduction

We propose to develop the first low-LET electron microbeam system using carbon nanotube field emission technology. The unique feature of the microbeam system is that it has not one but several hundreds to thousands of microbeam pixels, each of which is individually controlled. Such a multi-pixel microbeam array system allows simultaneous irradiation of selected cells or cellular regions under microscrope observation. Carbon nanotubes are planted on a chip in a pixelated pattern, and each pixel can be individually controlled to emit electrons that form a microbeam (*1, 2*). Our long-term objective is to develop a high-packing-density multi-pixel microbeam array using the microbeam on a chip nanotechnology. Instead of using the ''step and shoot'' method that all single-source microbeam devices rely on for multiple cell/cellular region irradiation, the proposed multi-pixel microbeam array simultaneously turns on only the individual microbeam pixels that share the same coordinates with the corresponding target cells. This portal cell irradiation system offers radiobiologists a small spatial and temporal scale radiation research tool that may be used to unravel the complex microprocesses in cellular level immediately after deposition of radiation energy. Once developed, the proposed device could revolutionize the study of signal transduction in response to ionizing radiation. Both basic and translational research would be facilitated by the new device, such as studies that identify which branch points and networks in critical signal transduction pathways, such as EGFR/RAS/RAF/ERK, MEKK/MAPK and PI3K/AKT, are important to radiosensitivity, which kinases, substrates and interacting partners are activated in response to ionizing radiation, the role of tumor/stromal interactions in cellular motility and invasiveness, which DNA damage and cell cycle regulatory pathways determine cell proliferation and cell death, and the screening of putative radiation sensitizers or protectors for their effects on downstream signaling pathways. Here we report some of our preliminary results in the initial stage of research and development-feasibility demonstration through developing a single-pixel microbeam system based on carbon nanotube field emission technology and validating its ability to deliver radiation dose to living cells.

Methods and Materials

Carbon nanotube field emission technology. Since the historic discovery by Iijima in 1991 (*3*), carbon nanotubes (CNTs) have attracted the interests of many scientists worldwide because of their unique properties. CNTs are excellent field emission electron sources. Different from the thermionic emission process in conventional electron cathodes today, field emission is a quantum-mechanical phenomenon in which electrons tunnel through the electric potential barrier at the surface of a solid metal when it is under a strong external electric field (*4*). The control of electron current and pulsation can be done easily through the control of the applied electric field. We have shown that CNT electron cathodes can produce high current density and high pulsing frequency electron beams for imaging and display (*5, 6*). CNT can also be formed into different patterns for unique applications such as the multi-pixel microbeam system (*7*).

CNT field emission single-cell microbeam system. We propose to develop a high packing density CNT cathode pixel array on a chip—approximately 2,500 microbeam pixels, each of which is generated by an individually controlled CNT pixel. The electron energy is tunable between 30–60 keV. The dose rate is controlled by the emission current and pulsation. The microbeam size is defined by the electron exit window.

The proposed microbeam pixel array can simultaneously irradiate a selected single cell or large number of individual cells *in vitro.* The device is also expected to offer flexibility in the irradiation pattern, spatially discrete or uniform, temporally continuous or pulsed.

Development of the prototype microbeam system. The initial stage of our research is feasibility demonstration by developing a prototype single-pixel CNT microbeam device. Inside a large vacuum chamber we have assembled a prototype single-pixel microbeam system without the vacuum enclosure that it would have in the finished product. This allowed us quick access to change experimental components and thus increased the research efficiency. The single-pixel microbeam system has a single triode-type CNT pixel with carbon nanotube deposited on the metal substrate using the electrophoresis deposition method developed in our laboratory. The CNT field emission electron current is controlled by the gate voltage applied on the gate electrode. Another focusing electrode is used for both isolating the gate structure from high anode voltage and first-stage electron beam focusing. A 400-μm-thick silicon wafer with a layer (200 nm) of Si_3N_4 is used to fabricate the vacuum window, which is also the electron microbeam beam portal. The thick silicon wafer acts as an electron collimator. The Si_3N_4 window is fabricated using a photolithography technique that carefully etches away the silicon in the intended location to form the Si_3N_4 window. The etching chemical selectively etches certain crystal planes and forms the inverted pyramidal opening.

Dosimetry of the prototype system was tested using 30 keV voltage and a pulsed current with a 2-μA peak and 1% duty cycle. The microbeam dosimetry for a 25-s irradiation was measured using GAFCHROMIC® film (HD-810) placed outside the Si_3N_4 window. The film optical density distribution was measured and converted to radiation dose. The film dosimetry indicated that the prototype single-pixel CNT microbeam irradiation system delivered a microbeam size of 20 μm and dose rate of 5 Gy/s. Monte Carlo simulation using PITS on the microbeam dosimetry considering the Si_3N_4 window was also performed. The Monte Carlo results indicated that the actual microbeam size should be significantly smaller than the film-measured size. We have identified several possible causes of the discrepancies between the film and Monte Carlo data and are in the process of identifying the exact cause.

Summary

We have developed the first prototype microbeam cellular irradiation system using carbon nanotube field emission technology and performed initial dosimetry measurements and Monte Carlo simulations. Our preliminary data demonstrated that the CNT-based low-LET microbeam system can be used to deliver a large dose-rate range (1 cGy to 100 Gy per second) and single-cell (10–20 μm) microbeam irradiation. The knowledge we gain in this feasibility study is essential for the development of a standalone multi-pixel CNT microbeam system.

Acknowledgments

The Monte Carlo package PITS was kindly provided by J. Miller of Washington State University. This work is partially funded by North Carolina Biotechnology Center (05MRG1111).

References

1. M. Sowa and W. Morgan, Microbeam developments and applications: A low linear energy transfer perspective. *Cancer Metastasis Rev.* **23**, 323–331 (2004).
2. M. Sowa, M. K. Murphy, J. H. Miller, J. C. McDonald, D. J. Strom and G. A. Kimmel, A variable-energy electron microbeam: A unique modality for targeted low-LET radiation. *Radiat. Res.* **164**, 695–700 (2005).
3. S. Iijima, Helical microtubules of graphitic carbon. *Nature* **354**, 56–58 (1991).
4. R. Gomer, *Field Emission and Field Ionization.* Harvard University Press, Cambridge, MA, 1961.
5. G. Z. Yue, Q. Qiu, B. Gao, Y. Cheng, J. Zhang, H. Shimoda, S. Chang, J. P. Lu and O. Zhou, Generation of continuous and pulsed diagnostic imaging x-ray radiation using a carbon-nanotube-based field-emission cathode. *Appl. Phys. Lett.* **81**, 355 (2002).
6. Y. Cheng, Y. Z. Lee, B. Gao, S. Dike, W. Lin, J. P. Lu and O. Zhou, Dynamic X-ray radiography using a carbon nanotube field emission x-ray source. *Rev. Sci. Instrum.* **75**, 3264–3267 (2004).
7. J. Zhang, G. Yang, Y. Cheng, B. Gao, Q. Qiu, Y. Z. Lee, J. P. Lu and O. Zhou, Stationary scanning x-ray source based on carbon nanotube field emitters. *Appl. Phys. Lett.* **86**, 184104 (2005).

Development of the GCI Multitarget X-Ray Microprobe

M. Folkard,[a] K. D. Atkinson,[a] G. Flaccavento,[a] P. R. Barber,[a] R. J. Locke,[a] G. Pierce,[a] S. Gilchrist,[a] A. G. Michette,[b] K. M. Prise[a] and B. Vojnovic[a]

[a]The University of Oxford, Gray Cancer Institute, Mount Vernon Hospital, Northwood, HA6 2JR, United Kingdom; and [b]King's College London, Strand, London WC2R 2LS, United Kingdom

Introduction

Cellular microirradiation techniques are being used increasingly for understanding how ionizing radiation interacts with living cells and tissues. The majority of facilities make use of collimated or focused ions; however, the Gray Cancer Institute (GCI) has pioneered the use of X-ray focusing techniques for microirradiating individual cells and subcellular targets *in vitro* (*1*). Our prototype ''tabletop'' X-ray microprobe has been optimized for focusing 278 eV C_K X rays and has been used successfully for a number of years (*2*). However, C_K X rays have very little penetration in tissue; almost all will be absorbed within one cell layer. Therefore, we have developed a new ''multitarget'' soft X-ray microprobe capable of delivering focused C_K (0.28 keV), Al_K (1.48 keV) and Ti_K (4.5 keV) X rays. Ti_K X rays are capable of penetrating several cell layers and are therefore much better suited to studies involving tissues and multicellular layers. Also, from a microdosimetric point of view, Ti_K X rays produce a spectrum of energy depositions in DNA-sized targets that more closely resembles those of conventional low-LET radiations. However, the lower efficiency of Ti_K X-ray production (by electron bombardment) and the increased X-ray penetration in tissue both conspire to reduce the effective dose rate. Furthermore, the zone-plate lenses used to focus the X rays are harder to manufacture at higher energies and tend to be less efficient. For this reason, one aspect of this study has been to develop a new X-ray microfocus source that is capable of higher outputs than our current system. At the same time, we have designed and implemented a much-improved automated cell-finding and irradiation capability that takes full advantage of recent developments in the performance of desktop computers and electronic imaging hardware. With the new facility, we have introduced a number of improved strategies for aligning the zone plate assembly and the microscope assembly, such that swapping X-ray-producing targets and zone plates (with a wide range of focal lengths) is relatively straightforward.

Methods

As with our prototype source, zone-plate diffractive optics are used to microfocus characteristic K-shell X rays generated by the focused electron bombardment of a target. The X-ray source comprises of two standard six-way ''vacuum cubes'' with 114-mm sides. One cube is fitted with the electron gun, while the other supports the target and X-ray focusing assembly. The cubes are joined by a 125-mm-long mid-section to which is mounted the electron gun anode, two sets of scan coils, and the electron focusing magnet. Each vacuum cube is pumped by its own turbomolecular pump that drops through a hole in a 1-m × 1.5-m optical table on which the source is mounted. The source is supported by linear bearings so that it can be aligned with the microscope and sample stage. Separate gauges are used to monitor the vacuum in each cube, which is typically 10^{-7} mbar or better.

The electron gun is custom-built, fitted with a high-brightness lanthanum hexaboride cathode, and designed to operate up to 15 kV. The gun is mechanically decoupled from its vacuum cube by a ''pan and tilt'' positioning device such that it can be aligned precisely with the anode. A number of gun-anode geometries have been tested; the most satisfactory with regard to ease of alignment and electron beam spot definition is the so-called Pierce gun arrangement. Electron beam transport to the focusing magnet is optimized by the two sets of scan coils mounted to the mid-section. They allow for modest ''dog-legging'' of the beam to correct any minor mechanical misalignments. The electrons are focused onto a target using a permanent neodymium-iron-boron magnet assembly. As the magnet strength is fixed, focusing is achieved by fine-tuning the target position through a vacuum position feedthrough. To aid this focusing procedure, a custom-built microscope (fitted with an infrared camera) is used to image the focused electron beam on the target through a vacuum window on the side of the cube. To simplify swapping between targets, a number of target assemblies have been constructed.

The X rays emerge vertically upward through a 0.5-mm^2 silicon nitride window that is 100 nm thick. The window is part of a zone-plate assembly coupled to the top of the target vacuum cube by a translating stage such that the zone plate assembly can be positioned precisely with respect to the X-ray source. The translating stage also supports an adjustable mirror within the vacuum that reflects the X rays at grazing incidence to the zone plate assembly. The mirror serves to remove unwanted Bremsstrahlung radiation at higher energies, which would otherwise be incorrectly focused. Delivery of X rays to the sample is controlled by means of a small solenoid-operated shutter just above the zone plate.

The cell finding and positioning stage comprises an epifluorescence microscope and a feedback-controlled three-axis cell positioning stage, also mounted on the optical table. The whole microscope-stage assembly can be raised or lowered precisely to adjust for large differences in the focal length of the X-ray zone plates. Independent vertical micropositioning of the microscope objective turret allows the focus of the microscope and the X-ray focus to coincide in space (i.e., at the point at which the cell should be positioned for exposure). All aspects of the source are controlled and monitored using a desktop computer. The same computer is used for the automated cell finding and irradiation procedures (see Barber *et al.* in these proceedings).

Results

The X-ray intensity, the energy spectra and the alignment of the zone-plate assembly have been analyzed using a proportional counter with a 0.9-μm Mylar window and filled with an argon/methane mix at atmospheric pressure. So far, most of the performance-related experiments have used C_K X rays. The X-ray flux through the vacuum window as a function of the electron beam current on target is about 3000 photons s^{-1} μA^{-1}. This corresponds to about 1.5×10^6 photons s^{-1} at the anticipated typical operating conditions for cell exposures (~500 μA).

Critical to the operation of the source is the alignment of the order-selecting aperture (OSA) at the focus of the zone plate. The OSA is necessary to allow only first-order diffracted X rays to reach the sample, and we are currently testing OSAs with diameters as small as 20 μm. To align the OSA, it is mounted to the three-axis stage that would normally support the cell dish. Automated procedures can then be used to scan the OSA and search for the correct alignment. Once this is established, the microscope is used to image the OSA and log its position in space precisely. It is then decoupled from the microscope stage and supported on an adjustable mount that is part of the zone-plate assembly, using the logged microscope position to achieve the correct location. Using a 100-μm-diameter zone plate with a 10-mm focal length, we have recently been successful in aligning a 25-μm OSA. Experiments are under way to establish the focused spot size, currently estimated to be less than 10 μm in diameter. The eventual goal is to achieve 1 μm or less.

Acknowledgments

The authors acknowledge the support of Cancer Research UK and the U.S. Department of Energy (award: DE-FG02-01ER63236).

References

1. M. Folkard, G. Schettino, B. Vojnovic, S. Gilchrist, A. G. Michette, S. J. Pfauntsch, K. M. Prise and B. D. Michael, A focused soft X-ray microbeam for targeting cells individually with submicrometer accuracy. *Radiat. Res.* **156**, 796–804 (2001).
2. G. Schettino, M. Folkard, K. M. Prise, B. Vojnovic, K. D. Held and B. D. Michael, Low-dose studies of bystander cell killing with targeted soft X rays. *Radiat. Res.* **160**, 505–511 (2003).

Performance of the GCI Multitarget X-Ray Microprobe

G. Flaccavento,[a] K. D. Atkinson,[a] P. R. Barber,[a] R. J. Locke,[a] G. Pierce,[a] S. Gilchrist,[a] A. G. Michette,[b] K. M. Prise,[a] B. Vojnovic[a] and M. Folkard[a]

[a]Gray Cancer Institute, Mount Vernon Hospital, Northwood, HA6 2JR, United Kingdom; and [b]King's College London, Strand, London WC2R 2LS, United Kingdom

Currently, the Gray Cancer Institute (GCI) is working on the final stages of development of a microirradiation system that uses X-ray focusing to irradiate individual cells. The design and construction of the facility have been described previously (see Folkard *et al.* in these proceedings). Presently, we are implementing improved procedures for aligning the X-ray focusing assembly that is located at the output of the system. To do this, we have developed an automated system to find the optimum position of the focusing components. The automated algorithm for this alignment is described below. Also discussed are preliminary results that quantify the size of the focused X-ray beam.

Focus Assembly Alignment

The X rays exit the system through a 500-μm^2 vacuum window made of 100-nm-thick silicone nitride. X rays are focused using zone-plate diffractive optics. A microscope is used to center the zone plate 2 mm above the vacuum window. Different zone plates are used to focus the beam depending on the type of X rays being produced. So far, all experiments have been performed using a 200-μm-diameter zone plate to focus C_K X rays (278 eV). Future experiments will also be performed using Al_K X rays (1.5 keV) and Ti_K X rays (4.5 keV). The zone plate for C_K X rays has an effective focal length of 9.4 mm (first-order diffracted X rays). Additionally, unwanted zero and higher-order X rays are present and must be prevented from reaching the cell dish. To do this, a 100-μm-diameter X-ray blocking stop mounted centrally on the zone plate and an order-selecting aperture (OSA) are used. The OSA consists of a pinhole, typically 20 μm or less in diameter, that must be positioned precisely at the first-order focus.

To align the OSA, it is first rigidly coupled to the cell micropositioning stage. This stage is computer controlled using the software designed primarily for cell finding and positioning (see Barber *et al.* in these proceedings). Initial alignment is performed with a 50-μm OSA. Once the approximate position of the X-ray focus is established, progressively smaller OSA diameters are used to refine the alignment. The cell-finding microscope can be used to visualize the OSA *in situ* and is used to assist in this alignment procedure. A proportional gas counter with a 0.9-μm-thick Mylar window is attached to the stage above the OSA. It is used to count the X rays as the OSA is moved to various positions. The measurements from the proportional counter are recorded using an MCA8000A multichannel analyzer (MCA) (Amptek).

Data Collection and Results

The stage is moved initially in 25-μm steps, in a 2D spiral path, beginning at a position determined geometrically to be close to optimum alignment of the zone plate and OSA. Using automated procedures, the stage pauses briefly at every step, and the number of counts per second is logged. The end result is a map of the dose rate for a predetermined region around the starting point. With this coarse stage movement of 25 μm, we find just one position where the dose rate was significantly higher than neighboring positions. It can therefore be assumed that the first-order focus lies entirely within this region. Then the process is repeated using finer 10-μm steps, beginning at the peak position found previously. In this instance, a region of high dose rate is found. Notably, the transition between high dose rates and low dose rates occurs within one 10-μm step, which indicates that the actual focus spot is much smaller than the size of the 50-μm OSA.

Next we replace the 50-μm OSA with a 25-μm OSA. The stage is moved until the smaller OSA is at the center of the peak area found in the previous measurements. Again, the measurements are repeated, this time moving the stage in increments of 5 μm. The results show a peak area approximately 20 μm in diameter with a dose rate significantly higher than its surroundings. Taking into account the diameter of the OSA, these results indicate that the spot size is approximately 10 μm. This spot size is larger than anticipated and may indicate that the OSA is not at the correct distance from the zone plate. Further experiments are planned to improve the alignment by using smaller-diameter OSAs and by adjusting the OSA position in all three axes.

Acknowledgments

The authors acknowledge the support of the EC Marie Curie Research Training Network (CELLION) and Cancer Research UK.

X-Ray Microbeam Irradiation Systems at the Photon Factory—Present Status and Future Plans

K. Kobayashi,[a] N. Usami,[a] H. Maezawa,[b] T. Hayashi,[c] K. Hieda,[d] K. Takakura[e] and Y. Furusawa[f]

[a]Photon Factory, Institute of Materials Science, KEK, Tsukuba 305-0801, Japan; [b]School of Health Sciences, University of Tokushima, Tokushima 770-8509, Japan; [c]Hayashi So-ken Inc., Sengen, Tsukuba 305-0047, Japan; [d]Department of Life Science, College of Science, Rikkyo University, Tokyo 171-8501, Japan; [e]College of Liberal Arts, International Christian University, Mitaka 181-8585, Japan; and [f]National Institute of Radiological Science, Inage, Chiba 263-8555, Japan

We have developed an X-ray microbeam irradiation system using monochromatic synchrotron X rays. The energy of X rays is restricted to 5.35 keV, since the beam is deflected at a right angle upward using diffraction of a Si(311) lattice plane, to irradiate the samples through the bottom of the dish. Improvements in this system and development of an energy-tunable microbeam irradiation system are described here.

Improvement of the System

Presently we are usually using a microbeam defined by a slit system. The beam size can be changed from 5 μm square to any larger size of rectangular shape. The photon density at the sample position is concentrated by using asymmetric diffraction of Si(311), and the dose rate is about 40 R/s (10.32 mC/kg s^{-1}), which corresponds to about 10^4 photons/s per 100 μm^2. With the experience of using this system, we have established a procedure to irradiate all the cells in a designated area automatically. With this mode we can obtain survival data with statistical significance, and hypersensitivity in the low-dose region can be observed.

For efficient use of the system, we have set up another fluorescence microscope with a motorized stage (off-line system) into which information about the coordinates of the cell irradiated by the irradiation system (on-line system) can be transferred. This system is dedicated to observing biological effects in irradiated cells. Recently, we have installed a confocal laser microscope into this microscope, which enables highly sensitive detection of fluorescent images of the irradiated cells. Many users are using this system to study the postirradiation induction or accumulation of response-related proteins by either immunostaining or using GFP-integrated cell lines.

Development of an Energy-Tunable X-Ray Microbeam System

One of the advantages of using synchrotron radiation as the light source is that we can choose any energy of monochromatic X rays with practical intensity. Using this technique we have a long experience in studying the energy dependence of radiation-induced biological effects, including the effects of inner-shell photoabsorption and Auger effects. According to recent reports using microbeams, it has been revealed that radiation-induced signaling in the cell plays an important role in determining the final biological effects. To study the signal induction process as a function of photon energy, we are planning to build an energy-tunable X-ray microbeam system with which we can irradiate with the monochromatic X rays of inner-shell absorption edges of certain elements. We have to use the horizontal beam as emitted from the electron storage ring; hence we need to overcome some difficulties such as vertical positioning and design of an appropriate sample chamber contain the cells. The final test is scheduled for autumn 2006.

Development of a Soft X-Ray Microbeam at RARAF

G. Schettino, G. Randers-Pehrson and D. J. Brenner

Center for Radiological Research, Columbia University, New York, New York

Nearly all microbeam facilities currently employed for radiobiological applications use charged particles: from protons to heavy ions with LET ranging from a few tenths to several hundred keV/μm. There are, however, considerable benefits in using soft X-ray microbeams for both mechanistic and risk estimation end points. The higher spatial resolution achievable with modern state-of-the-art X-ray optics elements combined with the localized damage produced by the absorption of low-energy photons (~1 keV) represents a unique tool to investigate the radiosensitivity of subcellular and eventually subnuclear targets. Moreover, since X rays do not suffer from scattering, by using higher-energy X rays (~5 keV), it will be possible to irradiate with submicrometer precision individual cells and/or parts of cells up to a few hundred micrometers deep inside a tissue sample to investigate the relevance of effects such as the bystander effect in well-organized 3D structured cell systems. Finally, several recent studies (*1, 2*) have highlighted the phenomenon of an adaptive response with a small ''priming'' dose of X rays being able to stimulate cell repair mechanisms and reduce the effect of a subsequent higher-dose or higher-LET exposure. Such studies require more accurate head-to-head comparisons of X rays and charged particles and require facilities able to perform mixed irradiations.

We are planning to improve the RARAF charged-particle microbeam by including soft X rays (characteristic K_α X rays from aluminum, 1.49 keV, and titanium, 4.5 keV) since higher energies are not feasible due to Compton scattering effects. The X-ray microbeam will then be in the same physical location of the charged particle facility, sharing the same geometry, image analysis and micropositioning setup, favoring head-to-head comparisons between X rays and charged particles and facilitating mixed irradiation experiments. X rays will be generated by proton bombardment by using the existing electrostatic lens setup to focus protons [best cross sections at 2.9 MeV for aluminum and 4.5 MeV for titanium (*3*)] into a thin foil. By using the already focused proton microbeam to generate characteristic X rays, it is possible to obtain a nearly monochromatic X-ray beam (very low bremsstrahlung yield) and a reasonably small X-ray source (~10 μm diameter), reducing the requirement on the

TABLE 1
Results of Target Simulations with Expected Dose Rate to Samples

Source diameter (μm)	Maximum total power (mW)	Proton current (nA)	K_α X-ray yield	Dose rate (Gy/s)	Spot size (μm)
Aluminum target (three foils, each 10 μm thick with a 5-μm gap in between; helium-cooled)					
5	1.1	0.44	1.21×10^9	0.02	0.4
10	4.4	1.8	4.83×10^{10}	0.08	0.8
25	27.6	11	3.03×10^{10}	0.5	2.1
Titanium target (three foils of 10, 20 and 10 μm thickness with a 5-μm gap in between; helium-cooled)					
5	0.102	22.7	6.40×10^9	0.033	0.4
10	0.36	80	2.26×10^{10}	0.12	0.8
25	1.44	320	9.04×10^{10}	0.46	2.1

subsequent X-ray focusing device. Extended simulations performed using a finite element analysis (ANSYS) have provided an indication of the size of the X-ray source and the maximum power with which it is possible to proton bombard the aluminum and titanium foil. The final target design consists of three thin foils (different thickness for aluminum and titanium) separated by a 5-μm gap through which cooled helium is blown. Such a target is able to cope with a substantial amount of power dissipated by a focused proton beam increasing the characteristic X-ray production and the overall final dose rate to the samples (Table 1). The emerging X-ray beam is then focused down to a submicrometer size spot by the use of a custom-made circular diffraction grating (i.e. zone plate). The parameters have been optimized for the aluminum and titanium zone plates to obtain a final demagnification >10 at a distance of 150 mm from the X-ray source and with the same focal length of 12 mm, making it easier and quicker to switch between the two X-ray energies. The zones will be 200-nm-thick gold (deposited on silicon) with the center zone covered by a conductive beam stop that prevents protons from reaching the cells. The beam stop, in conjunction with the collimated beamline exit window, also prevents both the zero and high-order diffracted X rays from reaching the samples, resulting in an optimal beam spot size. Although zone plates are quite efficient in focusing X rays in this energy range and are widely available, alternative optics devices such as polycapillaries are also being considered.

A critical aspect of the RARAF microbeam will be a quick switching between charged particles and X rays. To avoid the long time required for the accelerator beamline to reach operating vacuum after it is opened to air, a routable turret will hold both the charged-particle and the X-ray snouts. The latter will contain the aluminum or titanium target with the zone plate properly aligned. Roller bearings will be used to rotate the snouts without disrupting the vacuum conditions allowing operating conditions to be reestablished quickly.

References

1. E. I. Azzam, G. P. Raaphorst and R. E. J. Mitchel, Radiation-induced adaptive response for protection against micronucleus formation and neoplastic transformation in C3H 10T1/2 mouse embryo cells. *Radiat. Res.* **138** (Suppl.), S28–S31 (1994).
2. K. M. Prise, O. V. Belyakov, H. C. Newman, S. Patel, G. Schettino, M. Folkard and B. D. Michael, Non-targeted effects of radiation: Bystander responses in cell and tissue models. *Radiat. Prot. Dosim.* **99**, 223–226 (2002).
3. J. D. Garcia, R. J. Fortner and T. M. Kavanagh, Inner-shell vacancy production in ion-atom collisions. *Rev. Mod. Phys.* **45**, 111–175 (1973).

Biological Experiments Visualizing Radiation-Induced Responses with Synchrotron X-Ray Microbeam at the Photon Factory

N. Usami,[a] K. Eguchi-Kasai,[b] M. Mori,[b] H. Maezawa[c] and K. Kobayashi[a]

[a]Photon Factory, High Energy Accelerator Research Organization (KEK), Tsukuba 305-0801, Japan; [b]National Institute of Radiological Sciences, Chiba 263-8555, Japan; and [c]Faculty of Medicine, University of Tokushima, Tokushima 770-8509, Japan

An X-ray microbeam irradiation system using synchrotron radiation has been developed at the Photon Factory, KEK, Japan and is now being used for various biological experiments. The energy of microbeam X rays is 5.35 keV, which is suitable for experiments using mammalian cells, because the X rays can penetrate the thickness of cells and the range of secondary electrons is a few micrometers. Details of the system and future developments are presented elsewhere in this proceedings.

The synchrotron radiation has extremely low divergence, so it is easy to get an X-ray beam with micrometer dimensions. The high-precision slit installed in the system is the simplest way to get a microbeam without focusing. The minimum beam size with the slit is 5 μm square, and the size of the microbeam can be changed quickly and arbitrarily. This specification might be ideal to investigate localization of the damage in cells or cell nuclei irradiated with subcellular-sized beam. We tried to visualize the DNA damage produced in the microbeam-irradiated human cells by immunostaining of phosphorylated histone H2AX (γ-H2AX).

Human fibroblast cells (NB1RGB) were grown in α-MEM containing 10% FBS and inoculated to the specially designed dishes, the bottom of which was made of a thin polymer film (Mylar or polypropylene). The cells were incubated for 12 h to allow them to attach to the surface of the polymer. Before irradiation, the cell nuclei were stained with the medium containing 1 μ*M* Hoechst 33258 for 30 min. The dish was set on the microbeam system; the positions of cell nuclei were recorded with the specially developed software, and the nuclei were irradiated with the X-ray microbeam. The cells were irradiated with two different microbeams, either 5 or 10 μm square. The fluence of microbeam was 1.4×10^4 photons/$(10\ \mu m)^2$ per second, which is equivalent to X rays at 0.4 Gy per second. After irradiation, cells were incubated at 37°C for 15 min and fixed in 100% methanol for 20 min and 100% acetone for 10 s at 0°C. Then cells were blocked with 1% FBS for 10 min, incubated with the γ-H2AX antibody (provided by Sawady Technology), washed and incubated with FITC-conjugated donkey anti-rabbit IgG (Santa Cruz Biotechnology, Inc). The nuclei of the cells were also stained with 1 μg/ml of propidium iodide after the immunostaining process. The dish was set on the microbeam system again, and the system automatically revisited the positions of the targeted cells. The targeted cells were viewed with the epifluorescence microscope installed in the system. We also observed the cells by a confocal laser scanning microscope installed recently to the ''off-line detection system'' in which the information of targets can be shared in common with the irradiation system.

All the irradiated cells could be found at the revisited positions and could be distinguished from surrounding unirradiated cells by their high yield of fluorescence of γ-H2AX. Most fluorescent foci were observed in localized areas in cell nuclei, the sizes of which were almost the same as the beam size. Differences in the sizes of the stained areas can easily be recognized between cells irradiated using the 5-μm beam and those irradiated with the 10-μm beam. This result also demonstrates that the system has enough accuracy and repeatability to target a part of the individual cell nucleus. Dose dependence of γ-H2AX induction was also clearly observed within the dose range equivalent to 2–6 Gy X rays.

Recently, we have started an investigation to visualize the accumulation of DNA repair-related proteins by using Chinese hamster cells with GFP-Rad51. Within 2 h after irradiation, significant numbers of foci of GFP-Rad51 were clearly observed in the nuclei of the microbeam-irradiated cells. Experiments to determine the time course of the protein accumulation are now in progress.

SESSION 3: MICROBEAM ENDSTATIONS

Chair: Gerhard Randers-Pehrson

The GCI Multitarget X-Ray Microprobe: Imaging, Control and Software Automation

P. R. Barber, R. J. Locke, G. P. Pierce, R. G. Newman, M. Folkard and B. Vojnovic

The University of Oxford, Gray Cancer Institute, Mount Vernon Hospital, Northwood, Middlesex, HA6 2JR, United Kingdom

Introduction

A new X-ray microprobe is being developed at the Gray Cancer Institute and will operate alongside two existing microirradiation facilities: a charged-particle microbeam and a prototype X-ray microprobe optimized for focused C_K X rays. It generates X rays through bombardment of carbon, aluminum or titanium targets by a focused electron at acceleration energies of up to 15 kV (see Folkard *et al.* in these proceedings). The new facility takes advantage of advances in technology that have arisen since the original microprobe was commissioned some 10 years ago. Specifically, dramatic improvements in the processing power of desktop computers and the availability of affordable, sensitive CCD cameras have enabled much improved automated procedures for cell recognition, positioning and irradiation to be implemented.

Dose delivery is controlled either by presetting irradiation times or through integration of electron beam current: When the required counts are reached, a shutter in the X-ray path is activated. All aspects of the source can be computer-controlled or overridden using manual controls.

Automated Microirradiation and Microscopy

A microirradiation experiment requires a high degree of hardware automation to fulfill the requirements for speed, reliability and reproducibility, particularly when large numbers of cells (10^2–10^4) are involved. The control of the radiation source and dose delivery is essential alongside the control of a cell positioning system as well as some means of cell detection or imaging, usually based on standard microscopy techniques. A convenient way to control, in a flexible manner, such disparate hardware is through the use of a desktop computer and appropriate software. This approach also allows ''intelligent'' experiments to be performed, during which decisions about ''where'' to irradiate can be made automatically. For example, the cellular nucleus or cytoplasm can be targeted through the use of appropriate image processing algorithms. The recent construction of the microfocus X-ray source has led to a push to develop a faster and more accurate software-driven system, as described below. This approach is equally applicable for performing fast and complex irradiations with particle microbeams and addresses current and future experimental needs.

This software control system uses a modular approach, whereby individual programs are developed to control each specific hardware subsystem. These modules are combined to form the final program but, for them to remain self-contained, message passing is used to allow the modules to communicate. Self-containment is important since debugging is simpler and it allows code reuse between projects. Just as importantly, it forces the code developer to consider this aspect. Furthermore, this approach aids hardware testing and complements the design of the hardware control systems. We implement hardware control using an expandable, daisy-chain bus approach, based on the use of the I^2C bus. In turn, this is controlled through a single, standard USB link to the host PC. This allows us to readily add devices perhaps not envisaged at the design stage.

Modern computers are able to run more than one program at once, and true parallel processing can be achieved by installing multiple processors or by using ''multiple core'' processors that are now available. We can make effective use of these by implementing multithreaded programs; this has been used extensively not only to speed up processor-intensive tasks but also to add a degree of system adaptability during automated, repetitive tasks. For example, differences in dose delivery or camera exposure times will exist between experiments; an adaptable automated system easily copes with this.

Image Processing and Performance

There are two aspects to a ''typical'' microirradiation experiment. These are (1) cell finding, i.e., *XYZ* coordinate mapping and target identification, and (2) individual target revisiting and irradiation. Many variations on how these are sequenced can be envisaged, e.g., all targets within a field of view identified, followed by their irradiation or all targets within a dish region identified and then irradiated. The most common imaging method is based on widefield steady-state fluorescence microscopy, usually performed with a 40× water-dipping objective (0.9 na) which restricts the field of view to around 220 × 290 μm but provides diffraction-limited resolution (215 nm/pixel) and high sensitivity. Some 10^4 cells/hour can be processed under these circumstances using interpolated three-point focusing; i.e., where a focus plane is defined, image stitching is used to provide a true dish map of cells and targets along with classification of different object ''types'', e.g., nuclei, debris, overlapping/binucleated cells, etc. A range of image processing functions is performed during automated experiments, ranging from image corrections for variations in fluorescence excitation illumination to cell finding and the delineation of the nucleus. The more sophisticated of algorithms use a Compact Hough Transform And Radial Map (CHARM) approach, whereby the centers of objects of approximately circular shape are found by a modified Hough Transform and their outlines are found by searching outward from these centers to form radial maps. Importantly, fast shape processing can be performed on these radial maps to improve outlines and resolve conflicts in overlapping shapes or cells in contact. In particular, our algorithm is rugged and insensitive to minor variations in focus where features may not be perfectly delineated, with much enhanced performance over the more usual watershed- or threshold-based approaches. A range of morphological and intensity features are logged to aid cell cycle-related studies. By searching outwards from the ''found'' object, we make use of edge strength, edge completeness and mean radius measures to aid the classification process. Live overlays are used extensively to mark objects, targets and source beam positions.

System Hardware

The imaging hardware is implemented from standard Nikon components and accessories, modified to allow other imaging modes (e.g., polarized light epi-illumination to aid alignment of the X-ray source zoneplate and order-selecting aperture). Other imaging modalities (e.g., time-resolved fluorescence detection) can be added readily. The assembly is integral to the tabletop source (see Folkard *et al.* in these proceedings) and uses a closed-loop motorized sample positioning stage (*x,y* axes) complemented by two *z*-axis motorized drives, one controlling the optical focus, the other the X-ray source focus, as well as other motorized optical components. Images are stored using the Imaging Cytometry Standard (ICS, http://libics.sourceforge.net/), and all operating conditions (e.g., objective, filter cubes, camera setup) are monitored and logged as metadata in these files.

The host computer uses dual hyperthreading Intel P4 processors, and modular experiment user interfaces are available on dual graphics screens. The software is developed in the C and C++ programming languages and runs under the National Instruments CVI LabWindows environment.

The X-ray source hardware is similarly controlled and its performance continuously monitored, displayed and logged. In this instance, in-house developed hardware is used, the main components of which are electron gun filament and grid supplies, an electron beam acceleration supply (15 kV, 100 W maximum), magnetic beam deflection supplies, and a range of shutter and status control and monitoring systems. This integrated approach allows us to easily monitor and control the source vacuum system, to sequence the various power supplies, to condition the safe starting,

stabilization and shutdown of the source, and to implement specific sequences, e.g., during conditioning of a new filament/cathode assembly. Once aligned, the intensity of the electron beam may be stabilized through control of the grid voltage, using a hardware-implemented feedback loop that compares the electron beam current collected at the source target with a set-point value, up to currents in excess of 5 mA.

Acknowledgments

The authors acknowledge the support of Cancer Research UK (Programme Grant: C133/A/1812) and the US Department of Energy (award: DE-FG02-01ER63236).

Multiphoton Microscope Design for the Columbia University Microbeam II Endstation

A. W. Bigelow, G. J. Ross, G. Randers-Pehrson and D. J. Brenner

Columbia University, Radiological Research Accelerator Facility, Irvington, New York 10533

At the Radiological Research Accelerator Facility (RARAF), we are developing a multiphoton microscope at the endstation of our single-cell single-particle microbeam irradiator for detecting and observing the short-term molecular kinetics of radiation response in living cells. A multiphoton microscope is an infrared laser-based, 3D, minimally damaging imaging tool that, when compared to conventional confocal microscopy, has greater penetration depth and has reduced phototoxicity and photobleaching in the sample bulk (*1*). The guiding principle of the multiphoton microscope is that when two photons are spatially and temporally coincident within the excitation cross section of a fluorophore molecule, they can act as one photon with twice the energy to induce an electronic transition.

Our multiphoton microscope design incorporates our current cell-imaging platform, a Nikon Eclipse E600-FN research fluorescence microscope. This Nikon microscope was modified to function over a vertical ion beam; the base was removed from the microscope, which was mounted to a pivot arm for switching between on-line and off-line positions. To improve the kinetic mount for the microscope, a new pivot arm has been designed with a spring-loaded ball and socket connection at the pivot point.

The excitation light source is a Chameleon (Coherent Inc.) tunable titanium sapphire laser that provides 140-fs pulses at a 90 MHz repetition rate. In obtaining our laser, an extensive evaluation was made between two similar one-box titanium sapphire laser systems: the Chameleon made by Coherent Inc. and the Mai Tai made by Spectra Physics. After comparing the laser specifications and after consulting references from both companies, our conclusion was that either laser would work well for our application. Slight advantages that swayed our decision to purchase the Chameleon were (1) superior user feedback, (2) a manual control mode in addition to a computer control interface, (3) Coherent's favorable ''Advanced Replacement Service Strategy'', (4) an internal spectrometer instead of a look-up table to monitor the lasing frequency, and (5) a user-friendly diode replacement process.

Along the incident laser beam path, a waveplate and polarized beam splitter are placed in the beam path to control the laser beam power. Mirrors direct the laser up through the microscope pivot shaft and into a scan head. A scan lens then focuses the scanned laser beam to a point in an image plane for the microscope (a CCD camera is often placed at such an image plane). The incident light path continues through the side of the trinocular tube where a retractable mirror directs the laser beam down through the tube lens and the objective lens to a focal point within a specimen. The scanned laser establishes an optical cross section within the specimen, where multiphoton absorption preferentially occurs. Wavelengths available from our titanium sapphire laser can be made to penetrate to depths of about 100 μm in a biological sample by varying the *Z*-position of the specimen stage. Returning along the collection pathway, light emitted from the specimen is selectively deflected by a series of dichroic mirrors to an array of photomultiplier tubes (PMTs). An additional PMT for transmitted light collection is available for the microscope in the off-line position. Images are constructed through comparing PMT signal to scan head position.

For control of our multiphoton microscope, we are adopting Karel Svoboda's design from Cold Spring Harbor. Svoboda's control software, ScanImage (*2*), runs in the MatLab platform and was obtained through an Internet download. Continuing with these suggestions, we have purchased the recommended multifunction DAQ device (NI-6110, National Instruments) and its break-out box. Test for scanning voltage waveforms were successful and the microscope assembly process continues.

References

1. W. Denk, J. H. Strickler and W. W. Webb, Two-photon laser scanning fluorescence microscopy. *Science* **248**, 73–76 (1990).
2. T. A. Pologruto, B. L. Sabatini and K. Svoboda, ScanImage: Flexible software for operating laser scanning microscopes. *Biomed. Eng. Online* **2**, 13 (2003).

Ion Beam Quality Assessment at the INFN-LNL Single-Ion Microbeam Facility. A Combined Approach: Simulations and Measurements

S. Gerardi and R. Cherubini

INFN-Laboratori Nazionali di Legnaro, Viale dell'Università 2, I-35020 Legnaro, Padova, Italy

Introduction

To undertake a systematic investigation of the action of a single charged particle in a single mammalian cell, an accelerated low-intensity ion beam, well defined in energy (monoenergetic) and with a cross section reduced to a few square micrometers (at least comparable to cell dimensions), is required. Among the available approaches, the use of an appropriate microcollimator allows the production of a single-ion microbeam. The choice of the microcollimator, in terms of materials and geometry, is one of the fundamental tasks to be accomplished to obtain monoenergetic ion beams with a micrometer spot in air. The energy and angular distributions of scattered ions strongly depend on particle type and energy, thicknesses and materials traversed by the particles traveling toward the target. To optimize the beam quality in air, by reducing the scattering components and the beam spot size at the cell position and increasing the percentage of full-energy particles on cells, a careful study of the material and geometry for a microcollimator has to be undertaken. Usually such an experimental investigation is time consuming and requires a lot of allotted accelerator beamtime. Appropriate Monte Carlo codes could serve as useful tools, complementary to the measurements.

To assess the contribution of the different factors on the beam quality and to optimize the microcollimation system developed at the INFN-Laboratori Nationali de Legarno (INFN-LNL) single-ion single-cell microbeam facility (*1*), a simulation code for the transport of light ions along the facility has been developed using the GEANT4 toolkit (*2*). The roles of the various parameters influencing the beam quality at the cell position (type and energy of the beam, extraction window, microcollimator geometry and material, air gap before the cell sample, etc.) have been analyzed. Specific measurements have been performed to validate the simulation. Different microcollimator devices have been tested on the ion beams, and a systematic simulation activity has been undertaken.

The INFN-LNL Single-Ion Single-Cell Microbeam Facility

The single-ion single-cell microbeam apparatus (*1*) has been set up at the Radiobiology irradiation facility of the 7 MV Van de Graaff CN accelerator of the INFN-LNL, which delivers horizontal light ion beams

(protons, deuterons, $^{3}He^{+,2+}$ and $^{4}He^{+,2+}$ ions in the energy range 0.8 to 13 MeV in air).

The primary CN VdG accelerator ion beam intensity, reduced along the Radiobiology beampipe by means of two gold scatter foils, is defined in vacuum by a three-tantalum-collimator (13-mm-diameter) telescope and extracted in air through a thin window (2-mm-diameter, 10-μm-thick bi-aluminized Mylar). The extracted light ion beam is homogeneously broadened (with an uncertainty less than 1% over the sample) over a circular area 2 mm in diameter with a low-intensity beam current.

As a distinctive feature of the INFN-LNL single-ion microbeam facility, the microcollimator device is positioned in air in front of the extraction window by means of a separate, tilting support flange. The alignment of the microcollimator with respect to the incoming beam direction is achieved by moving the tilting support, which is mounted at a distance of 2 mm (properly adjustable) from the extraction flange by three tongs and is driven by two remotely controlled stepper motors coupled to two motor eccentrics and pistons.

Collimators of different geometries (slit assembly or pinhole microcollimators) and materials (titanium, tantalum, silicon) have been tested. The performances of the various microcollimators have been assessed in terms of the quality of the beam energy spectrum in air (full-energy peak/whole energy spectrum) as well as of the particle counts as measured by a silicon detector at the position of the cells to be irradiated.

The collimators in use consist of a single tantalum disc (200-μm thickness) with either a 5-μm- or 2-μm-diameter central pinhole. Novel microcollimator devices on silicon wafers have been developed by using the Deep Reactive Ion Etching (DRIE) technique at the Semiconductors and Sensors Laboratory of Physics Department-Ferrara University, in the framework of a joint collaborative project. Silicon collimators of different apertures (8×8, 8×4, 4×4, 2×2 μm^2) have been tested on beam.

Simulation Code for the INFN-LNL Single-Ion Single-Cell Microbeam Facility and its Validation

Considering protons and α particles as primary ions with energy in the range 3–6 MeV and 5–14 MeV, respectively, GEANT4 standard and low-energy electromagnetic processes (ionization, multiple scattering) and hadronic (elastic and inelastic) processes have been included in the physics list of the simulation. For secondary electrons produced by interaction of primary ions with the traversed materials, standard and low-energy electromagnetic processes (ionization, multiple scattering, bremsstrahlung) have been defined.

The basic components of the facility (scattering chambers with collimators and gold scatters, beam pipe, three-collimator telescope, extraction flange, Mylar vacuum-air window, microcollimator) have been built with GEANT4 by defining a volume for each beamline component.

The simulation code has been validated by making a comparison between experimental data and simulation results in terms of beam energy spectrum, spatial particle distribution and beam profile after a 4-mm-thick air gap (before the beam is microcollimated) for protons and alpha particles. The ion energy spectrum has been measured with a silicon surface barrier detector (depletion region thickness: 500 μm), with a 1-mm-diameter collimator, placed at a distance of 4 mm from the extraction window. The horizontal and vertical beam profiles in air have been determined by moving, with micrometric mechanisms, the silicon detector in the plane perpendicular to the direction of the incident beam, along the *Y* and *Z* axes. To register the spatial particle distribution, a CR39 solid-state nuclear track detector has been positioned in front of the extraction window at a distance of 4 mm. After irradiation, the detector has been etched and a 3-mm-diameter beam spot has been evaluated and compared with simulation results.

Then the energy spectrum and the spatial particle distribution of a 10 MeV α-particle beam microcollimated by the 5-μm tantalum pinhole has been measured after the 2-mm-thick air gap and compared with simulation results.

The comparison of simulation results with experimental data, in terms of energy loss and particle scattering, showed a good agreement. Therefore, the GEANT4-based simulation code can be considered a reliable tool to support experiments in the energy region of interest in this application and to perform a systematic simulation activity on the geometry and the materials of the different microbeam facility components, and in particular of the microcollimation system, to optimize the beam quality in air.

Ion Microbeam Quality Assessment

Tantalum and silicon collimators with apertures down to few square micrometers have been simulated and compared to assess the effects of different materials (silicon and tantalum) and geometry (square and circular section) on the ion beam quality in air at the cell sample position.

Multiple collisions encountered by particles traversing the different elements mounted along the beamline broaden the beam before hitting the cell sample. This effect also depends on the thicknesses and materials that have been traversed. The influence on beam quality of the various element thicknesses and materials, of the vacuum window (Si_3N_4 or bi-aluminized Mylar membranes), and of the air gap between the collimator and the cell sample has been considered.

On the basis of the preliminary results of simulations, the following statements can be made about the optimization of the collimation system:

1. The collimator aperture shape (circular or square) does not appear to be relevant for the beam quality in air (at least for the configurations considered).
2. Tantalum and silicon appear to be equivalent material in terms of particle spatial distribution; tantalum more than silicon allows reducing the particle energy straggling.
3. Using a Si_3N_4 membrane (200 nm thick) rather than a bi-aluminized Mylar as vacuum window allows reduction of the particle scattering component, but no relevant improvement in energy definition is observed at the cell sample position. The air gap has a major effect.
4. Reducing as much as possible the air gap between the microcollimator and the cell sample allows significant reduction of the beam spot size in air.

The air gap between the microcollimator and the cell sample appears to be the parameter that influences the beam spot size at the cell position more than the others in the facility configuration considered. A 200-μm-thick air gap seems a good practicable compromise to get a small beam size and to have enough free space to move safely the cell sample and place each cell in front of the beam during irradiation without scratching the Mylar base of the petri dish (*1*). Further simulations and additional specific measurements are needed and planned.

Acknowledgments

The authors are grateful to Maria Grazia Pia and Susanna Guatelli (INFN-Genova, Italy) for their kind support and assistance in the introduction to GEANT4. The Semiconductors and Sensors Laboratory of Physics Department of Ferrara University (Giuliano Martinelli, Vincenzo Guidi and Francesco Logallo) is acknowledged for the development of silicon microcollimators.

References

1. S. Gerardi, G. Galeazzi and R. Cherubini, A microcollimated ion beam facility for investigations of the effects of low-dose radiation. *Radiat. Res.* **164**, 586–590 (2005).
2. GEANT4: http://wwwasd.web.cern.ch/wwwasd/geant4/geant4.html.

Progress Report on the IFJ PAN Microprobe for Living Cell Irradiations: Technical Setup and First Experimental Data

J. Lekki,[a] W. Polak,[a,c] R. Ugenskiene,[b] O. Veselov,[a] Z. Stachura,[a] J. Styczen,[a] M. Zazula[b] and J. Stachura[b]

[a]Henryk Niewodniczanski Institute of Nuclear Physics PAN, Cracow, Poland; [b]Jagiellonian University Collegium Medicum, Cracow, Poland; and [c]Ion Beam Centre, University of Surrey, Guildford, United Kingdom

During the last 2 years, significant modifications have been introduced at the IFJ PAN Cracow ion microprobe to allows the possibility of its application to single-ion irradiation studies. This overview presents current status of the facility and the results of the first radiation measurements performed with living cells.

Technical Setup

The Cracow microprobe facility is built around a Van de Graaff accelerator that can supply H^+ and He^+ ions accelerated by a voltage of 2.5 MV in the horizontal direction. The ion beam passes the 90° analyzing magnet and, after forming in a system of quadrupoles and diaphragms, is focused by two doublets of quadrupoles (MARC, Melbourne). The total length of the microprobe is only 2.3 m. Just prior to the focusing end stage, the beam blanking plates driven by a dedicated system are installed. The main measurement stage consists of an ion exit chamber, a precise 3D moving stage equipped with a petri dish holder, a particle detector for ion counting, and an optical system with a CCD camera. Ions leave the vacuum through a thin Si_3N_4 (200 nm) exit window that serves also as an illumination window for the microscope (a high-brightness LED diode is mounted inside the chamber). This arrangement allows observation of the unstained cells in transmitted light using a standard microscope objective. Due to the requirement for observation of cells during all steps of an experiment, another off-line optical system is provided that consists of an Olympus BX51 microscope with bright-field illumination, fluorescence microscopy and quantitative phase microscopy (*1*).

The experiment is controlled by a personal computer, which directly runs positioning and blanking tasks and processes information from the optical system and the detector acquisition system using self-developed software. Particular attention has been paid to development of a robust image processing code. Its task is to find the coordinates of the subsequently irradiated cells based on a microscopic image. Although the image processing encompasses a great number of transformation procedures (filters, logical operations, morphological transformations, etc.), there is no standard way to achieve the required result. Thus the developed software allows adjusting and modifying the applied algorithm by the application of adjustable command scripts. This enables convenient processing both in simple cases (suitable for fast preliminary investigations) and also in circumstances requiring complex sequences of image transformations.

Several standard protocols for system testing and setup have been developed. A beam blanking system provides sufficient performance (>98%) for ion intensities up to $\sim 10^3$ protons/s. The positioning system provides 0.5 μm accuracy and enables an automatic beam location procedure. However, in spite of ensuring a very small (~200–300 μm) distance between the exit window and irradiated cells, the ion hit resolution of the beam in the atmosphere is rather poor; tests using a CR39 solid-state detector revealed a targeting accuracy of only about 30 μm. This effect is mainly due to imperfections in microprobe setup that were accidentally introduced during ion guide rearrangement. The ongoing system adjustment should vastly improve this parameter.

Materials and Methods

For our first microbeam experiments, we used human skin fibroblasts. Cells were grown in DMEM with supplements. One day before irradiation, approximately 500 cells were seeded directly on a 500-nm-thick, 3 × 3-mm^2 silicon nitride window glued with paraffin over a hole drilled centrally in a standard 35-mm petri dish. Just prior to the irradiation, the medium was removed and cells were washed with PBS. Then the petri dish was covered with Mylar foil to prevent cells from drying and inserted into an irradiation holder.

We have focused on several end points: micronucleus assay, double-strand breaks (DSBs), and cell survival. This gives a wider overview of the radiation-induced damages. For the micronucleus assay, after the irradiation, cells were incubated in DMEM with 1.5 μg/ml of cytochalasin B for 72 h, washed with PBS, fixed with methanol-acetone solution, and stained with a mixture of Acridine Orange and Hoechst 33342 (*2*). The micronuclei were scored according to the IPCS guidelines (*3*). For the detection of DSBs, immediately after the irradiation, samples were placed on ice and fixed. A common immunohistochemistry procedure for cell permeabilization and unspecific blocking was applied. H2AX monoclonal primary antibody was used at a concentration of 1:500 for 1 h at room temperature and Alexa Fluor 488 secondary antibody at the same concentration and duration. Additionally, cell nuclei were stained with DAPI. For the evaluation of the DSBs, cell dish images were taken and brightly shining spots representing DSBs were counted. Survival was determined by Hoechst and propidium iodide staining at concentrations of 0.5 μ*M* and 1 μ*M,* respectively. Cell cultures were stopped at different time ranging from 1 h to 72 h after irradiation.

Samples were irradiated with doses of 1 and 6 Gy (corresponding to 500 and 3000 of 2 MeV protons, respectively). The procedure lasted from 10 to 30 min depending on the dose and the number of irradiated cells. Every irradiation was carried out for at least three cell samples.

Results of First Irradiations

The results were scored using Olympus BX51 fluorescence microscope. For the micronucleus test, at least 75 binucleated cells were counted in every experiment for a given dose. The yield of micronuclei was scored 72 h after irradiation and ranged from 1.6% in the control sample to 8.9% in a 1-Gy sample and 13.9% in a 6-Gy sample. Since only two doses were studied, it is difficult to rule out whether the results are in linear dependence. The first test with DSBs revealed a significant difference in the DSB yield between unirradiated and irradiated cells. There is also a visible difference in the DSB yield between the cells irradiated with 1 Gy and those irradiated with 6 Gy. In spite of the fact that only one-third to one-fourth of the cells in the dish had been irradiated, many more cells showed DSBs. However, all these observations are preliminary, and at the current stage of experiment they are only qualitative.

It remains unclear whether there is any direct relationship between micronucleus formation and DSB numbers. Such a dependence could allow a cross-check of the results and/or estimations based on observation of only one of these factors. Nevertheless, both of them showed an increase with proton dose. In evaluations of cell survival, propidium iodide and Hoechst staining did not appear to be sensitive enough to determine the difference in cell survival, apoptosis and necrosis for the different doses. The results did not show a correlation between the number of dead cells in the dish and the dose of proton radiation. A colony-forming assay will be used in the future to study cell survival and DNA end-labeling to analyze apoptosis.

The results obtained show that the irradiation facility has reached the routine operation stage. Further irradiations are planned to increase the statistical significance of the data to investigate more proton doses and to develop and expand more biological tests.

Acknowledgment

This study was supported by the project CELLION of the EU 6th Framework Programme, MRTN-CT-2003-503923.

References

1. O. Veselov, J. Lekki, W. Polak, D. Strivay, Z. Stachura and J. Styczen, The recognition of biological cells utilizing Quantitative Phase

Microscopy system. *Nucl. Instrum. Methods Phys. Res. B* **231**, 212–217 (2005).
2. R. J. Albertini, D. Anderson, G. R. Douglas, L. Hagmar, K. Hemminki, F. Merlo, A. T. Natarajan, H. Norppa, D. E. Shuker and A. Aitio, IPCS guidelines for the monitoring of genotoxic effects of carcinogens in humans. *Mutat. Res.* **463**, 111–172 (2000).
3. K. M. Prise, O. V. Belyakov, M. Folkard and B. D. Michael, Studies of bystander effects in human fibroblasts using a charged particle microbeam. *Int. J. Radiat. Biol.* **74**, 793–798 (1998).

Cellular Geometry Modeling for Monte Carlo Microdosimetry

T. Pouthier, H. Seznec, S. Incerti, O. Boissonnade and Ph. Moretto

Centre d'Etudes Nucléaires de Bordeaux-Gradignan, CNRS/IN2P3, Université Bordeaux 1, UMR 5797, Chemin du Solarium, BP 120, 33175 Gradignan Cedex, France

Monte Carlo Microdosimetry for Cellular Irradiation

Microbeams provide a unique opportunity to investigate the radiobiological effects of low doses of ionizing radiation at the cellular level. Since 1998, a single-ion single-cell irradiation facility has been developed at CENBG. This setup is able to deliver in air α particles of a few MeV onto individual cultured cells with a spatial resolution of a few micrometers, allowing subcellular targeting (*1–3*). A computer simulation of this facility based on the Geant4 Monte Carlo toolkit has recently been developed at CENBG (*4*). This simulation allows the prediction of the absorbed dose in the targeted cells, assuming reasonable cellular geometries. Up to now, geometries were rather simple, based on parallelepiped or ellipsoid mathematical volumes (*5*). Using high-resolution confocal microscopy imaging, we are now able to extract realistic geometries that can be directly included as 3D phantoms into the simulation platform.

Protocols

The cellular volumes of several cell lines available at CENBG were determined. The keratinocyte HaCaT, expressing the chimeric recombinant histone GFP-H2B, identified as HaCaT/(GFP-H2B)Tg, the human primary keratinocyte and the IMR 90 fibroblast cell types were plated on a cover glass and were grown in dedicated growing medium supplemented with 10% FCS with 100 μg/ml streptomycin/penicillin at 37°C in a 95% air/5% CO_2 and water-saturated atmosphere. After 4 or 24 h of incubation, the cells were fixed in a 1% PFA solution before immunocytofluorescence treatment with Hoechst 33342 dye (10 m*M*) that would stain cell nuclei and with phalloidin-AF350 (6 U/ml) targeted against F-actin. Cover slips were then mounted in an antifade reagent, glued and stored overnight at −20°C. High-resolution imaging of interphase nuclei and cytoskeleton were acquired by confocal microscopy with a Leica DMR TCS SP2 microscope. Cells were reconstructed in three dimensions using the Leica Confocal Software and data were transferred into the Amira software to create 3D phantoms that could be imported into the Geant4-based simulation.

Results

Nuclear and cytoplasmic cell volumes were observed using high-resolution imaging confocal microscopy. These realistic volumes were included in the Geant4 simulation as voxelized volumes. A first estimation of the absorbed dose in targeted HaCaT/(GFP-H2B)Tg human keratinocyte nuclei after α-particle irradiation showed a strong dependence of the dose on the nucleus geometry obtained after 4 h or 24 h of incubation. Plating protocols could be adjusted as a consequence.

Conclusion

These preliminary data demonstrate that the Geant4-based simulation in combination with 3D confocal microscopy techniques is suitable to estimate the absorbed dose in irradiated cells. We plan to identify inner cellular volumes more precisely using different subcellular markers. In addition, the new CENBG nanobeam line will soon bring new insight on cell density and elemental chemical composition (STIM, RBS, PIXE) at the voxel level, allowing even more realistic modeling of cellular geometries for Monte Carlo simulations.

Acknowledgment

This study is partially supported by CELLION project, MRTN-CT-2003-503923.

References

1. C. Michelet, Ph. Moretto, Ph. Barberet, A. Balana, R. K. Dutta and P. Aguer, A focused microbeam for targeting cells with counted multiple particles. *Radiat. Res.* **158**, 370–371 (2002).
2. Ph. Moretto, C. Michelet, A. Balana, Ph. Barberet, W. Przybylowicz, J. P. Slabbert, V. Prozesky, C. Pineda and F. Lhoste, Development of a single ion irradiation system at CENBG for applications in radiation biology. *Nucl. Instrum. Methods Phys. Res. B* **181**, 104–109 (2001).
3. Ph. Barberet, A. Balana, S. Incerti, C. Michelet-Habchi, Ph. Moretto and T. Pouthier, Development of a focused charged particle microbeam for the irradiation of individual cells. *Rev. Sci. Instrum.* **76**, 015101 (2005).
4. S. Incerti, Ph. Barberet, R. Villeneuve, P. Aguer, E. Gontier, C. Michelet-Habchi, Ph. Moretto, D. T. Nguyen, T. Pouthier and R. W. Smith, Simulation of cellular irradiation with the CENBG microbeam line using Geant4. *IEEE Trans. Nucl. Sci.* **51**, 1395–1401 (2004).
5. S. Incerti, N. Gault, C. Habchi, J. L. Lefaix, Ph. Moretto, J. L. Poncy, T. Pouthier and H. Seznec, A comparison of cellular irradiation techniques with alpha particles using the Geant4 Monte Carlo simulation toolkit. *Radiat. Prot. Dosim.,* in press.

Update on Incorporating No-Stain Imaging into Microbeam Endstation

G. J. Ross, B. Ponnaiya, A. W. Bigelow, G. Randers-Pehrson and D. J. Brenner

Center for Radiological Research, Columbia University, New York, New York

Two techniques for rapid location and targeting of cells for microbeam irradiation without use of stain have been added to the microbeam endstation and have undergone continued testing (*1*): (1) quantitative phase microscopy (QPm) and (2) an interim, test version of a novel immersion-based Mirau interferometry (IMI) lens. Both approaches accommodate our requirement, due to the location of the incoming ion beam, of using reflected light microscopy (*2*).

With QPm, reflected light-based images are obtained in focus and with the focus set slightly above and below the sample plane. These images are then used to approximately solve the light transport equation using the Fourier transform-based software from Iatia (*3, 4*). The results are used to create a new 2D map of the sample that is then fed back into the custom microbeam irradiation software. The additional processing time required to convert the raw images into usable images only adds 10% to the time the dish spends on the endstation. While the parameters used for obtaining the approximate solution to the light transport equation are optimized by the operator, there can still be dishes that are not successfully imaged by this method. Several variables have been isolated to determine the cause or causes, including plating time, cell type, cell phase, light color, cell growth surface, amount of medium (depth), percentage of medium and buffer, and use of a cover slip. All of these tests found no correlation to image quality. Continued efforts are now aimed at finding a combination of these variables that may affect the images and at exploring other variables that have not yet been considered.

The immersion-based Mirau interferometric objective is under con-

struction and has been designed to function as an immersion lens with standard interferometric techniques using a short coherence length (*1*) and to otherwise accommodate the endstation requirements at the Columbia University microbeam at RARAF. The preliminary results in air on 10-μm polystyroid beads were sufficiently encouraging to warrant the efforts to design the new objective. As part of the testing for the design process, we modified an off-the-shelf Mirau objective such that it served as a water immersion lens, and we confirmed that the two equal-arm light pathways will indeed be restored and will then provide interference fringes in the environment with sufficient contrast to perform the biological experiments.

In comparing the two techniques, IMI is slightly faster than QPm as it adds about 5–8% to the time the dish spends on the endstation. Immersion-Mirau interferometry is currently reliable in detecting the cells and has a low count of false positives (none in approximately 100 cells imaged) according to the preliminary, interim-lens testing. QPm is a software solution and does not require introduction of fluids or cleaning, whereas immersion-Mirau interferometry does. QPm does not require any additional equipment and can work in air, while the immersion-Mirau interferometer requires the use of a custom objective and an immersion-based approach. It appears likely that the immersion-Mirau approach will ultimately be favored, but additional work will be done, especially on the QPm reliability.

References

1. G. J. Ross, A. W. Bigelow, G. Randers-Pehrson, C. C. Peng and D. J. Brenner, Phase-based cell imaging techniques for microbeam irradiations. *Nucl. Instrum. Methods Phys. Res. B* **241**, 387–391 (2005).
2. G. Randers-Pehrson, C. Geard, G. Johnson, C. D. Elliston and D. J. Brenner, The Columbia University single-ion microbeam. *Radiat. Res.* **156**, 210–214 (2001).
3. A. Barty, K. A. Nugent, D. Paganin and A. Roberts, Quantitative optical phase microscopy. *Optics Lett.* **23**, 817–819 (1998).
4. E. D. Barone-Nugent, A. Barty and K. A. Nugent, Quantitative phase-amplitude microscopy. I. Optical microscopy. *J. Microsc.* **206**, 194–203 (2002).

SESSION 4: MICROBEAM STATUS REPORTS

Chair: Hans Bichsel

Radiobiological Experiments at the Munich Microprobe SNAKE

A. A. Friedl,[a] G. A. Drexler,[a] M. Deutsch,[a] H. Strickfaden,[b] S. Dietzel,[b] T. Cremer,[b] A. Hauptner,[c] R. Krücken,[c] C. Greubel,[d] V. Hable[d] and G. Dollinger[d]

[a]Radiobiological Institute and [b]Biology Department II, University of Munich, Munich, Germany; [c]Physics Department E12, Technical University of Munich, Garching, Germany; and [d]Applied Physics and Metrology, LRT2, Bundeswehr University, Neubiberg, Germany

The ion microprobe SNAKE (Superconducting Nanoscope for Applied Nuclear Experiments) at the Munich 14 MV tandem accelerator has been used for a variety of radiobiological experiments since its adaptation for irradiation of cells in 2003 (*1*). The system can make use of a broad range of ions and ion energies, from 28 MeV protons to 250 MeV gold ions, thus covering an LET range from 2 keV/μm to several MeV/μm. Ions are focused by a superconducting quadrupole doublet to achieve a beam spot size of <500 nm (FWHM). A scanning unit, coupled with an ion detector placed behind the cell sample, allows targeting single ions in pre-programmed spatial patterns. So far, two types of irradiation setup have been used to study cellular response: (1) Cells are placed perpendicular to the horizontal beam and irradiated in geometric patterns. (2) Cells are placed at a 10° angle and a single-ion beam is scanned to achieve a regular irradiation pattern. After irradiation and postirradiation incubation, the cells are fixed and the accumulation of proteins or protein modifications in the vicinity of damaged chromatin regions is visualized by indirect immunofluorescence. Here we give an overview of radiobiological experiments currently performed, preliminary results, and future plans.

Experimental Methods

For the first setup (cells perpendicular to beam), HeLa cells are grown in specially designed cell chambers that consist of stainless steel plates between which 6-μm Mylar foils are clamped (*2*). During irradiation, this cell chamber is placed in an upright position and the cells in the irradiation window are not covered by medium, except for a thin medium layer that remains attached to the cells. In this position, medium collected at the bottom of the chamber provides a saturated atmosphere. Typically, the samples remain in this upright position for maximally 15 min during sample positioning and irradiation. We did not observe any indications for stress response reactions caused by this treatment. After irradiation, the medium is replaced by fresh, prewarmed medium, and the chamber is incubated in a 37°C, 95% air/5% CO_2 incubator. For irradiation at a small angle, a 6-μm Mylar foil is clamped between two stainless steel rings to form the bottom of a round chamber. For most experiments, the medium remains during irradiation, but it is also replaced by fresh medium after irradiation.

Under normal conditions, HeLa cells adhere strongly enough to the Mylar foil that cell loss during subsequent handling is negligible. In some applications, however, such as cell synchronization or pre-extraction of soluble proteins before fixation, stronger adherence is desirable. We therefore routinely treat Mylar foils with CellTak (BD Bioscience, 1 μg/cm^2) prior to cell seeding. Fixation of cells after irradiation and indirect immunofluorescence were described (*1*). For microscopy, first a round cover glass is mounted with Vectashield anti-fading solution (Vector Laboratories). Then the Mylar foil adhering to the cover glass is cut from the cell chamber, using specifically modified soldering tools, and the foil-cover glass sandwich is mounted on a glass slide and sealed using nail polish.

Experiments Performed at SNAKE

For irradiation in geometric patterns, the cell chamber is placed perpendicular to the beam and single ions are applied, e.g., a matrix-like pattern, where individual hits are separated by 6 μm in both directions (*x,y*), or a line pattern, where individual hits are separated by 1 μm in the *x* direction (thus forming a line) and 6 μm in the *y* direction. A major application of this setup is the study of the mobility of damaged chromatin over time after irradiation in a line pattern (*3*). Cells are fixed at various times after irradiation, and damaged chromatin is visualized by immunofluorescence detection of γ-H2AX. The positions of the γ-H2AX foci after incubation are related to the original irradiation pattern to obtain a function of mobility over time. Preliminary data show that this mobility is compatible with a diffusion process. Currently, we are investigating the dependence of the diffusion coefficient on damage density, cell cycle position, and the presence of certain genes. The same irradiation setup can also be used to determine how focus sizes change during postirradiation incubation. The first data hint at a complex time course, with an initial increase followed by a sharp decrease and a subsequent plateau phase. Currently, we are investigating the genetic requirements determining this time course.

Another major application of geometric irradiation is in investigating whether cellular response mechanisms are altered by prior irradiation. If, for example, cells are first irradiated in a horizontal line pattern and then, after incubation for a certain period, in a vertical line pattern, foci originating from the two irradiation treatments can be differentiated by their locations. Geometric irradiation patterns may also be helpful in differentiating targeted, radiation-induced reactions from untargeted or spon-

taneous reactions. This holds especially in situations where damage-related signals are not very distinctive or when the loss of a signal (e.g., a certain histone modification) in the vicinity of damaged chromatin is being investigated.

Irradiation at a small angle was inspired by work of Gisela Taucher-Scholz and coworkers at GSI, Darmstadt. This setup is useful if enhanced microscopic resolution along the track is desired, e.g., when investigating how the number of foci along a track depends on damage density. Clustering of foci during repair incubation renders a quantitative evaluation of the focus numbers difficult, since it is affected by the definition of a focus (macrostructure or microstructures) and by the image processing parameters. We are currently testing a new evaluation procedure that is based on determination of the number of structures formed by interconnecting voxels as a function of the fluorescence intensity thresholds applied.

Conclusion and Future Plans

In its present configuration, the microbeam facility SNAKE is used for a variety of experiments, some of which have only become possible using the geometric irradiation setup. We are currently extending the range of experiments possible at SNAKE by integrating a live-cell imaging facility.

Acknowledgments

Radiobiological experiments at SNAKE are supported by grant Str.Sch.4450 of the Bundesamt für Strahlenschutz and grant 02S8264 of the Bundesministerium für Bildung und Foschung to AAF, by Eurodyna grants of the European Science Foundation to AAF, TC and GD, and by the Maier Leibnitz Laboratorium of the TU Munich and the University of Munich. We thank the technical staff of the Munich tandem accelerator.

References

1. A. Hauptner, S. Dietzel, G. A. Drexler, P. Reichart, R. Krücken, T. Cremer, A. A. Friedl and G. Dollinger, Microirradiation of cells with energetic heavy ions. *Radiat. Environ. Biophys.* **42**, 237–245 (2004).
2. G. Dollinger, V. Hable, A. Hauptner, R. Krücken, P. Reichart, A. A. Friedl, G. Drexler, T. Cremer and S. Dietzel, Microirradiation of cells with energetic heavy ions. *Nucl. Instrum. Methods Phys. Res. B* **231**, 195–201 (2005).
3. V. Hable, G. Dollinger, C. Greubel, A. Hauptner, R. Krücken, S. Dietzel, T. Cremer, G. A. Drexler, A. A. Friedl and R. Löwe, Methods for quantitative evaluation of dynamics of repair proteins within irradiated cells. *Nucl. Instrum. Methods Phys. Res. B,* in press.

New Capabilities and Experimental Programme of the PTB Microbeam

Klaus Greif,[a] Ulrich Giesen,[a] Ferya Banaz-Yasar,[b] Alexandra Gellhaus,[b] Maria Gomolka,[c] Ute Rößler[c] and Dieter Frankenberg[a]

[a]Physikalisch-Technische Bundesanstalt, Bundesallee 100, D-38116 Braunschweig, Germany; [b]Institute of Anatomy, University Hospital Essen, Hufelandstraße 55, D-45122 Essen, Germany; and [c]Bundesamt für Strahlenschutz, Ingolstädter Landstraße 1, D-85764 Oberschleißheim, Germany

At the PTB ion accelerator laboratory, a charged-particle microbeam optimized for radiobiological research has been in routine operation since 2002 (*1*). An important feature of this PTB facility is the wide energy range available for protons (up to 20 MeV) and α particles (up to 25 MeV). Thus the PTB microbeam covers an LET of 3–200 keV/μm and allows the investigation of radiation effects in the low- and high-LET domains. The spatial confinement of the beam is done by focusing, and a beam diameter of approximately 2 μm (FWHM) is typically achieved. Recently, an electrostatic scanning device has been added to the facility that allows the targeting of each cell within a few milliseconds. This and other improvements led to an increase in the experimental speed of the system, including all experimental steps such as scanning the dish and cell recognition procedures, to a maximum of 50,000 cells per hour.

The capabilities of the facility have been further improved by a customized software module for the automatic quantification of immunocytochemical staining. This allows the measurement of protein activation for each individual cell, including the positional information of the irradiation. Thus the signals of irradiated and unirradiated cells on the same dish can be measured separately and the signal of bystander cells could, for instance, be correlated to the distance from the next irradiated cell. The module accomplishes the effective removal of artifacts and an appropriate image enhancement and guarantees a quick and unbiased protein quantification.

The module described is used to investigate the effects of gap junctional communication in mediating radiation-induced bystander effects on short time scales. The expression of TP53 is measured by immunofluorescence as a marker for the induction of bystander effects 15 min after targeting nuclei of selected single cells with different numbers of α particles. The induction of TP53 is an indication of the activation of the G_1 checkpoint and an accepted marker molecule for evaluating radiation-induced cell damage. For the experiments we used a noncommunicating malignant trophoblast cell line, Jeg3, which was stably transfected with the inducible gap junction protein Connexin43.

Another major project investigates the expression of bystander effects in human and rodent cells for high- and low-LET radiation. Primary human skin fibroblasts (HSF) were irradiated with 4.5 MeV α particles (LET = 100 keV/μm) and 10 MeV protons (LET = 4.7 keV/μm). For α particles, an exponential survival curve was obtained and no bystander effect was observed. For protons, a significantly higher survival in the low-dose domain (70 particles corresponding to approximately 300 mGy) was observed for both the 100% irradiation and the 10% irradiation, thus demonstrating a positive bystander effect. At higher doses, the cells did not show any detrimental bystander effect. The results have recently been accepted for publication (*2*). The experiments are currently being continued with Chinese hamster ovary cells (CHO). We use the wild-type AA8 and the mutant lines V3 and irs1-SF, which are deficient in NHEJ and HR, respectively. Preliminary data show that, in contrast to the HSF results, the cells exhibit no positive bystander effects with low doses of protons. Additionally, a cell line-dependent detrimental bystander effect was found at high doses of protons.

Together with the German Federal Institute for Radiation Protection (BfS—Bundesamt für Strahlenschutz), the PTB has just started experiments at various energies, using the alkaline comet assay as an end point. This assay provides an excellent method to detect direct DNA damage and its subsequent repair at the single-cell level. Our primary goal is to correlate the DNA hits with the resulting DNA damage in human lymphocytes and cells of a gastric cancer cell line (HSC45-M2) for several radiation qualities. The resulting dose–response relationship can then be used as a calibration curve, for example for DNA damage induced by radioactively labeled antibodies used in medical treatments. Further goals are the investigation of repair processes and the detection of possible bystander effects.

References

1. K-D. Greif, H. J. Brede, D. Frankenberg and U. Giesen, The PTB single ion microbeam for irradiation of living cells. *Nucl. Instrum. Methods Phys. Res. B* **217**, 505–512 (2004).
2. D. Frankenberg, K. Greif and U. Giesen, Radiation response of primary human skin fibroblasts and their bystander cells after exposure to counted particles at low and high LET. *Int. J. Radiat. Biol.,* **82**, 59–67 (2006).

Update and Performance of the Scanning Ion Microprobe at GSI

M. Heiß,[a] B. E. Fischer,[a] Ph. Barberet,[a] G. Du,[a] B. Jakob,[b] G. Becker[b] and G. Taucher-Scholz[b]

[a]Materials Research and [b]Biophysics, Gesellschaft für Schwerionenforschung (GSI), 64291 Darmstadt, Germany

Introduction

The possibility to place a single ion or a counted number of ions precisely into a selected living cell makes ion microprobes an interesting tool for fundamental studies in radiation biology, like the analysis of the sensitivity of subcellular targets or the radiation response of cells not directly hit, a phenomenon called the bystander effect.

Since 2003, these kinds of experiments can also be carried out at the focusing heavy-ion microprobe at GSI. Since there are almost no scattered ions in this focused microprobe compared to collimated beams (*1, 2*), it offers the advantage of a better-defined LET, smaller beam spots, and therefore potentially higher aiming accuracy. Additionally the beam can be deflected rapidly from cell to cell and therefore, compared to stationary beams where the cells have to be moved into the focus, a higher throughput can be reached. Furthermore, at this microprobe, it is possible to work with ions from helium to uranium with energies up to 11.4 MeV/nucleon, and therefore a broad range of LET inside the cells can be used.

This abstract gives an overview on the latest improvements to the facility and the performance of the setup.

Technical Advances

The main issue affecting the aiming precision was variations in temperature. Heat, mainly generated by the heat of the UV lamp, caused thermal expansions of the setup and therefore slowly increasing targeting inaccuracies, which made frequent readjustments of the irradiation settings necessary. To prevent this, the whole irradiation area was temperature stabilized, the microscope lamp was thermally isolated from the setup, and a temperature-controlled fan was installed that blows cool prefiltered air into the irradiation chamber. By filtering the air, the sterility of the system could be enhanced, decreasing the risk of contaminating the samples during the irradiation.

A further change that reduced the effect of thermal expansions was to demount the microscope objective from the large optical platform that holds all optical components and to fix it close to the flange that carries the sample holder on a stable mounting that allows its movement for focusing and centering. Thus any thermal displacement of the optical platform will shift only the camera against the 20× magnified image of the sample, and the errors in position measurements are considerably smaller.

In some experiments, such as the irradiation of densely seeded cells, it is desirable to be able to change the magnification of the microscope during the investigation of the sample. In this way, a fast cell finding can be done in an overview mode while the positioning of the beam is done with higher precision. To achieve this, an inverted telescope has been built that can be placed into the light path of the microscope to temporarily decrease its magnification without affecting the targeting accuracy of the 20× objective.

Further updates have been made in the development of the microscope used for cell detection. Since it is possible to illuminate the sample through the vacuum window, a high-intensity white LED was placed behind it, allowing transmitted light microscopy. Additionally, a second LED was positioned off axis in a transition region between bright-field and dark-field illumination to get a simple phase-contrast image.

To test the precision of the beam deflection over the whole optical field of view, a method for a fast online aiming verification was developed. A thin copper microgrid and an energy-resolving particle detector are placed at the sample position. After an automatic recognition of the grid, single ions are targeted onto its bars. All accurately targeted particles have to traverse the copper and will reach the detector with reduced energy while misplaced ions reach the detector with full energy. By plotting the coordinates of the ions with full energies, the areas of misaligned particles can easily be visualized.

To verify targeting precision inside the cells, the ion tracks were visualized by immunocytochemical staining of DNA damage response proteins (e.g. 53BP1), which are known to accumulate as foci at sites of DNA lesions (*3*). To easily distinguish tracks from background foci, the ions were placed in cross patterns. The irradiation accuracy was then estimated by calculating the differences between the barycenter of the crosses and the barycenter of the cell nuclei that were targeted with the cross. The result after evaluating 30 cells was a misalignment of only 1.34 μm ± 0.67 μm between these two positions.

The same immunostaining technique was applied to estimate the maximum focal diameter of the beam in the fibroblast cell nuclei after irradiation with a 4.8 MeV/nucleon carbon-ion microbeam. For this purpose, the crosses were written by either one or 20 ions per point. While the one-hit spots had an average diameter of about 1.1 μm, the spot size increased for the 20-hit spots to roughly 1.8 μm (100 spots analyzed). From these data we conclude that all of the 20 ions per spot were accurately placed in an area with a diameter of about 1 μm.

Conclusions

The technical advances at the heavy ion microprobe at GSI improved its performance, allowing a targeted irradiation of cells with a precision better than 2 μm.

Acknowledgment

This work was partly supported by EU Grant CELLION MRTN-CT-2003-503923.

References

1. M. Folkard, B. Vojnovic, K. M. Prise, A. G. Bowey, R. J. Locke, G. Schettino and B. D. Michael, A charged-particle microbeam: I. Development of an experimental system for targeting cells individually with counted particles. *Int. J. Radiat. Biol.* **72**, 375–385 (1997).
2. G. Randers-Pehrson, C. R. Geard, G. Johnson, C. D. Elliston and D. J. Brenner, The Columbia University single-ion microbeam. *Radiat. Res.* **156**, 210–214 (2001).
3. M. Heiß, B. E. Fischer, B. Jakob, C. Fournier, G. Becker and G. Taucher-Scholz, Targeted irradiation of mammalian cells using a heavy-ion microprobe. *Radiat. Res.* **165**, 231–239 (2006).

The LPS Saclay Single-Ion Microbeam Facility

H. Khodja, L. Daudin, M. Hanot, J. Hoarau, M. Carrière and B. Gouget

Laboratoire Pierre Süe, CEA-CNRS UMR9956, CEA Saclay, 91191 Gif sur Yvette, France

Introduction

The LPS microbeam facility is based on a KN3750 Van de Graaff accelerator devoted to microbeam analysis (*1*). It is equipped with two horizontal microbeam lines used in various fields such as material science, geological science, nuclear material science and biology. Research conducted at the laboratory in biology are focused on heavy-metal toxicity in cultured cells. Uranium, as a heavy metal, induces both a chemical and a radiological toxicity. To study this toxicity locally, the decision was made in spring 2004 to build a setup for performing single-ion irradiation at controlled doses and locations.

Experimental Setup

The facility was designed with the following guidelines:

1. The irradiation direction was chosen as vertical, to offer a convenient and fast access, without the usual requirement of cell or culture medium transfers in the case of a horizontal beam. Thus a 90° bending magnet was inserted in one of the two beamlines, with a 0° exit port allowing beam transport to the analysis chamber when required.
2. The microbeam is produced at the exit of the 90° bending magnet by using a collimator rather than a focusing unit. Obviously microbeam performances using focusing lenses are better under vacuum than collimating slits or capillaries but are strongly deteriorated by window, air gap traversals, detector and cell dish bottom. Our optical arrangement optimizes the current density close to the exit of the bending magnet by adopting an object definition plane far from the bending magnet entrance port. The irradiation plane is close to the exit port and no extra building is required at all.
3. To compensate for the fact that a collimator arrangement was chosen, thus limiting the throughput by the mechanical performances of the *XY* culture dish stage, a piezo actuator stage will be used to place the collimator promptly under the selected cells. This arrangement will considerably enhance the irradiation speed.
4. Other parameters are similar to those found on single-ion microbeam setups. A fluorescence *in situ* microscope (Olympus BX FM) is mounted on an anti-vibration table surrounding the exit port. It is equipped with a CCD camera (Roper Scientific), and images are acquired using Image Pro Plus software. Beam extraction is performed using a 150-nm Si_3N_4 window, and culture dishes are based on standard plastic petri dishes with a 100-nm-thick Si_3N_4 insert. Ion detection is performed using a photomultiplier tube (Hamamatsu R7400P) collecting photons emitted by a 9-m BC400 foil inserted between the exit window and the culture dish. When a predefined number of ions have been counted, a fast signal triggers a high-voltage amplifier (Technishes Büro Fisher) connected to an electrostatic shutter.

Results and Discussion

Extracted beam properties were evaluated by using CR39 nuclear track detectors and a silicon surface barrier detector. CR39 images gave an estimate of the lateral straggling, and the diode was used to measure the energy straggling. Both effects are mainly due to ion scattering on the inner wall of the collimator and are very sensitive to alignment (K. J. Hollis, Microbeam design in radiobiological research. Ph.D. thesis, Brunel University, 1995). Several arrangements were tested using electron microscopy collimators (down to 30 μm diameter) or fused silica capillaries (down to 1 μm inner diameter). Optimal arrangement was found using a 1-mm-long 5-μm-inner-diameter silica capillary. We obtained a high-quality beam (90% of the particles have the expected energy and 97% were found in a 10-μm-diameter circle).

Living cell irradiations were performed with cells of the ROS 17/2.8 cell line (osteoblast-like bone cells originating from a rat osteosarcoma cell clone). The 3 MeV extracted α-particle beam intensity was reduced to a few ions per second, and the petri dish seeded with cells at 50% confluence was placed over the exit window on different locations, thus covering a cumulative area limited to 1% of the Si_3N_4 insert. We expect that a similar fraction of the cell population was effectively irradiated. Each irradiated cell received approximately 30 ions during this experiment, inducing a dose deposition estimated to be 3 Gy/cell. The end point investigated was the induction of reactive oxygen species (ROS) by radiation. ROS were detected using the fluorescent probe CM-H_2DCFDA (Molecular Probes) and compared to the cell distribution, estimated using Hoechst 33258 stain (*2*). It was found that ROS expression of cells from the irradiated dish was twofold higher than that of cells from a sham-irradiated dish.

Future work will focus on fast cell recognition and irradiation at lower doses.

Acknowledgment

This work is partially supported by Conseil Général de l'Essonne.

References

1. H. Khodja, E. Berthoumieux, L. Daudin and J. P. Gallien, The Pierre Süe Laboratory nuclear microprobe as a multi-disciplinary analysis tool. *Nucl. Instrum. Methods Phys. Res. B* **181**, 83–86 (2001).
2. C. Shao, M. Folkard, B. D. Michael and K. M. Prise, Bystander signaling between glioma cells and fibroblasts targeted with counted particles. *Int. J. Cancer* **116**, 45–51 (2005).

Current Status of Heavy-Ion Microbeams at JAEA-Takasaki

Y. Kobayashi,[a,d] T. Funayama,[a] T. Sakashita,[a] S. Wada,[a] Y. Yokota,[b] T. Kakizaki[a,c] and N. Hamada[a,d]

[a]Microbeam Radiation Biology Group, and [b]Gene Resource Research Group, Japan Atomic Energy Agency (JAEA), 1233 Watanuki-machi, Takasaki, Gunma 370-1292, Japan; [c]Laboratory of Veterinary Radiology and Radiation Biology, Department of Veterinary Medicine, Kitasato University Graduate School of Veterinary Medicine and Animal Sciences, 35-1 Higashi-nijuu-san-ban-cho, Towada, Aomori 034-8628; and [d]Department of Quantum Biology, and The 21st Century Center of Excellence (COE) Program, Gunma University Graduate School of Medicine, 3-39-22 Showa-machi, Maebashi, Gunma 371-8511, Japan

We have upgraded the Japan Atomic Energy Agency (JAEA) single-cell irradiation system (*1, 2*), which allows selected cells to be hit individually with a defined number of heavy charged particles. The system has been incorporated into the collimated heavy-ion microbeam apparatus, which was installed below a vertical beam line of the azimuthally varying field (AVF) cyclotron at the Takasaki Ion accelerators for Advanced Radiation Application (TIARA) of the JAEA-Takasaki. The collimated heavy-ion beams are extracted into air through a microaperture on a 100- or 200-μm-thick tantalum disk perforated using an electrical discharge machining (spark erosion) method. The smallest microaperture, 5 μm in diameter on a 100-μm-thick disk, was used to cell irradiate cells with a precise number of 11.5 MeV/nucleon ^{40}Ar and 13.0 MeV/nucleon ^{20}Ne ions, and a microaperture 20 μm in diameter on a 200-μm-thick disk was used for 17.5 MeV/nucleon ^{20}Ne-ion and 18.3 MeV/nucleon ^{12}C-ion irradiation.

This system has been developed to study radiobiological processes in hit cells and bystander cells exposed to low-dose and low-dose-rate high-LET radiations in ways that cannot be achieved using conventional broad-field exposures (*3*). Individual cultured cells grown in special dishes were irradiated in air with a single or defined numbers of heavy ions. However, the targeting accuracy and overall irradiation throughput should be improved to carry out further complicated analyses of the effect of high-LET ions. Therefore, two points of the system were recently upgraded.

First, we have replaced the sample positioning microscope stage used previously with a BIOS-213T (Sigma Koki, Co., Ltd., Tokyo, Japan). The procedure for irradiating cultured cells with microbeams contains many steps: cell-image acquisition and processing, setting of fiducials, automatic stage movement, and irradiation with counted ions. Almost all these steps contain an event that contributes to the targeting errors. Among these steps, the automatic stage movement is the most frequent action during the whole irradiation process, and it affects the overall targeting accuracy. The improvement of cell targeting accuracy was measured between the previous and new automatic stage by irradiating cells with five ^{40}Ar ions. The samples irradiated using the previous stage included more than 25% unhit cells. The distribution of ion hits with the new stage indicated that 70% of the cells were irradiated with three to five ions and less than 5% of the cells remained unhit.

Second, the focus-control unit of the cell targeting system has been

replaced and the microscope-stage driver software has been improved. The new focus-control unit consists of a stepping motor (1000 pulses = 1 rotation = 100 μm focus movement) and its controller, jog-dial control pad with full remote control function, and optical upper and lower limit sensor. The stage driver software was modified for the new unit. Before this improvement, we inserted a waiting code to make stage movement stable, because occasional instability (software hanging up, etc.) was observed with the previous hardware configurations. With the insertion of the waiting code, the instability of system, which was mainly caused by instability of the previous focus unit, was decreased. However, the movement of the microscope stage was slower because of the architecture of the combined control of both *X-Y* sample stage and focus control unit in stage driver software. To verify the effects of the improvement, the movement speed of the stage using both the previous driver and the improved driver was measured with an online microscope system. The overhead time of the driver software with a single stage action was reduced markedly from 1.37 s to 0.62 s due to the deletion of the waiting code.

Besides bystander effect studies using Chinese hamster ovary (CHO-K1) cells (*2*) and normal human foreskin fibroblast AG01522 cells (*4, 5*), radiobiological studies using tobacco BY-2 protoplasts (*6*) and germline cells of the nematode *Caenorhabditis elegans* (*7*) are in progress.

Acknowledgments

This work was supported by a grant from the Ministry of Education, Culture, Sports, Science and Technology, Japan. Part of this study was financially supported by the Budget for Nuclear Research of the Ministry of Education, Culture, Sports, Science and Technology, based on the screening and counseling by the Atomic Energy Commission of Japan.

References

1. Y. Kobayashi, T. Funayama, S. Wada, M. Taguchi and H. Watanabe, System of cell irradiation with a precise number of heavy ions. *Radiat. Res.* **161**, 90–91 (2004). [extended abstract]
2. T. Funayama, S. Wada, Y. Kobayashi and H. Watanabe, Irradiation of mammalian cultured cells with a collimated heavy-ion microbeam. *Radiat. Res.* **163**, 241–246 (2005).
3. Y. Kobayashi, T. Funayama, S. Wada, Y. Furusawa, M. Aoki, C. Shao, Y. Yokota, T. Sakashita, Y. Matsumoto and N. Hamada, Microbeams of heavy charged particles. *Biol. Sci. Space* **18**, 235–240 (2004).
4. C. Shao, Y. Furusawa, Y. Kobayashi, T. Funayama and S. Wada, Bystander effect induced by counted high-LET particles in confluent human fibroblasts: A mechanistic study. *FASEB J.* **17**, 1422–1427 (2003).
5. Y. Furusawa, M. Aoki, C. Shao, Y. Kobayashi, T. Funayama, T. Sakashita and S. Wada, Development of irradiation procedure to detect distance the signal transfer of GJIC bystander effect. *JAERI Rev.* **2004-025**, 88–90 (2004).
6. Y. Yokota, T. Funayama, Y. Kobayashi, T. Sakashita, S. Wada, Y. Hase, N. Shikazono, A. Tanaka and M. Inoue, Development of an ion microbeam system for irradiation single plant cell[s]. *Biol. Sci. Space* **17**, 298–601 (2003).
7. T. Sugimoto, K. Dazai, T. Sakashita, T. Funayama, S. Wada, N. Hamada, T. Kakizaki, Y. Kobayashi and A. Higashitani, Cell cycle arrest and apoptosis in *Caenorhabditis elegans* germline cells following heavy-ion microbeam irradiation. *Int. J. Radiat. Biol.* **82**, 31–38 (2006).

Status of the New Single-Ion Hit Facility for Irradiation of Living Cells at LIPSION

C. Nilsson, S. Petriconi, T. Reinert and T. Butz

Faculty of Physics and Geosciences, University of Leipzig, Linnéstrasse 5, 04103 Leipzig, Germany

Introduction

At the LIPSION nanoprobe laboratory, single-ion irradiation experiments on single living cells have been carried out since 2003. Previous cell irradiation experiments include patterned irradiations of HeLa cells and primary fibroblasts with a low number of protons and α particles (*1, 2*). Biological end points include changes in the rate of apoptosis and radiation-induced DNA double-strand breaks. This is a report on the current status of the new single-ion hit facility (SIHF), an upgrade that will allow for truly targeted cell irradiation.

The LIPSION Nanoprobe Laboratory

The LIPSION laboratory consists of a 3.5 MV Singletron™ accelerator with a horizontal beam line where H^+ or He^+ ions are accelerated to energies up to 3 MeV (*3*). The cell irradiation experiments have been carried out at an energy of 2.25 MeV. Using this system, a focused beam spot size of less than 350 nm in air can be achieved. Due to the horizontal orientation of the beam line, a vertical petri dish arrangement is required, and such an arrangement has been successfully implemented and tested at the facility.

New Developments Regarding the Beam Line

Currently, a major rebuilding of the target chamber is being carried out to increase the versatility and accessibility of the nanoprobe. The old target chamber, a system of cylinders and flanges, which has been part of the setup since the facility became operational in 1998, will be replaced by a new target chamber that is the shape of a box with a removable top, with the dimensions 450 mm × 300 mm × 480 mm. The new chamber will be equipped with a new translation stage as well as with a separate irradiation platform for the irradiation of single, living cells with single ions. The implementation of the new chamber is planned for the second quarter of 2006.

The new seven-axis translation stage with goniometer has been custom-manufactured (Feinmess Dresden, Germany). It is movable in the *x, y* and *z* directions as well as in the θ, *x, y′* and φ directions (the goniometer will be needed, e.g., for STIM tomography and channeling experiments). The translation part consists of two piezo motors that control the horizontal motion and the motion in the axial (beam) direction and one stepper motor that controls the vertical motion. Initial tests indicate that a positioning accuracy and repeatability of about 1 μm can be achieved for this stepper motor-controlled axis. The rotation part consists of four piezo motors that control rotation in two axes as well as additional horizontal and vertical motion.

New Developments Regarding the Cell Irradiation

To enable irradiation of living cells, one key issue is to extract the beam into air through a vacuum window. In the case of the LIPSION SIHF, this extraction will be realized by attaching an exit nozzle to the beam entrance in the chamber wall.

This solution is space saving and allows not only for cell irradiation experiments but also for other kinds of in-air ion beam analysis, such as PIXE investigations of archeological samples. The end piece of the nozzle is exchangeable and can be made either of stainless steel, to be used for cell irradiation experiments, or of aluminum, for PIXE measurements.

The exit window on the nozzle is a 100-nm-thick Si_3N_4 vacuum window with an area of 1 × 1 mm^2, which has proven to withstand the pressure difference well. Other new vacuum windows that will be tested are ones that are 50 nm thick as well as circular windows.

The new irradiation platform will consist of several separate components to ensure maximum flexibility. The integral component is the petri dish holder, a holder for the particle detector, a p-i-n diode that is placed after the Petri dish microscope objectives, and a holder for the microscope eyepiece and the CCD camera.

This combination with a downstream microscope enables online cell recognition. Another possibility is to use fiducial markers on the petri dish itself, thereby allowing recognition of the cells offline. At the LIPSION facility, such fiducial markers could be fabricated using proton beam writing.

Software Development

In parallel with the upgrades of the beam line, software improvements are also under way. These include the development of completely new scan control software that runs in a hard real-time environment under Linux/RTAI. First measurements of response times have given encouraging results, suggesting that beam blanking may be triggered reliably directly from software. The limiting factor to the current system's accuracy appears to be the slow ADC conversion time of 20 μs during which the beam remains unblanked. Various strategies to improve the accuracy are currently being investigated. With an adaptive blanking algorithm, irradiation rates in excess of 200 s^{-1} have been reached without relying on external hardware blanking triggers, and a single-hit accuracy of better than 99% has been observed.

Future development efforts will focus on providing a user-friendly graphical user interface for the scan control as well as for the control of the new translation stage and goniometer. The stage control will run over a network and use the software under development at the division, using C++ and Qt, a C++ class library and application framework. Likewise, cell recognition software will also be developed at the division, using C++ together with the commercially available software package ImagePro Plus. The use of cell recognition software will make automated and/or semi-automated truly targeted cell irradiation possible, as opposed to the predetermined patterns (dots, lines, bands and crosses) that have been used so far.

Acknowledgments

This work was supported by the Marie Curie Research Training Network CELLION, MRTN-CT-2003-503923, under the EU 6th Framework Programme.

References

1. A. Fiedler, J. Skopek, T. Reinert, J. Tanner, J. Vogt, J. Österreicher, L. Navratil and T. Butz, First irradiation experiments with living cells at LIPSION. *Radiat. Res.* **161**, 95–96 (2004). [extended abstract]
2. T. Reinert, A. Fiedler, J. Skopek, J. Tanner, J. Vogt and T. Butz, Single ion bombardment of living cells at LIPSION. *Nucl. Instrum. Methods Phys. Res. B* **219–220**, 77–81 (2004).
3. T. Butz, R-H. Flagmeyer, J. Heitmann, D. N. Jamieson, G. J. F. Legge, D. Lehmann, U. Reibetanz, T. Reinert, A. Saint and J. Zhu, The Leipzig high-energy ion nanoprobe: A report on first results. *Nucl. Instrum. Methods Phys. Res. B* **161–163**, 323–327 (2000).

Biological Validation of the Ion Microbeam Developed at CENBG to Generate Localized Ionizing Radiation-Induced Damage on Keratinocyte Cells Expressing GFP-Tagged Protein

H. Seznec, T. Pouthier, S. Incerti, M. Heiss, Ph. Barberet and Ph. Moretto

Centre d'Etudes Nucléaires de Bordeaux-Gradigan, IN2P3/CNRS, Université Bordeaux 1, Chemin du Solarium, 33175 Gradignan Cedex, France

The CENBG Microbeam Line and the Irradiation Procedure

The CENBG cellular irradiation facility is based on a focused microbeam line that has been described extensively elsewhere (*1, 2*). This setup allows single cell irradiation with precise control of the delivered dose; a predetermined number of α particles can be sent to a selected cell within a population. The layout and irradiation procedure using the microbeam at the CENBG have been presented elsewhere (*1, 2*). Approximately 1500 exponentially growing cells were plated into ''home-made'' microbeam dishes. The DNA content of attached cells was visualized without the use of chemical agents (like Hoechst 33342) but using the transgenic and chimeric fluorescently labeled protein histone GFP-H2B. The position of individual nuclei was determined by optical imaging of the fluorescent staining pattern at $\lambda = 490$ nm. The image analysis system then located the centroid of each nucleus, and the nuclei were irradiated one at a time with an exact number of α particles.

On average, it took less than 90 min to localize and irradiate up to 1500 cells. We used 3×1500 irradiated cells per group per experiment in the present study. The overall spatial precision of the setup is about ±10 μm. Because the average cross-sectional area of the nucleus of live attached HaCaT/(GFP-H2B)tg cells was determined to be 100 μm^2, we estimated by Monte Carlo modeling that the particle beam would hit the target nucleus 97% of the time. The average energy of the α particles after the cell-polypropylene plating foil was 2.37 ± 0.01 MeV (*3*) delivered at a dose rate of about 1000 α particles per second. Due to the lag time of the shutter closure, cells were illuminated during 400 ms. After irradiation, the dish was removed from the stage, and the cells were maintained for 24 h in normal culture.

The HaCaT/(GFP-H2B)tg Transgenic Cell Line

We chose HaCaT cells because they would attach to a surface as a monolayer to ensure reasonably uniform radiation doses over the cell population (*1*). Exponentially growing HaCaT cells were transfected by lipofection with the GFP-H2B expression vector (*1*). After 2 weeks of drug selection (G418, 5 μg/ml), several GFP-positive colonies were isolated using fluorescence-activated cell sorting (FACS). Before irradiation, HaCaT/(GFP-H2B)]tg cells were grown in DMEM supplemented with 10% fetal calf serum with 100 μg/ml streptomycin/penicillin at 37°C in a 95% air, 5% CO_2 and water-saturated atmosphere. The exposure of the cells to α particles was accomplished as follows: 1500 HaCaT/(GFP-H2B)tg cells were plated onto 3.8-μm-thick polypropylene film-bottomed tissue culture dishes and incubated 24 h before exposure to α particles.

Results

We used transfected immortalized HaCaT cells expressing the chimeric recombinant histone GFP-H2B. This GFP-H2B protein is involved in the DNA architecture and precisely localizes the DNA in the cell nucleus. *In vivo*, these cell nuclei are visualized under a visible-light microscope and targeted in full control mode (down to the ultimate dose of one α particle per cell). The behavior of the GFP-H2B protein also allows us to determine the integrity of chromatin and chromosomes and the induction of cell death. Thus we are able to identify dividing cells, genetic instability, and living and apoptotic cell nuclei. This newly established cell line has been characterized to validate its proliferative capacity and the integrity of its cellular response; and no significant differences were found between transgenic and non-transgenic cells. High-resolution images of interphase nuclei were acquired by confocal microscopy with a Leica DMR/TCS/SP2 microscope. In combination with immunocytochemical techniques using antibody targeted against the specific phosphorylated form of the histone H2AX (called γ-H2AX) (*6*), DNA DSBs were analyzed 24 h after irradiation with α particles. Digital monochrome images were collected for each appropriate channel and were analyzed using the Metamorph software. The quantitative analyses were performed in all regions of the nucleus, and the fluorescence intensities in both channels were calculated in the presence of predetermined masks applied to the whole stack of images after filtering of serial acquisition images. Data were acquired from different cells for each double labeling condition (GFP-H2B and γ-H2AX). Discrete foci of γ-H2AX can be seen distributed homogeneously in the whole cell nucleus of nonirradiated control cells. In contrast, in irradiated cells, we have observed an inhomogeneous distribution of intense and bright γ-H2AX foci, indicating a clear increase of DNA DSBs and also suggesting the putative α-particle impacts. We have also observed a correlation between the number of DNA DSBs generated (γ-H2AX foci) and the number of initial incident α particles.

Concluding Remarks

These preliminary data demonstrate that the CENBG microbeam line setup is a suitable tool to investigate the molecular pathways involved in the response to ionizing radiation. We plan to (1) define biological indicators as a function of dose and (2) improve and validate *in silico* biological models of radiation-induced-damage (Monte Carlo simulation).

Acknowledgment

This study is partially supported by CELLION project, MRTN-CT-2003-503923.

References

1. C. Michelet, Ph. Moretto, Ph. Barberet, A. Balana, R. K. Dutta and P. Aguer, A focused microbeam for targeting cells with counted multiple particles. *Radiat. Res.* **158**, 370–371 (2002). [extended abstract]
2. Ph. Moretto, C. Michelet, A. Balana, Ph. Barberet, W. Przybylowicz, J. P. Slabbert, V. Prozesky, C. Pineda, G. Brut and F. Lhoste, Development of a single ion irradiation system at CENBG for applications in radiation biology. *Nucl. Instrum. Methods Phys. Res. B* **181**, 104–109 (2001).
3. S. Incerti, Ph. Barberet, R. Villeneuve, P. Aguer, E. Gontier, C. Michelet-Habchi, Ph. Moretto, D. T. Nguyen, T. Pouthier and R. W. Smith, Simulation of cellular irradiation with the CENBG microbeam line using GEANT4. *IEEE Trans. Nucl. Sci.* **4**, 1395–1401 (2004).
4. P. Boukamp, R. T. Petrussevska, D. Breitkreutz, J. Hornung, A. Markham and N. E. Fusenig, Normal keratinization in a spontaneously immortalized aneuploid human keratinocyte cell line. *J. Cell Biol.* **106**, 761–771 (1988).
5. K. T. Kanda, K. F. Sullivan and G. M. Wahl, Histone-GFP fusion protein enables sensitive analysis of chromosome dynamics in living mammalian cells. *Curr. Biol.* **8**, 377–385 (1998).
6. E. P. Rogakou, D. R. Pilch, A. H. Orr, V. S. Ivanova and V. M. Bonner, DNA double-stranded breaks induce histone H2AX phosphorylation on serine 139. *J. Biol. Chem.* **273**, 5858–5868 (1998).

SESSION 5: DNA REPAIR PROBED WITH MICROBEAMS

Chair: William F. Morgan

DNA DSBs and HSP70 Expression in Proton-Irradiated Living Cells at LIPSION

A. Fiedler,[a,b] T. Reinert,[a] J. Tanner[c] and T. Butz[a]

[a]Faculty of Physics and Earth Science, University of Leipzig, Germany; [b]Faculty of Biology, Pharmacy and Psychology, University of Leipzig, Germany; and [c]Clinic and Polyclinic for Radiation Oncology, University of Halle-Wittenberg, Germany

Introduction

Ionizing radiation can initiate direct and indirect radiation effects in biological systems. One direct effect of ionizing radiation is DNA double-strand breaks. The immunostaining of phosphorylated H2AX (γ-H2AX) visualizes the DNA DSBs as a focus. Our objective was to test the feasibility of using γ-H2AX staining for direct visualization of single proton hits. The system could be used as a ''biological track detector'', replacing the solid-state track detector CR39 for hit verification tests. At this point it was not clear whether single protons would produce detectable foci.

Radiation-produced free radicals *indirectly* damage and denature proteins, which can either get refolded into a functional structure or degraded by the protecting heat-shock protein 70 (HSP70). Ionizing radiation can recruit of HSP70 to special cell compartments and can lead to an overall increased expression of HSP70. However, this effect has been shown mostly for heavy ions and γ and X rays but rarely for proton irradiation (*1–6*). Therefore, we investigated the expression of the cellular stress response protein after focused proton-beam irradiation.

Materials and Methods

The high-energy ion nanoprobe LIPSION at the University of Leipzig supplies H^+ or He^+ ion beams by a 3.5 MV Singletron™ accelerator. The horizontal beam can be focused down to below 50 nm in diameter in the low current mode. The hit accuracy for protons is better than 0.5 μm in air (*7*). However, targeted irradiation at LIPSION is still under development. To easily recognize the irradiated area and the ion hits, specific irradiation patterns with a selected number of ions to each target position were used. A cross pattern, 7 × 7 pixels with a 1-μm distance per cross and an intercross distance of 5 μm, and a line pattern (spacing 4 μm × 2 μm or 6 μm × 3 μm) were applied.

For cell irradiation, 35-mm petri dishes with a Si_3N_4 irradiation window (200 nm thick, 2 mm × 2 mm) were used. The dish can be positioned in front of the beam exit window (Si_3N_4 of 1 mm × 1 mm, 100 nm thick) with a minimal air gap. The energy loss of the ions after transmission through the cells is measured with a PIN diode, which acts as a particle detector.

For cell irradiation experiments, primary human skin fibroblasts were transferred into sterilized irradiation dishes 2 days before irradiation. They attached well on the Si_3N_4 window (*8*). Since we have the particle detector behind the cells, we have to remove as much medium possible. The irradiation experiments were carried out at ambient conditions (21°C, 55% relative humidity), but later the cells and the sample holder were cooled on ice before irradiation. The confluent cells were irradiated with 5, 10, 20 or 40 2.2 MeV protons/pixel or with one or two 2 MeV α particles (He^+)/pixel with a particle rate of about 1000 cps. The dose for protons, calculated for the cell nucleus, was approximately 0.7–12 Gy/nucleus (~10 mGy/proton, ~100 mGy/α particle). After irradiation, the petri dishes were refilled with culture medium and incubated at 37°C. The whole procedure, during which the cells were without medium took less than 2 min.

For immunohistochemistry, the incubation time at 37°C was stopped 1 h (for DSBs) or 1.5 h (for HSP70) after the irradiation. For the HSP70 expression, an additional positive control was done by heat-shocking the cells for 30 min at 42°C. The DSBs were identified with anti-phospho-H2AX (Ser139) rabbit polyclonal antibody, and the HSP70 was identified with polyclonal rabbit-anti-HSP70 antibody, both followed by secondary Alexa Fluor 488 goat anti-rabbit antibody. For the optical analysis with a laser scanning microscope, the cells were covered with mounting medium and a cover slip.

Results

1. DSBs

After α-particle irradiation, the irradiation pattern was observed in some cell nuclei showing a cross of DSB foci in the nucleus. However, several pixels of the cross were fusing together and therefore were hardly visible as defined dots. The signal did not get brighter when using two α particles per pixel.

In the case of proton irradiation at 21°C, already five protons/pixel (~1.5 Gy/cell nucleus) reflected the irradiated area with an increased number of foci. The number of DSBs increased with the number of protons. However, the lines of the irradiation pattern itself generally were not clearly recognizable. In a few cells the focus lines were barely visible. It appeared that delocalization of foci took place. The cooled cells showed many fewer diffuse proton hits with more local DSB inductions. Even in the case where single foci were hardly visible, the irradiation cross was clearly recognizable in many cells.

2. HSP70

Control and sham-irradiated cells showed a weak expression of HSP70. The HSP70 expression in heat-shocked cells was generally increased, and

in particular the expression in the cell nucleus was increased notably relative to the results obtained for proton irradiation. Proton irradiation leads to a stronger signal of HSP70 in the cytoplasm than in the nucleus. After an irradiation of 10 protons/pixel (line pattern), bright HSP70 aggregates were observed in the cytoplasm. The intensity and the number of these punctual protein aggregates tended to be increased with increasing numbers of protons per pixel. However, the irradiated area could not be recognized; all cells on the Si_3N_4 window showed a homogeneous expression pattern.

Discussion

Irradiation with α particles (higher LET than protons) induces relatively localized DSBs in the cells. On the other hand, the proton-induced DSBs appear to be more delocalized than was expected by the ion hit accuracy. Possibly due to the less dense ionizing processes, the DSBs are induced predominantly by indirect, secondary effects after proton irradiation. This assumption is based on the observation that cooling reduces the delocalization of DSBs, probably as a result of reduced diffusion of DNA-damaging agents. For DSB-based proton hit localization/verification, cell cooling is mandatory.

The dominant localization of HSP70 in the cell nucleus after heat shock leads to the assumption that HSP70 mainly induces gene expressions to avert heat damage and may even participate in DNA repair. In the contrast, proton irradiation appears to provoke protein damages mainly in the cytoplasm, as indicated by the cytoplasmic HSP70 aggregates. Perhaps these protein damages are more pronounced than damages in the cell nucleus, where no increased HSP70 expression was observed. The different expression patterns after heat shock and proton irradiation lead to the assumption that the HSP70 pathways depend on the type of the stressor and its damages. These are preliminary results that remain to be investigated in more detail.

Acknowledgments

The European Commission within the CELLION project supported this work. J. Tanner gratefully acknowledges support from the Wilhelm Roux program (NBL3).

References

1. E. Sierra-Rivera, G. J. Voorhees and M. L. Freeman, Gamma irradiation increases hsp-70 in Chinese hamster ovary cells. *Radiat. Res.* **135**, 40–45 (1993).
2. H. S. Melkonyan, T. E. Ushakova and S. R. Umansky, Hsp70 gene expression in mouse lung cells upon chronic gamma-irradiation. *Int. J. Radiat. Biol.* **68**, 277–280 (1995).
3. S. Sadekova, S. Lehnert and T. Y. Chow, Induction of PBP74/mortalin/Grp75, a member of the hsp70 family, by low doses of ionizing radiation: A possible role in induced radioresistance. *Int. J. Radiat. Biol.* **72**, 653–660 (1997).
4. C. M. Kang, K. P. Park, C. K. Cho, J. S. Seo, W. Y. Park, S. J. Lee and Y. S. Lee, Hspa4 (HSP70) is involved in the radioadaptive response: Results from mouse splenocytes. *Radiat. Res.* **157**, 650–655 (2002).
5. S. H. Park, S. J. Lee, H. Y. Chung, T. H. Kim, C. K. Cho, S. Y. Yoo and Y. S. Lee, Inducible heat-shock protein 70 is involved in the radioadaptive response. *Radiat. Res.* **153**, 318–326 (2000).
6. S. J. Lee, S. A. Choi, K. H. Lee, H. Y. Chung, T. H. Kim, C. K. Cho and Y. S. Lee, Role of inducible heat shock protein 70 in radiation-induced cell death. *Cell Stress Chaperones* **6**, 273–281 (2001).
7. T. Reinert, A. Fiedler, J. Skopek, J. Tanner, J. Vogt and T. Butz, Single ion bombardment of living cells at LIPSION. *Nucl. Instrum. Methods Phys. Res. B* **219–220**, 77–81 (2004).
8. A. Fiedler, J. Skopek, T. Reinert, J. Tanner, J. Vogt, J. Österreicher, L. Navratil and T. Butz, First irradiation experiments with living cells at LIPSION. *Radiat. Res.* **161**, 95–96 (2004). [extended abstract]

Effect of Heavy-Ion Radiation on Phosphorylation of Histone H2AX

T. Funayama,[a] S. Wada,[a] N. Hamada,[a,b] T. Kakizaki,[a,c] T. Sakashita[a] and Y. Kobayashi[a,b]

[a]Microbeam Radiation Biology Group, Japan Atomic Energy Agency (JAEA), 1233 Watanuki, Takasaki, Gunma 370-1292, Japan; [b]Department of Quantum Biology, and The 21st Century Center of Excellence (COE) Program, Gunma University Graduate School of Medicine, 3-39-22 Showa, Maebashi, Gunma 371-8511, Japan; and [c]Laboratory of Veterinary Radiology and Radiation Biology, Department of Veterinary Medicine, Kitasato University Graduate School of Veterinary Medicine and Animal Sciences, 35-1 Higashi-nijuu-san-ban-cho, Towada, Aomori 034-8628, Japan

Heavy-ion radiation induces dense energy deposition along with its track and consequently induces greater biological effects. However, because the spatial distribution of ion hits follows a Poisson distribution, the radiation dose on the target becomes uneven, especially in a case of lower-fluence radiation. This uneven distribution of dose results in a mixture of hit and nonhit cells within a cell sample. In the mixture of hit and nonhit cells within the same sample, various biological effects, which are called bystander effects, are induced on nonhit cells based on transduction of a signal(s) from a hit cell. Therefore, exploring the mechanisms of bystander effects is necessary to understand the biological effects induced by heavy-ion radiation.

The analysis of bystander effects requires distinguishing hit cells and nonhit cells individually. Using a microbeam to target specific cells in a cell population is one means to address this issue. Thus we developed a heavy-ion microbeam targeting system in JAEA-Takasaki (*1, 2*). The system is capable of targeting individual cells with a heavy-ion microbeam and distinguishing hit and non-hit cells even long after irradiation.

The cell responses revealed in the bystander effect, such as cell killing, mutation and induction of DNA repair genes, are known to be triggered in hit cells by DNA damage, especially DSBs. However, whether the responses in bystander cells are also trigged by DSBs is still not clear. Therefore, as a first step to discover the mechanisms of the bystander response, we examined the formation of DSBs in bystander cells using heavy-ion microbeam irradiation. As a molecular marker of DSBs, we used the phospohorylated form of histone H2AX (γ-H2AX), which can be detected in individual cells *in situ* by immunohistochemistry.

For microbeam irradiation of cultured cell samples, we used a sample holder whose bottom was made of a 100-μm-thick film of a plastic ion-track detector, CR39. The CHO-K1 cells were kept in exponential growth phase, and 2500–3000 cells were inoculated within an area of 5 mm × 5 mm at the center of a sample holder. Among the inoculated cells, 25 cells were selected and their positions were stored in the object database. Thereafter the cells were irradiated with five $^{40}Ar^{13+}$ ions (11.5 MeV/nucleon, LET = 1260 keV/μm). The irradiated cells were postincubated for 30 min to 6 h and then fixed and stained with antibody specific against γ-H2AX. The frequency of γ-H2AX-positive cells increased for postincubation times longer than 30 min in a range of 3–4%. This result suggested that the heavy-ion radiation induced a bystander effect on the phosphorylation of histone H2AX in CHO-K1 cells.

References

1. T. Funayama, S. Wada, Y. Kobayashi and H. Watanabe, Irradiation of mammalian cultured cells with a collimated heavy-ion microbeam. *Radiat. Res.* **163**, 241–246 (2005).

2. Y. Kobayashi, T. Funayama, S. Wada, M. Taguchi and H. Watanabe, System of cell irradiation with a precise number of heavy ions. *Radiat. Res.* **161**, 90–91 (2004). [extended abstract]

Dynamics of DNA Repair Proteins after Directed Heavy-Ion Cell Irradiation

V. Hable,[a] G. Dollinger,[a] C. Greubel,[a] A. Hauptner,[b] R. Krücken,[b] S. Dietzel,[c] T. Cremer,[c] G. A. Drexler[d] and A. A. Friedl[d]

[a]Angewandte Physik und Messtechnik LRT2, UniBw-München, 85577 Neubiberg, Germany; [b]Physik Department E12, TU-München, 85748 Garching, Germany; [c]Department Biologie II, LMU-München, 82152 Martinsried, Germany; and [d]Strahlenbiologisches Institut, LMU-München, 80336 München, Germany

Various proteins that are involved directly or indirectly in repair processes accumulate as clusters (so-called foci) at DNA double-strand breaks (DSBs). To study the spatiotemporal dynamics of foci formed by the phosphorylated histone γ-H2AX, living HeLa cells were irradiated with directed single 100 MeV oxygen ions in a line pattern. The irradiation was performed using the ion microprobe SNAKE, the Superconducting Nanoscope for Applied Nuclear (= Kern-) Physics Experiments, at the Munich 14 MV tandem accelerator. The γ-H2AX foci were made visible by indirect immunofluorescence techniques and three-dimensional microscopy. Techniques to evaluate, from the microscopic images, the time-dependent changes in focus size and the movement of foci within the chromatin were developed based on the data analysis software ''ROOT'' (available online at http://root.cern.ch/).

The source of the evaluation is a deconvolved fluorescence image of γ-H2AX foci induced by a line irradiation (single ion hits separated by 1 μm). Gaps in the lines colocate with nucleoli, where focus formation is strongly reduced, presumably because of the limited amount of DNA present. Along every horizontal pixel line perpendicular to the vertical irradiation line, the gray shadestones of the microscopic image were determined and fitted by a Gauss function. The x value of the mean of each Gaussian was determined and plotted as a function of the y coordinate. A straight line was fitted to the distribution of the means, which is taken as a representation of the irradiated line. Movements of the foci during postirradiation incubation can be evaluated relative to this irradiation line. Thus one obtains a relative measure that is independent of movements of the whole cell nucleus.

The distance of every data point from the best-fit straight line was determined. The variance of this distance plotted as a function of the time between irradiation and fixation of the cells reveals movements of the foci. The data obtained are compatible with a pure diffusion process, within the limits of the accuracy of these measurements.

To reveal how focus sizes evolve over time, we have determined the average line width by analyzing the FWHMs of the fitted Gaussians. This line width plotted as a function of time shows complex time dependence. Up to 2 h after irradiation, the foci increase in size, but in the next 2 h their size decreases to a value which is nearly constant for at least 24 h. Whether this decline is due to chromatin clustering is currently being investigated. It also was discovered that foci in z planes in the center of the cell nucleus are about 0.4 μm larger than foci in z planes at the upper edge of the nucleus, possibly reflecting different chromatin compaction grades.

Acknowledgments

Radiobiological experiments at SNAKE are supported by grant Str.Sch.4450 of the Bundesamt für Strahlenschutz and grant 02S8264 of the Bundesministerium für Bildung und Foschung to AAF, by Eurodyna grants of the European Science Foundation to AAF, TC and GD, and by the Maier Leibnitz Laboratorium of the TU Munich and the University of Munich. We thank the technical staff of the Munich tandem accelerator.

References

1. A. Hauptner, S. Dietzel, G. A. Drexler, P. Reichart, R. Krücken, T. Cremer, A. A. Friedl and G. Dollinger, Microirradiation of cells with energetic heavy ions. *Radiat. Environ. Biophys.* **42**, 237–245 (2004).
2. V. Hable, G. Dollinger, C. Greubel, A. Hauptner, R. Krücken, S. Dietzel, T. Cremer, G. A. Drexler, A. A. Friedl and R. Löwe, Methods for quantitative evaluation of dynamics of repair proteins within irradiated cells. *Nucl. Instrum. Methods Phys. Res. B,* in press.

Monte Carlo Simulation of Interactions of Radiation with Biological Systems at the Cellular and DNA Levels: The Geant4-DNA Project

S. Chauvie,[a] Z. Francis,[b] S. Guatelli,[c] S. Incerti,[d] B. Mascialino,[c] G. Montarou,[b] Ph. Moretto,[d] P. Nieminen[e] and M. G. Pia[c]

(The Geant4-DNA Collaboration)

[a]Azienda Ospedaliera Santa Croce e Carle Cuneo and INFN Sezione di Torino, I-10125 Torino, Italy; [b]Laboratoire de Physique Corpusculaire, CNRS/IN2P3, Université Blaise Pascal, F-63177 Aubière Cedex, France; [c]INFN Sezione di Genova, I-16146 Genova, Italy; [d]Centre d'Etudes Nucléaires de Bordeaux-Gradignan, CNRS/IN2P3, Université Bordeaux 1, F-33175, Gradignan Cedex, France; and [e]European Space Agency, 2200 AG Noordwijk, The Netherlands

The Geant4-DNA collaboration is developing a fully integrated simulation toolkit based on the general-purpose state-of-the-art Monte Carlo software Geant4 (*1, 2*) for the modeling of radiation interactions with biological systems at the cellular and DNA levels (*3*). These new extensions will be part of the Low Energy Electromagnetic package (*4*) included in Geant4 that has already shown a remarkable ability to model low-energy light-ion cellular irradiation setups based on focused microbeams (*5–7*) or on more classical irradiation facilities like macrobeams or radionuclide emitters (*8*).

At the cellular level, Geant4-DNA will provide the user with a wide set of radiobiological models currently under implementation to describe the macroscopic survival rates of cell populations irradiated with low- (photons) and high-LET (light ions) particles. These models could for example include among others the target theory of cell killing, the repair-misrepair model, the lethal-potentially lethal model, the Scholz and Kraft model, etc. On a smaller scale, at the DNA level, a full set of physics models has been included in the toolkit; this set takes into account elastic scattering, excitation, ionization and charge transfer for electrons, protons, and α particles and their charge states in liquid water down to the electronvolt scale and up to a few tens of MeV.

These new software developments follow a rigorous object-oriented software design using policy-based classes within the framework of the Geant4 simulation toolkit. This architecture allows the flexibility and extensibility to include future chemistry (production and tracking of oxidative radical species) and biological damage (production of DNA strand breaks and DNA fragments) models, as well as realistic voxelized 3D cellular geometries and new solid target materials for applications at the submicrometer level. The Geant4-DNA collaboration will benefit from experimental cellular irradiation facilities to validate the developed extensions: neutron cellular irradiation at the Laboratoire de Physique Corpusculaire in Aubière, France, and proton and α-particle cellular irradiation in single-ion/single-cell mode at the Centre d'Etudes Nucléaires de Bordeaux-Gradignan, France. Applications of this Monte Carlo tool will not only involve radiobiology at low doses but also radiotherapy and radioprotection for future manned space missions.

Acknowledgment

This study is partially supported by CELLION project, MRTN-CT-2003-503923.

References

1. S. Agostinelli, J. Allison, K. Amako, J. Apostolakis, H. Araujo, P. Arce, M. Asai, D. Axen, S. Banerjee and D. Zschiesche, Geant4: A simulation toolkit. *Nucl. Instrum. Methods Phys. Res. A* **506**, 250–303 (2003).
2. J. Allison, K. Amako, J. Apostolakis, H. Aroujo, P. A. Dubois, M. Asai, G. Barrand, R. Capra, S. Chauvie and H. Yoshida, Geant4 developments and applications. *IEEE Trans. Nucl. Sci.,* in press.
3. R. Capra, S. Chauvie, Z. Francis, S. Incerti, B. Mascialino, G. Âontarou, Ph. Moretto, P. Nieminen and M. G. Pia, Geant4 simulation of very low energy interactions in liquid water. *Radiat. Prot. Dosim.,* in press.
4. K. Amako, S. Guatelli, V. N. Ivanchenko, M. Maire, B. Mascialino, K. Murakami, P. Nieminen, L. Pandola, S. Parlati and L. Urban, Comparison of Geant4 electromagnetic physics models against the NIST reference data. *IEEE Trans. Nucl. Sci.* **52**, 910–918 (2005).
5. S. Incerti, P. Barberet, B. Courtois, C. Michelet-Habchi and P. Moretto, Simulation of ion propagation in the microbeam line of CENBG using Geant4. *Nucl. Instrum. Methods Phys. Res. B* **210**, 92–97 (2003).
6. S. Incerti, Ph. Barberet, R. Villeneuve, P. Aguer, E. Gontier, C. Michelet-Habchi, Ph. Moretto, D. T. Nguyen, T. Pouthier and R. W. Smith, Simulation of cellular irradiation with the CENBG microbeam line using Geant4. *IEEE Trans. Nucl. Sci.* **51**, 1395–1401 (2004).
7. S. Incerti, R. W. Smith, M. Merchant, G. W. Grime, F. Méot, L. Serani, P. Moretto, C. Touzeau, P. Barberet and D. T. Nguyen, A comparison of ray-tracing software for the design of quadrupole microbeam systems. *Nucl. Instrum. Methods Phys. Res. B* **231**, 76–85 (2005).
8. S. Incerti, N. Gault, C. Habchi, J. OL. Lefaix and Ph. Moretto, A comparison of cellular irradiation techniques with alpha particles using the Geant4 Monte Carlo simulation toolkit. *Radiat. Prot. Dosim.,* in press.

Study of the Dynamics and Regulation of Fanconi Proteins using the Microbeam Technique

A. Lyakhovich and J. Suralles

Group of Mutagenesis, Department of Genetics and Microbiology, Universitat Autonoma de Barcelona, Barcelona, Spain

Fanconi anemia (FA) is a genetic syndrome characterized by chromosome fragility, congenital malformations, progressive pancytopenia and cancer susceptibility. Exposure to ultraviolet radiation leads to formation of DSBs as a result of replication arrest since most of the DNA polymerases are unable to replicate templates containing UV-radiation-induced DNA lesions. We have developed a novel functional assay of the FA/BRCA pathway to study the dynamics and regulation of Fanconi protein relocation to locally induced stalled replication forks. In this research, we created DSBs in cells of several fibroblast cell lines by sequentially exposing the cells to pulse laser microbeam irradiation (390 nm). The sites of irradiation were visualized with antibodies against CPD and the relocation of the key Fanconi proteins (FANCD2, BRCA1, etc.) to the site of damage was measured at different times using specific antibodies. Cells have been fixed after several periods of exposure and the number of fluorescent foci per cell has been calculated by confocal image analysis software. More than 200 locally irradiated foci per time were analyzed to measure the percentage of UV-irradiated spots containing the proteins of interest. Many components of the DNA damage response including BRCA1, the MRN complex, 53BP1, MDC1 and RAD51 formed foci and colocalized with pre-existing γ-H2AX foci. These studies led us to discover that the ATR substrate histone H2AX is a novel component of the FA/BRCA pathway. Importantly, microbeam irradiation is not unique in producing protein relocation to the damage sites but rather models the clinical situation after treatment of patients with DNA-damaging drugs. Therefore, it may potentially be used for prescreening studies.

Dynamics of DSB Sensing and Repair Proteins at DNA Double-Strand Breaks in Living Cells

N. Uematsu,[a] B. P. Chen,[a] B. Jakob,[b] G. Taucher-Scholz[b] and D. J. Chen[a]

[a]Division of Molecular Radiation Biology, Department of Radiation Oncology, University of Texas Southwestern Medical Center, Dallas, Texas 75390-9187; and [b]Department of Biophysics, Society for Heavy Ions Research, 64291 Darmstadt, Germany

Introduction

DSBs are considered to be the most lethal form of DNA damage. In eukaryotes, cells have evolved two mechanisms for the repair of DSBs: homologous recombination (HR) and nonhomologous end joining (NHEJ). Despite tremendous progress in understanding the genetic and biochemical aspects of DSB-induced genome surveillance and repair mechanisms, little is known about the organization of these molecular pathways in time and space. In particular, the *in vivo* kinetics of the individual pathway responses and the mechanism of pathway choice are not well understood. Our main intention is to visualize the key molecular events in DNA damage recognition, processing and repair in their physiological environment and to investigate how DSB-induced molecular pathways operate in time and space. Our final goal is to obtain a systematic overview of the organization of these molecular pathways based on *in vivo* imaging. We hypothesize that the accumulation and dissociation of DNA repair proteins at DSB sites would be strictly regulated through coordination with each other, especially phosphorylation events and subsequent conformational changes that would affect the DNA damage recognition events.

UV Microbeam Laser System

To analyze the dynamics of DNA repair proteins assembling at DSBs *in vivo,* we used a UV microbeam laser system (Photonic laser) with a 365-nm laser interface combined with a fluorescence microscope. The laser is focused through a 63× Plan-Apochromat objective to yield a spot size of approximately 1 μm. The laser can be operated at a rate of 1 to 20 pulses per second, and the movement of the microscope stage can be automatically controlled by self-made software. This technique is based on a relatively old finding by Limoli and Ward that DNA presensitized by BrdU, IdU and/or DNA intercalating dyes (Hoechst 33258) becomes hypersensitive to light within the UVA spectrum (*1*). Applying laser microdissection equipment with this approach allowed the placement of DNA lesions in a specified area within a single nucleus, such that it was possible to investigate the dynamics of a certain protein at a specific DNA break site. Although it is still not clear what kind of DNA lesions would occur in response to microirradiation, it has been suggested that a single pulse of 365 nm laser microirradiation at the lower dose (0.75 μJ) generates only single-strand breaks, whereas irradiation at the higher dose (2.5 μJ) produces double-strand breaks and base damage in addition to single-strand breaks (*2*). Several groups have used a microlaser to generate local DSBs without the use of agents for presensitization of the DNA (*3, 4*). The obvious advantage of such an approach is that it eliminates the concerns about the background DNA damage potentially caused by the exposure of cells to UV-radiation sensitizers. We currently have established a microbeam laser system that may produce mainly DSBs without any contaminant presensitizers and could give the exact equal energy to multiple cells by using the automatic controller of the microscope stage.

Experimental Procedures

We generated DNA-dependent protein kinase (DNA-PKcs) mutant V3 cell lines complemented with yellow fluorescent protein (YFP)-tagged DNA-PKcs. The cells were grown in α-MEM on grid cover slips with a 1-mm-thick silicon gasket to form a chamber and placed on the stage of the microscope. After irradiation, the cells were subjected to time-lapse recording of an initial assembly of YFP-DNA-PKcs. Signal intensities of the accumulation of YFP-DNA-PKcs at the damage site and background intensity within the same nucleus were obtained by using Axiovision software (Carl Zeiss). To avoid nonspecific fluorescence bleaching during the repeated image acquisition, the signal of accumulation at each time was subtracted by the background of each image. Relative fluorescence (RF) was calculated as $RF_{(t)} = (I_t - I_{preIR})/(I_{max} - I_{preIR})$, where I_{preIR} is the fluorescence intensity of the region within the irradiated area before laser irradiation, and I_{max} represents the maximum fluorescence signal in the damaged region after irradiation. Ten irradiated cells were measured for statistical analysis.

Results and Discussion

UV laser-induced DNA lesions were monitored by TUNEL labeling and γ-H2AX that colocalized with YFP-DNA-PKcs, suggesting that the accumulation of DNA-PKcs indicates DSB-associated DNA-PKcs foci. *In vivo* imaging analysis revealed that the localization of YFP-DNA-PKcs to laser-induced DSBs was observed within seconds and that its intensity reached a maximum around 20 s after irradiation, which was identical to the kinetics of irradiation by uranium ions (11.4 MeV/nucleon). To investigate whether kinase activity regulates the accumulation of DNA-PKcs to DSBs, we also tested the kinetics of kinase-dead DNA-PKcs. Although the initial kinetics displayed no difference between wild-type and kinase-dead DNA-PKcs, kinase-dead dissociated from DSBs faster than wild-type. Furthermore, we found that YFP-DNA-PKcs failed to localize to laser-induced DSBs in Ku80-deficient Xrs6c cells, suggesting that Ku80 is essential for localization of DNA-PKcs to DSBs. We also found cell cycle-dependent activation of DNA-PKcs upon DNA double-strand breaks.

Conclusion

A method for irradiating individual cells with a UV microbeam laser has been established. *In vivo* imaging provides us with accurate information about the temporal and spatial dynamics of DSB sensing and repair proteins after DNA damage. With this method, we can observe the kinetics of a large number of sensing and repair proteins and can compare the kinetics of these proteins. This method will be quite useful to study the mechanisms for the repair of DSBs as well as for the regulation of NHEJ and HR pathways after DNA damage.

References

1. C. L. Limoli and J. F. Ward, A new method for introducing double-strand breaks into cellular DNA. *Radiat. Res.* **134**, 160–169 (1993).
2. L. Lan, S. Nakajima, K. Komatsu, A. Nussenzweig, A. Shimamoto, J. Oshima and A. Yasui, Accumulation of Werner protein at DNA double-strand breaks in human cells. *J. Cell Sci.* **118**, 4153–4162 (2005).
3. L. Lan, S. Nakajima, Y. Oohata, M. Takao, S. Okano, M. Masutani, S. H. Wilson and A. Yasui, In situ analysis of repair processes for oxidative DNA damage in mammalian cells. *Proc. Natl. Acad. Sci. USA* **101**, 13738–13743 (2004).
4. J. S. Kim, T. B. Krasieva, V. LaMorte, A. M. Taylar and K. Yokomori, Specific recruitment of human cohesin to laser-induced DNA damage. *J. Biol. Chem.* **277**, 45149–45153 (2002).

SESSION 6: CELLULAR RESPONSE PROBED WITH MICROBEAMS

Chair: Michael Cornforth

Inter- and Intraindividual Differences in Genomic Instability after Targeted Microbeam Irradiation

S. R. Moore,[a] D. A. Macdonald,[a] M. Folkard,[b] G. Patel,[b] K. M. Prise[b] and M. A. Kadhim[a]

[a]Radiation and Genome Stability Unit, Medical Research Council, Harwell, United Kingdom; and [b]Gray Cancer Institute, Mount Vernon Hospital, Northwood, United Kingdom

Introduction

Radiation exposure can lead to a number of cellular changes that resemble those observed during tumorigenesis. A hallmark of tumorigenesis, genomic instability, is defined by an increased rate in the accumulation of new genetic alterations and is frequently assessed using cytogenetic analysis of chromosomes. In addition to being observed in a large fraction of the progeny of irradiated cells, genomic instability has also been reported in unirradiated cells (bystander cells) that are in the vicinity of, and are permitted to communicate with, irradiated cells. Understanding such bystander effects is crucial for a complete comprehension of radiation dosimetry and radiotherapy, particularly because of the need to determine the relevance of out-of-field (abscopal) effects.

Radon and its daughters are ubiquitous in the environment, and exposure has been linked to lung cancer. Measurement of cytogenetic aberrations in peripheral lymphocytes is commonly used to estimate dosimetry and risk in exposed populations. Exposure to radon for the vast majority of the population is very low and is generally such that very few cells in the lung will ever be traversed and those that do will only ever see a single charged-particle traversal. Charged-particle microbeams have emerged as powerful tools to target exact numbers of cells for irradiation by precise numbers of particle tracks. Using lymphocytes from a single donor, we have reported that nuclear traversal of all cells in a population with a single or two $^3He^{2+}$ particles results in a significant induction of genomic instability (*1*). Also, nuclear traversal of fractions of the cell population with a single $^3He^{2+}$ particle results in a significant induction of genomic instability, suggesting a significant contribution of bystander effects. In the same study, we noted that antibody-mediated inactivation of the pro-inflammatory cytokine tumor necrosis factor alpha (TNFA) is sufficient to significantly reduce genomic instability when all cells are irradiated but not when fractions of the population are irradiated, suggesting a role for TNFA signaling in irradiated but not bystander cells. In this study we couple the measurement of aberrations in primary lymphocytes with targeted microbeam irradiation to address the hypothesis that interindividual differences in radiation sensitivity will be evident between healthy lymphocyte donors and that differences between treatment groups will exist within individuals.

Materials and Methods

Primary human T lymphocytes were isolated from four healthy donors, and one donor over two collection times separated by 4 years, and made to adhere transiently to a specially designed dish with a Mylar base for microbeam irradiation using the Gray Cancer Institute charged-particle microbeam as described previously (*1, 2*). Briefly, charged particles from a 4 MV Van de Graff accelerator were collimated to a spot size of 2 μm (radius) and individually detected as they exited the collimator. The detector triggers a fast shutter after a preselected number of particles are delivered to each cell. The system is computer-aided such that cells stained with 0.8 μ*M* Hoechst 33258 are automatically positioned over the collimator for irradiation. The efficiency of delivering a single particle to a specified target (±2 μm) is >99%, in comparison to the size of human lymphocytes (6–7 μm diameter). Fractions of the population,

down to a single cell, were irradiated at G_1/G_0 with precisely one $^3He^{2+}$ particle (105 keV/μm) delivered through the center of the nucleus. After irradiation, cells were removed from the Mylar dish with gentle aspiration and cultured, and exponentially growing cells were harvested using standard cytogenetic techniques. At least 50 well-spread and isolated, Giemsa-stained metaphases were analyzed per sample. Comparisons between treatments and between donors were made using the nonparametric Mann-Whitney *U* test. Regression analysis (nonparametric Spearman rank correlation) was performed on all irradiated groups (grouped after Kruskal-Wallis ANOVA) to determine any correlation between the number of cells on a dish and the level of genomic instability. In all tests, $P \leq 0.05$ was the significance cutoff. All statistical comparisons were made using GraphPad InStat software (version 3.06, GraphPad Software, Inc.).

Results and Discussion

Interindividual differences in the level of genomic instability induced after targeted microbeam irradiation were evident, with one of four donors susceptible to the induction of genomic instability and three of four donors being resistant to the induction of genomic instability.

Furthermore, for lymphocytes from a single donor at two collection times separated by 4 years, we observed a substantially different pattern in the induction of genomic instability, where one collection time showed genomic instability across doses and the other collection time showing no genomic instability. The inter- and intraindividual differences that we report are not related to donor age or seasonal temperature variations at the blood collection times, T-lymphocyte cell cycle kinetics (FACS analysis), general T-lymphocyte radiosensitivity (measured in X-irradiation experiments), or distinct donor T-lymphocyte cytokine profiles after microbeam irradiation.

We did notice, however, that there seemed to be a relationship between the number of cells on each microbeam dish at the time of irradiation and the level of genomic instability in the resulting culture. To explore this further, data from all donors were pooled and sorted by the number of cells per dish at time of irradiation, and a correlation between genomic instability and the number of cells per dish was analyzed using a nonparametric Spearman rank test. Interestingly, in the bystander groups, we observed a significant correlation between the number of cells on the dish and the level of genomic instability in the resulting culture; this trend was not evident in the control or fully irradiated groups. Furthermore, there appears to exist a threshold for genomic instability as a function of cells on the dish. Since we observed a similar threshold for the bystander groups, we hypothesize that under bystander conditions in our system, the number of unirradiated cells is a more crucial determinant of genomic instability than the number of irradiated cells. Overall, these data suggest that the number of unirradiated bystander cells on the dish is inversely related to the level of genomic instability and that the amplification of the bystander signal through communication between bystander cells is critical for the initiation of genomic instability. This interpretation is supported by recent intercellular communication experiments from our group that demonstrate that communication between irradiated cells and communication between bystander cells is critical for genomic instability (*3*).

References

1. S. R. Moore, S. Marsden, D. A. Macdonald, S. Mitchell, M. Folkard, B. Michael, D. T. Goodhead, K. M. Prise and M. A. Kadhim, Genomic instability in human lymphocytes irradiated with individual charged particles: Involvement of tumor necrosis factor alpha in irradiated cells but not bystander cells. *Radiat. Res.* **163**, 183–190 (2005).
2. M. A. Kadhim, S. J. Marsden, D. T. Goodhead, A. M. Malcolmson, M. Folkard, K. M. Prise and B. D. Michael, Long-term genomic instability in human lymphocytes induced by single-particle irradiation. *Radiat. Res.* **155**, 122–126 (2001).
3. S. R. Moore, D. A. Macdonald and M. A. Kadhim. *Int. J. Low Radiat.,* in press.

Cell Survival Study Using KEK-PF Synchrotron X-Ray Microbeam Irradiation System

M. Maeda,[a] N. Usami[b] and K. Kobayashi[a,b]

[a]Department of Materials Structure Science, School of High Energy Accelerator Science, The Graduate University for Advanced Studies, Tsukuba, 305-0801, Japan; and [b]Photon Factory, Institute of Materials Structure Science, KEK, Tsukuba, 305-0801, Japan

Introduction

It is generally accepted that the majority of biologically important damage produced by ionizing radiation occurs in DNA, either by direct ionization or through reactions with free radicals produced nearby. Meanwhile, new phenomena such as the radiation-induced bystander effect have been discovered (*1*). Detailed mechanisms of these phenomena are not yet clear, although the important role of intracellular or intercellular signaling is suggested. In irradiation experiments using a broad irradiation field, we cannot distinguish individual cellular responses from those resulting from intercellular signaling. Therefore, a system in which we can observe cellular responses of both individual nonirradiated cells and individual cells irradiated by microbeams is needed. From this rationale, a synchrotron X-ray microbeam irradiation apparatus has recently been developed (*2*). Using this system, we can irradiate an arbitrarily defined target region with a desired number of X-ray photons. In this research, we compare the surviving fractions as an index for cellular responses of broad-field (broad-beam) irradiation and of microbeam irradiation.

Experimental Procedure

In microbeam experiments, Chinese hamster lung V79 cells were plated on specially designed Mylar-based dishes. To avoid interference between the colonies originating from single cells, the cells were seeded in a very low concentration (2×10^3 cells/dish). After a 4-h incubation, the nuclei of cells attached to the base film were stained with a 2 μM solution of Hoechst 33258. The positions of each target nuclei were automatically recognized and stored by the irradiation system. All targets were irradiated with a 10-μm square X-ray beam. The X-ray energy was 5.35 keV and the dose rate was about 30 R/s (7.74 mC/kg s^{-1}; 9.3×10^3 photons/s per 100 μm^2). After irradiation, the cells were incubated for 60 h and the nuclei were again stained with Hoechst 33258. To count the numbers of cells per colony, pictures were captured using a CCD camera. We drew a histogram of cell number per colony to determine the threshold for live or dead cells. Clear differences between irradiated cells and nonirradiated cells were observed in the histogram. Considering the doubling time of the cells, a threshold of 30 was determined in the histogram and surviving fractions were calculated. On the other hand, in broad-beam irradiation, approximately 1×10^5 V79 cells were seeded in a 35-mm dish. The entire plate was irradiated uniformly with 5.35 keV X rays. Cells were collected by trypsinization and surviving fractions were measured with the usual colony assay method.

The surviving fractions in microbeam experiments cannot be compared with the surviving fractions of cells irradiated with a broad beam, since the microbeam irradiates only a part of the cell nucleus and the energy of X rays is absorbed only by the targeted area. Here we propose a nuclear-averaged dose as a measure of dose, by which we can compare the biological effects in a microbeam experiment with those using a broad beam. We assumed that the cell has a thin double-cylindrical structure; the inner cylinder is the cell nucleus and the outer shell, the cytoplasm. We measured the area of the nucleus observed in the fluorescence microscope, 168.4 μm^2 on average, as the base area of the nucleus in this model.

Results and Discussion

1. The dose–survival curve obtained in the microbeam experiment was almost the same as or slightly higher than that obtained with broad-

beam irradiation. Considering the difference in the targeted area between microbeam and broad-beam experiments, these results may support the idea that the damage in the cell nucleus is critical in determining the death of the cell.

2. Low-dose hypersensitivity was clearly observed in the dose–survival curves obtained in microbeam experiments. In contrast, the low-dose hypersensitivity was not remarkable in the broad-beam experiments. In broad-beam experiments, the entire cytoplasm as well as the nucleus was irradiated uniformly with X rays, while the cytoplasm was not irradiated in microbeam experiments. Energy deposition in the nuclei was almost equal in both experiments. These results suggest that energy deposition in the cytoplasm might induce some kind of intracellular signaling and reduce the cell killing effect in the low-dose region.

Acknowledgments

The authors would like to express sincere thanks to Drs. K. Kasai-Eguchi, Y. Furusawa and H. Maezawa for valuable discussions concerning this work. We thank Dr. T. Konishi for his help in performing the broadbeam experiments. This work has been supported in part by Grant-in-Aid for Scientific Research (A) (14208069), MEXT, Japan. This work was performed under the approval of the Photon Factory Program Advisory Committee (Proposal No. 2002G333 and 2004G395).

References

1. H. Nagasawa and J. B. Little, Induction of sister chromatid exchanges by extremely low doses of alpha-particles. *Cancer Res.* **52**, 6394–6396 (1992).

2. K. Kobayashi, N. Usami, H. Maezawa, T. Hayashi, K. Hieda and K. Takakura, Development of photon microbeam irradiation system for radiobiology. *Int. Congr. Ser.* **1258**, 207–211 (2003).

Micronucleus Expression in Peripheral Lymphocytes Cultivated with Activated Cisplatin

N. P. Dikiy, N. A. Klimenko, E. P. Medvedeva and N. I. Onishchenko

National Science Center, Kharkov Institute of Physics and Technology, Kkharkov, Ukraine

At present, surgical treatment, radiation therapy and chemotherapy are the conventional treatments for cancer patients. It can be hypothesized that synergetic action of radioactive days would radically improve the efficiency of radiation and chemical therapy. In particular, radioactive cisplatin could reduce the toxic effects on the patient by lowering the dose of drug administered.

The objective of the study was to estimate the intensity of micronucleus expression in peripheral lymphocytes cultured with radioactive cisplatin and with normal cisplatin.

The radioactive isotopes of a platinum were obtained using a powerful electron accelerator with E = 21 MeV and current 1 mA in the reactions $^{194}Pt(\gamma,n)^{193m}Pt$, $t_{1/2}$ = 4.33 days, $^{195}Pt(\gamma,\gamma')^{195m}Pt$, $t_{1/2}$ = 4.02 days, and $^{196}Pt(\gamma,n)^{195m}Pt$, $t_{1/2}$ = 4.02 days. The abundance ratio of isotopes $^{194,195,196}Pt$ is 32.9, 33.8 and 25.2%, respectively. The ^{195m}Pt decay is accompanied by γ radiation of nuclear transactions, X rays and electrons of internal conversion. The Auger-MXY electrons have energy 2.417 keV, and the abundance is 3.22 per ^{195m}Pt decay. The LET of these Auger electrons is 9.5 keV/μm and the range is 0.25 μm. Therefore, for the incorporated cisplatin molecule, the range of Auger electrons is less than the size of cell nucleus. The Auger-LMM and Auger-LMX electrons with energies 7.4 and 9.7 keV are also less than the size of the cell nucleus (abundance 0.8 and 0.52 per ^{195m}Pt decay, respectively).

To obtain whole blood cultures for lymphocytes, 0.25 ml sterile blood was taken from the ulnar vein. The blood was added to 1.0 ml of RPMI 1640 medium + 20% FCS and incubated in the presence of PHA for 42 h. After cytochalasin B was added (final concentration 3 μg/ml; stock solution 1000 μg/ml DMSO), cells were incubated for another 24 h. The concentration of cisplatin in the medium was 7 μg/ml. After triple washing in Carnoy's fixative (methanol:glacial acetic acid 3:1, v/v), cells were dropped on glass slides and stained with 2% Giemsa. The numbers of micronuclei and the numbers of binucleated cells with micronuclei in 1000 binucleated cells were scored under a microscope (1000×).

It was established that intensity of micronucleus formation in human peripheral lymphocytes is higher in cells cultured with radioactive cisplatin compared to cells cultured with normal cisplatin. It can be hypothesized that radioactive cisplatin can be more effective in cancer treatment due to DNA damage by Auger electrons.

Acknowledgment

This research was partly supported by the STCU Project no. 1768.

A Mathematical Model of Cellular Behavior under Irradiation

M. Richard,[a,b] K. J. Kirkby,[a] R. P. Webb[a] and N. F. Kirkby[b]

[a]Ion Beam Center, Advanced Technology Institute, School of Electronics and Physical Sciences; and [b]Fluids and Systems Research Center, School of Engineering, University of Surrey, Guildford, GU2 7XH, United Kingdom

Introduction

There is now no doubt that low doses of radiation have a more effective killing effect than is predicted by the linear-quadratic assumption. Moreover, it is well known that radiation affects not only hit cells but also neighbors; this is called the bystander effect (*1*). For a further understanding of the cellular mechanisms involved and for improving treatment planning in fractionated radiotherapy, a model has been created that takes into account low-dose phenomena. The cellular automaton approach has been taken; the model handles two cellular automata, one that computes the evolution of biological cells and one that computes the diffusion of matter in the cellular milieu (such as glucose, oxygen and intercell signals).

Diffusion Rules

The diffusion rules have been adapted from ref. (*2*). The cellular milieu is represented by a square lattice; a lattice site has four neighbors, is divided into four quarters, north, south, east and west (N, S, E, W), and contains a given amount of matter. For convenience, the concentration of matter is computed by integers. The first step of the diffusion consists of matter diffusing between adjacent quarters of two neighboring sites; the second step averages the matter in the four quarters of a site.

Cell Cycle and Cell Division

The growth of cells is calculated on a second cellular automaton. Cells absorb the nutrients and oxygen available which are diffusing on the first cellular automaton.

The cell cycle has phases, G_1, S, G_2 and M; S and M are assumed to have fixed lengths, but the durations of G_1 and G_2 vary and are controlled by the state of the cell. Indeed, to be able to enter S or M phase, the cell must have absorbed a minimum amount of nutrients since the last division; the details are very similar to those of ref. (*3*). Also, in the case of radiation-induced DNA damage, the cell cycle is arrested in these two phases to allow time for repair. At any phase of the cell cycle, the cell cycle progress is arrested if the environmental level of oxygen becomes too low and the cell is assumed to enter a quiescent state.

A cell in mitosis divides in one of the eight neighboring directions: north, south, east, west, or northeast, northwest, southeast and southwest. If all these sites are already occupied, the cell waits before dividing. If no site is freed, the mitotic cell dies.

HRS/IRR and Bystander Effect

It is considered that a threshold dose of radiation, called d_e, is required to trigger cellular repair processes. The surviving fraction is described by a discontinuous splice of two linear-quadratic (LQ) curves; the first curve applies below d_e and the second one above. The parameters of the LQ curves are supposed to be the same for all the cells; however, they change throughout the cell cycle. On the other hand, the threshold d_e is normally distributed within the population, and its mean and standard deviation are also different for different phases of the cell cycle.

In addition to the killing due to direct irradiation, the bystander effect is computed. This is assumed to be a chemical secreted by hit cells, diffusing in the milieu and evolving on the first cellular automaton. Cells that have not been hit are affected by the chemical, which induces DNA damage; these cells then turn into secondary sources of the chemical. Little *et al.* describe a similar approach (*4*).

Results

So far, only the situation of no radiation has been considered in detail. A single cell in a uniform field of oxygen and nutrients is allowed to grow and gives rise to a circular colony of cells with a necrotic core, resulting from the depletion of nutrient and oxygen.

Discussion and Conclusion

The model has been checked in the case of no irradiation and gives consistent results. The modeling of the radiation effects should now be studied in more detail; however, some points can already be raised:

1. The assumption underlining the modeling of direct radiation effects is the one of threshold-induced cellular response, which has recently been challenged by Short *et al.* (*5*).
2. Other groups have stated that the bystander signal is produced only by directly hit cells (*6, 7*); little quantitative information is currently known about this signal.
3. The assumption that cells do not divide and do not diffuse if no free space is around may not be valid in case of some cancer cells (*8*).

Acknowledgments

The work is supported by the Marie Curie Research Training Network and is part of the Cellion project; the correspondent at the University of Surrey is Dr. G. W. Grime (Contract MCRTN-CT-2003-503923).

References

1. K. M. Prise, G. Schettino, M. Folkard and K. D. Held, New insights on cell death from radiation exposure. *Lancet Oncol.* **6**, 520–528 (2005).
2. S. Bandini, G. Mauri, G. Pavesi and C. Simone, Parallel simulation of reaction-diffusion phenomena in percolation processes–A model based on cellular automata. *Future Gen. Comp. Syst.* **17**, 679–688 (2001).
3. D. B. F. Faraday, P. Hayter and N. F. Kirkby, A mathematical model of the cell cycle of a hybridoma cell line. *Biochem. Eng. J.* **7**, 49–68 (2001).
4. M. P. Little, J. A. N. Filipe, K. M. Prise, M. Folkard and O. V. Belyakov, A model for radiation-induced bystander effects, with allowance for spatial position and the effects of cell turnover. *J. Theor. Biol.* **232**, 329–338 (2005).
5. S. C. Short, S. Bourne, C. Martindale, M. Woodcock and S. P. Jackson, DNA damage responses at low radiation doses. *Radiat. Res.* **164**, 292–302 (2005).
6. H. Nikjoo and I. K. Khvostunov, Biophysical model of the radiation-induced bystander effect. *Int. J. Radiat. Biol.* **79**, 43–52 (2003).
7. D. J. Brenner, J. B. Little and R. K. Sachs, The bystander effect in radiation oncogenesis: II. A quantitative model. *Radiat. Res.* **155**, 402–408 (2001).
8. K. R. Swanson, E. C. Alvord and J. D. Murray, Quantifying efficacy of chemotherapy of brain tumors with homogeneous and heterogeneous drug delivery. *Acta Biotheor.* **50**, 223–237 (2002).

SESSION 7: BYSTANDER RESPONSES

Chair: Edouard Azzam

Evaluation of the Role of Gap Junctional Communication in Mediating Radiation-Induced Bystander Effects in Jeg3 Trophoblast Cells

F. Banaz-Yasar,[a] K. Lennartz,[b] K-D. Greif,[c] U. Giesen,[c] G. Iliakis,[d] E. Winterhager[a] and A. Gellhaus[a]

[a]Institute of Anatomy, [b]Institute of Cell Biology and [d]Institute of Radiation Biology, University Hospital Essen, Hufelandstr. 55, 45122 Essen, Germany; and [c]Physikalisch Technische Bundesanstalt (PTB), Bundesallee 100, 38116 Braunschweig, Germany

It has been proposed that the radiation-induced bystander effect is mediated through gap junctional communication and/or diffusible cellular factors excreted from irradiated cells in the growth medium (*1*). Gap junction channels consisting of connexin (CX) proteins may mediate bystander effects by allowing direct intercellular exchanges of small molecules, ions and second messengers (cAMP, IP_3, Ca^{2+}) up to 1 kDa between irradiated and nonirradiated bystander cells. The effects of mediators of the paracrine effects, free radicals (ROS, NO) and soluble factors like cytokines such as tumor necrosis factor (TNF), interleukin 1 and 8 (IL1, IL8), and transforming growth factor β1 (TGFB1) are detected by performing medium transfer experiments (*2*). To discriminate between these two mechanisms, we used noncommunicating Jeg3 malignant trophoblast cells transfected with the inducible gap junction protein Conexin 43 using the tet-on system. This cell line is useful to analyze the different channel functions upon various mediators and stress factors. After induction of the connexins with doxycycline, the different cell lines demonstrate strong expression of connexin mRNA and protein correlated with a strong coupling efficiency (GJIC) as measured by Calcein dye transfer (*3*). These CX-inducible cell lines represent an appropriate system to evaluate radiation-induced bystander effects which can be studied in the presence or absence of GJIC within the same cell clone.

Investigation of Jeg3 Cell Lines for Modulation of CX43 Expression upon Irradiation

It is well known that the level of gap junctional communication is influenced by radiation. Azzam *et al.* (*4*) could demonstrate an up-regulation of CX43 in fibroblasts and epithelial cells after γ and α-particle irradiation. For this reason, the possible influence of X rays on modulation of CX43 expression was analyzed first before the bystander experiments were started. Upon irradiation, Jeg3 cells do not reveal any induction of endogenous changes in the exogenous level of CX43 transcript/protein and coupling efficiency (*5*). Thus this cell line represents an ideal cell system for analyzing bystander effects in association with and without the presence of gap junctional communication. The bystander effect was investigated using two different systems for long- and short-term evaluation.

Evaluation of Long-Term Bystander Effects Using a Coculture System and Cell Sorting

First we used a long-term coculture system with bystander cells cocultured with irradiated cells. After irradiation with 5 Gy X rays, the level of activated tumor suppressor protein TP53, an indicator for radiation-induced bystander effects, in the Jeg3 cells was already highly elevated 15 min after irradiation independent of gap junctional communication properties and decreased 1 h after irradiation. For coculturing, the directly irradiated and DiI membrane stained cells were mixed and cultivated with

unstained, nonirradiated bystander cells for 4 h. The coculture time of 4 h is needed for the formation of cell-cell membrane contacts between the two cell populations and is defined as the time leading to the strongest coupling efficiency. After cocultivation, irradiated cell populations were separated from nonirradiated cells by flow cytometry. In a parallel approach, the coupling properties were confirmed by measuring the degree of gap junctional coupling by fluorescence-activated cell sorting (FACS) using the gap junction permeable dye Calcein. The bystander effect evoked by radiation was measured analyzing activated TP53 in irradiated and nonirradiated cells. Independent of gap junctional communication, the nonirradiated bystander cell population revealed a significant up-regulation of TP53 compared to the nonirradiated control culture, but TP53 expression was less elevated compared to the irradiated cell population. The bystander effect could be verified by the analysis of the parental Jeg3 cells as a further control to exclude clonal specificity due to the transfection procedure. In conclusion, using a coculture system, we could find evidence for a bystander effect, but the bystander effect in the CX43-inducible Jeg3 cell line does not appear to be mediated through CX43 channels but rather by paracrine mechanisms through cellular factors excreted in the medium.

Evaluation of Short-Term Bystander Effects Using the Single-Cell Irradiation with the PTB Microbeam

Together with the group at the microbeam facility of the PTB, Braunschweig, we previously established and standardized the single-cell irradiation of parental Jeg3 and CX43 inducible Jeg3 cells with α particles using TP53 measured 30 min after targeting the nuclei of selected cells by immunofluorescence. In this second system, we want to analyze (1) whether these bystander responses also occur in a cell monolayer upon single-cell α-particle irradiation using the microbeam on short time scales (0–1 h) and (2) whether this bystander effect induced by different radiation types is dependent on gap junctional communication. Using the microbeam facility has the following advantages for the investigation of the role of GJIC in bystander effects:

1. Selectively irradiated cells and bystander cells are prepared identically within a single cell culture population.
2. Bystander effects that develop immediately after irradiation or on short time scales can be detected and compared with the long-term effects observed in coculture studies.
3. Precise radiation doses (selected number of particles) are delivered only to the cell nuclei or the cytoplasm.

In the present study, high-LET α particles with an energy of 4.5 MeV (typically 16 α particles) at the entrance of the attached cells were used for the irradiation (for experimental details, see the extended abstract by Greif *et al.* in these proceedings). Either 100% or 25% of all cells were exposed to α particles. The following cell lines were investigated: parental Jeg3 cells and CX43-expressing compared to CX43-nonexpressing cells. Nonirradiated Jeg3 cells served as a control. After cell irradiation, the TP53 induction in the whole cell monolayer was measured using immunofluorescence with an antibody against phosphorylated TP53. A special software module is used for automatic quantification of immunocytochemical TP53 staining that includes the positional information of the irradiation. Thus the TP53 signal of irradiated and nonirradiated cells on the same dish can be analyzed separately. The goal of the project is to correlate the signal of bystander cells with the distance from the next irradiated cell.

The first preliminary results show a tendency toward a bystander effect in Jeg3 cells after α-particle irradiation that seems to be independent of gap junctional communication.

References

1. E. I. Azzam, S. M. de Toledo and J. B. Little, Expression of CONNEXIN43 is highly sensitive to ionizing radiation and other environmental stresses. *Cancer Res.* **63**, 7128–7135 (2003).

2. E. I. Azzam, S. M. de Toledo and J. B. Little, Stress signaling from irradiated to non-irradiated cells. *Curr. Cancer Drug Targets* **4**, 53–64 (2004).

3. A. Gellhaus, X. Dong, S. Propson, K. Maass, L. Klein-Hitpass, M. Kibschull, O. Traub, K. Willecke, B. Perbal and E. Winterhager, Connexin43 interacts with NOV: A possible mechanism for negative regulation of cell growth in choriocarcinoma cells. *J. Biol. Chem.* **279**, 36931–36942 (2004).

4. E. I. Azzam, S. M. de Toledo and J. B. Little, Oxidative metabolism, gap junctions and the ionizing radiation-induced bystander effect. *Oncogene* **22**, 7050–7057 (2003).

5. F. Banaz-Yasar, R. Tischka, G. Iliakis, E. Winterhager and A. Gellhaus, Cell line specific modulation of connexin43 expression after exposure to ionizing radiation. *Cell Commun. Adhes.,* **12**, 249–259 (2005).

Studies on the Induction of the Cell Cycle Regulator CDKN1A (p21) in Bystander Cells Using the GSI Heavy-Ion Microbeam

Ph. Barberet,[a] C. Fournier,[b] F. Knauf,[b] M. Heiß,[a] B. E. Fischer[a] and G. Taucher-Scholz[b]

[a]Materials Research and [b]Biophysics, Gesellschaft für Schwerionenforschung, 64291 Darmstadt, Germany

Since the first successful targeted cellular irradiations in 2003, the GSI microbeam has been fully operational for the investigation of cellular responses to high-LET particles (*1*). The technical design of this setup as well as its ability to target cells precisely in culture has been described previously in detail (*2*). The high selectivity provided by microbeam facilities makes them particularly useful for the investigation of the radiation response in bystander cells, i.e., cells that have not been irradiated themselves but are in proximity to irradiated ones. During the last years, an increasing number of studies, and especially studies using microbeams, have reported the induction of radiation responses in bystander cells for various end points (*3, 4*). Up to now, these studies were performed mainly with low-LET or α-particle radiation. However, results indicating that such an effect could take place for higher-LET particles have recently emerged (*5*). A bystander radiation response may affect the space radiation risk assessment, and it is also interesting in connection to the normal tissue response after heavy-ion radiotherapy. Therefore, further investigations taking advantage of higher-LET microbeams are clearly desirable.

The aim of this study was to investigate the induction of the cell cycle regulator CDKN1A (p21), an important player in the cellular response to ion irradiation (*6, 7*). In various studies, the CDKN1A protein has been reported to be involved in bystander effects after low-LET and α-particle irradiations (*8, 9*). Furthermore, recent data obtained after exposure to low fluences of carbon ions have shown a slight overall increase of the protein level (*10*). Since irradiation with the GSI microbeam allows a clear identification of the targeted cells, this technique was used to assess the levels of CDKN1A in irradiated and unirradiated cells as well as the distribution of the amounts of CDKN1A in the potentially responding cells.

Cell Culture and Immunostaining

For this study, confluent monolayers of normal human fibroblasts (AG01522) were used. The cells were grown under standard conditions (95% air, 5% CO_2, 37°C) in cell dishes designed specifically for microbeam irradiations essentially as described previously (*2*). Briefly, 3 days before irradiation, 5000 cells were plated on the center of the 4-μm-thick polypropylene foil constituting the base of the microbeam cell dish. The foil was coated with Cell-Tak adhesive (Becton Dickinson, Bedford, MA) to enhance cell attachment. One hour prior to irradiation, the cell nuclei were stained with 200 n*M* Hoechst 33342 for automatic detection during the irradiation process.

Since the quantification of proteins using immunofluorescence staining requires identical experimental conditions, the irradiated cells, the bystander cells and the control cells should optimally belong to the same cell dish to undergo the same treatment during fixation and immunostaining. On the other hand, to account for a possible transmission of a bystander signal in the medium, a specific cell dish was designed to keep the control cells completely separated from the targeted ones. In this setup (referred to as a divided sample), a separating wall is introduced in the middle of the chamber to avoid any contact between the medium in the two compartments during the irradiation process. The water impermeability is ensured on the beam entry side by the candle wax (stearin) used to paste the polypropylene foil to the dish (*2*) and on the back side by a thin layer of silicon paste (G. E. Bayer Silicones, Baysilone-paste) applied between the cover glass and the wall. Up to now this setup has been used only in the case of carbon-ion irradiations.

The cells were fixed and immunostained 3 h after irradiation as described previously (*6*). In addition, the cells were co-stained for γ-H2AX to visualize the DNA damage induced by the ion traversals and thus to allow a reliable reidentification of the irradiated cells. After immunostaining and repositioning, the fluorescence intensities of the nuclei were visualized and recorded using a fluorescence microscope equipped with a CCD camera. The recorded signals were corrected for background fluorescence and inhomogeneities of the illumination.

Microbeam Irradiations

In each sample, 60 positions regularly distributed over the whole sample following a circular concentric pattern and ~500 μm distant from each other were visited by moving the sample positioning system of the microbeam. All these fields were exposed to UV radiation for cell recognition, but the cells were irradiated in only one half of the sample, the other half being used as a control. Depending on the sample, either one cell or six cells were targeted per field of view of the microbeam, leading to a proportion of 0.5% and 3%, respectively, of the total population. The same irradiation protocol was applied to the divided cell chamber, the only difference being the physical separation during the irradiation.

The irradiations were performed with either carbon (4.8 MeV/nucleon, 300 keV/μm) ions or argon (4.8 MeV/nucleon, 1950 keV/μm) ions. The single targeted cells were always irradiated with five ions per nucleus distributed on a cross pattern, allowing an easier reidentification after immunostaining. In all experiments, the few irradiated cells were unambiguously identified by means of the cross pattern of coimmunostained γ-H2AX foci.

Results and Discussion

The analysis of the immunofluorescence signal intensities revealed a broad distribution of the cellular levels of CDKN1A protein even in the control population, both by visual inspection and by quantitative analysis of the intensity distribution. This great heterogeneity could be reflecting a certain variability in the status of the cells within the population. In the samples where 0.5% to 3% of the cells were selectively irradiated with carbon ions, the cell population showed a slight but reproducible overall enhancement of the CDKN1A level compared to the mock-irradiated cell samples (either from control dishes or from the opposite side of the divided sample) measured 3 h after irradiation. A mean increase, close to 1.3-fold, was measured regardless of the percentage of cells irradiated, in good agreement with the results obtained after exposure to low fluences of carbon ions, when the same proportions of cells were hit (*10*). According to the measured distributions of the cellular CDKN1A levels, only a minor fraction of the bystander cells in the divided chamber setup showed a very high level of the protein, above a threshold defined as the mean intensity of the controls plus one standard deviation. Rather, the total population of bystander cells contributes to the enhanced overall response. Indeed, the intensity distribution in the bystander population was globally shifted to a higher mean value compared to the control population, but the distribution pattern was preserved.

Based on evaluation by eye, the cells showing an increased protein level were distributed randomly in the cell dish. To determine the spatial distribution of bystander cells showing elevated levels of CDKN1A, the immunofluorescence intensity was analyzed as a function of the radial distance to the irradiated cells for both carbon- and argon-ion irradiations. A clearly detectable average induction of CDKN1A (at least twofold) was found in the hit cells. The quantitative evaluation of CDKN1A in bystander cells located within concentric rings around the targeted cells showed that the nuclear levels of the protein were not dependent on the radial distance to the irradiated cells up to a distance of 200 μm. Thus, as also supported by visual evaluation, no clusters of bystander cells showing increased levels of CDKN1A were found in the direct neighborhood of the irradiated cells.

In conclusion, a bystander response for CDKN1A expression was observed in human fibroblasts after carbon-ion irradiations, i.e., for particles with an LET two times higher than for α particles. However, the induced bystander effect is weak and is in no case higher than the one observed after low-LET or α-particle irradiation (*8, 9*), although the different experimental conditions may hinder a direct comparison. The fact that in our experiments no clusters of responding cells were observed in the neighborhood of the targeted cells could be indicative of a medium-mediated signal transmission from the irradiated to the bystander cells coexisting with the gap junction communication pathways. Experiments involving medium transfer after ion irradiation to restrict the signals to secreted factors are in progress to clarify the underlying transmission mechanism.

Acknowledgments

This work was supported by BMBF (02S8203) and EU Grant CELLION MRTN-CT-2003-503923.

References

1. M. Heiss, B. E. Fischer and M. Cholewa, Status of the GSI microbeam facility for cell irradiation with single ions. *Radiat. Res.* **161**, 98–99 (2004). [extended abstract]
2. M. Heiß, B. E. Fischer, B. Jakob, C. Fournier, G. Becker and G. Taucher-Scholz, Targeted irradiation of mammalian cells using a heavy-ion microprobe. *Radiat. Res.* **165**, 231–239 (2006).
3. K. M. Prise, G. Schettino, M. Folkard and K. D. Held, New insights on cell death from radiation exposure. *Lancet Oncol.* **6**, 520–528 (2005).
4. E. J. Hall and T. K. Hei, Genomic instability and bystander effects induced by high-LET radiation. *Oncogene* **22**, 7034–7042 (2003).
5. C. Shao, Y. Furusawa, Y. Kobayashi, T. Funayama and S. Wada, Bystander effect induced by counted high-LET particles in confluent human fibroblasts: A mechanistic study. *FASEB J.* **17**, 1422–1427 (2003).
6. B. Jakob, M. Scholz and G. Taucher-Scholz, Immediate localized CDKN1A (p21) radiation response after damage produced by heavy-ion tracks. *Radiat. Res.* **154**, 398–405 (2000).
7. C. Fournier, C. Wiese and G. Taucher-Scholz, Accumulation of the cell cycle regulators TP53 and CDKN1A (p21) in human fibroblasts after exposure to low- and high-LET radiation. *Radiat. Res.* **161**, 675–684 (2004).
8. E. I. Azzam, S. M. de Toledo and J. B. Little, Direct evidence for the participation of gap junction mediated intercellular communication in the transmission of damage signals from alpha-particle irradiated to non-irradiated cells. *Proc. Natl. Acad. Sci. USA* **98**, 473–478 (2001).
9. H. Yang, N. Asaad and K. D. Held, Medium-mediated intercellular communication is involved in bystander responses of X-ray-irradiated normal human fibroblasts. *Oncogene* **24**, 2096–2103 (2005).
10. C. Fournier, F. Knauf, C. Sieben, G. Becker, M. Heiss, P. Barberet, B. Fischer, M. Scholz, S. Ritter and G. Taucher-Scholz, Advanced studies on the bystander response after exposure of human fibroblasts

to low fluences and targeted irradiation with heavy ions. In *GSI Annual Report 2004,* http://www.gsi.de/annrep2004.

Radiation-Induced Bystander Effects with a 12.5 keV X-Ray Microbeam

E. A. Blakely,[a] A. C. Thompson,[a] R. I. Schwarz,[a] P. Chang,[a,b] K. Bjornstad,[a] C. Rosen,[a] C. Wisnewski,[a] D. Mocherla[a] and B. Parvin[a]

[a]Life Sciences Division, Lawrence Berkeley National Laboratory, Berkeley, California; and [b]SRI International, Menlo Park, California

Introduction

There have been several approaches to quantitatively measure low-dose bystander effects from low-LET radiation sources, including studies involving medium transfer from irradiated cells to unirradiated cells, mixing irradiated cells with nonirradiated cells, and coculturing of cells labeled with tritiated thymidine with nonlabeled cells (*1*). Few studies, however, have been able to analyze the spatial range of effectiveness of bystander effects from directly targeted cells with sufficient measured precision of the dose profiles and adequate statistics (*2*). We are addressing these issues in bystander studies with human mammary epithelial cells (HMEC) irradiated with a unique synchrotron-based 12.5 keV X-ray Microbeam line 10.3.1 at the Advanced Light Source (ALS) at Lawrence Berkeley National Laboratory (LBNL) (*3*) with capability for a focused spot size of 2 μm^2 and a wide range of doses and dose rates.

Materials and Methods

Cultures of HMEC (*4*) that are phenotypically normal and nonmalignant but with an extended life span in culture were grown in Lab-Tek 4-well chamber plastic slides and irradiated in studies presented here with precise stripes of dose 18 mm long and up to 100 μm wide ranging from 10 cGy to 1 Gy. The 100-μm-wide 12.5 keV beam is produced with a multilayer monochromator and a precision slit system. The intensity of the beam is calibrated before sample irradiation with both an argon-filled ion chamber and a calibrated silicon diode. An on-axis optical camera is used to locate fiducial marks on the sample slide. Each well measures 10 mm × 22 mm. The slide is covered with a liquid-tight but gas-permeable membrane to permit it being held vertical during the 2–3-min irradiation of the slide with the fixed horizontal beam. A single X-ray exposure is delivered in three of the four wells to allow for an unirradiated control well. In some experiments, two dose stripes have been delivered per well with variable distances between them to determine whether bystander effects can be additive between two targeted sources.

Samples are processed for the expression of the radiation-induced protein marker $p53^{ser15}$ phosphorylation with fluorescence immunohistochemistry in a time course from 10 min to several hours after exposure with variable times of fixation by −20°C 100% methanol. Using fluorescence microscopy on a high-precision-controlled microscope stage and fiducial marked references, the physical locations of the dose stripes are mapped exactly to the location of the biological responses. Analysis of radiation-induced fluorescent signals was completed with a computer-based system that objectively measures the signal on individual DAPI-stained cell nuclei in both the targeted dose stripe and untargeted adjacent cells. In effect, we are able to objectively evaluate the widening of the dose stripe with time to include bystander cells using five or more montages of 30 images representing several thousand cells for each experimental sample. Data from replicate experiments are combined. Some samples were pretreated with 40 μ*M* lindane for 1 h to inhibit gap junction intracellular communication (GJIC).

Results and Discussion

We have completed a quantitative physical assessment of our 12.5 keV X-ray microbeam beam profile and measurements of dose- and time-dependent bystander effects on $p53^{ser15}$ phosphorylation in the untargeted regions adjacent to the dose stripe. Data analyses are in progress to evaluate the spatial range and duration of the bystander effects over the dose range studied as well as the effects of lindane and the double dose stripes separated by varying distances. We find that the time course of the integrated fluorescence response of targeted and untargeted cells shows both a time and dose dependence. We show that the spatial distance of bystander effects from our low-LET radiation is much less and has a shorter range of effectiveness compared to published reports of cells irradiated with high-LET microbeams.

Acknowledgments

This work was supported by the U.S. DOE Low Dose Radiation Research Program under Contract No. DE-AC02-05CH11231. The Advanced Light Source is supported by the Director, Office of Science, Office of Basic Energy Sciences, of the U.S. Department of Energy under Contract No. DE-AC02-05CH11231.

References

1. K. M. Prise, M. Folkard and B. D. Michael, Bystander responses induced by low LET radiation. *Oncogene* **22**, 7043–7049 (2003).
2. M. Sowa Resat and W. F. Morgan, Microbeam developments and applications: A low linear energy transfer perspective. *Cancer Metastasis Rev.* **23**, 323–331 (2004).
3. A. C. Thompson, E. A. Blakely, K. A. Bjornstad, P. Y. Chang, C. J. Rosen, D. Sudar and R. I. Schwarz, Micobeam studies of low-dose X-ray bystander effects on epithelial cells in fibroblasts using synchrotron radiation. *Radiat. Res.* **161**, 101–102 (2004). [extended abstract]
4. P. Briand, D. V. Nielsen, M. W. Madsen and O. W. Peterson, Trisomy 7p and malignant transformation of human breast epithelial cells following epidermal growth factor withdrawal. *Cancer Res.* **56**, 2039–2044 (1996).

Bystander Killing in Normal Human Fibroblasts by Heavy-Ion Microbeams

N. Hamada,[a,b] M. Ni,[b] T. Funayama,[b] T. Sakashita,[b] T. Kakizaki,[b] S. Wada,[b] Y. Yokota[c] and Y. Kobayashi[a,b]

[a]Department of Quantum Biology, and The 21st Century Center of Excellence (COE) Program, Gunma University Graduate School of Medicine, 3-39-22 Showa-machi, Maebashi, Gunma 371-8511, Japan; and [b]Microbeam Radiation Biology Group and [c] Gene Resource Research Group, Japan Atomic Energy Agency (JAEA), 1233 Watanuki-machi, Takasaki, Gunma 370-1292, Japan

We have developed a system of collimated microbeams, in which four kinds of heavy charged particles with a range of linear energy transfer (LET) from 103 to 1230 keV/μm are available at Takasaki Ion Accelerators for Advanced Radiation Application (TIARA) of JAEA (*1–3*). Using this system, the current investigation aims to characterize the dependence of bystander responses on LET in confluent density-inhibited normal human fibroblast AG01522 cells under conditions such that intercellular interactions are facilitated. Clonogenic survival assays preliminarily revealed that targeted irradiation of less than 0.005% of the whole population with a microbeam of carbon ions (220 MeV, 103 keV/μm) resulted in nearly 10% cell death, indicating the induction of bystander responses. In addition, apoptosis in the bystander population was detected with TdT-mediated dUTP nick end-labeling assay and was found to peak at 24 h postirradiation. The frequency of apoptotis increased at least up to 72 h after the random irradiation with 10% survival doses of broad beams of heavy ions. These preliminary results imply that the death modes are temporally distinct in irradiated cells and nonirradiated bystanders. Experiments to confirm the reproducibility of the data are ongoing.

Acknowledgments

This work was supported by a Grant-in-Aid for the 21st Century COE Program for Biomedical Research Using Accelerator Technology from the Ministry of Education, Culture, Sports, Science and Technology of Japan, and by the TIARA Research Program (51033).

References

1. T. Funayama, S. Wada, Y. Kobayashi and H. Watanabe, Irradiation of mammalian cultured cells with a collimated heavy-ion microbeam. *Radiat. Res.* **163**, 241–246 (2005).
2. Y. Kobayashi, T. Funayama, S. Wada, M. Taguchi and H. Watanabe, System of cell irradiation with a precise number of heavy ions. *Radiat. Res.* **161**, 90–91 (2004). [extended abstract]
3. Y. Kobayashi, T. Funayama, S. Wada, Y. Furusawa, M. Aoki, C. Shao, Y. Yokota, T. Sakashita, Y. Matsumoto and N. Hamada, Microbeams of heavy charged particles. *Biol. Sci. Space* **18**, 235–240 (2004).

Is the Plasma Membrane a Target for Generation of Signals to Bystanders?

J. H. Miller, B. Ginovska and W. E. Wilson

Washington State University Tri-Cities, Richland, Washington 99354

Radiation-induced bystander effects have been investigated extensively using microbeam probes. Studies at the Gray Cancer Institute with chromosomal damage as the biological end point suggested a strong dependence of bystander effects on radiation quality (*1*). When exposures were normalized to the same dose to the nucleus of targeted cells, ^{3}He ions were much more effective than soft X rays. Recognizing that ^{3}He ions at an initial stopping power of 100 keV/μm have much greater penetration than a carbon-K characteristic X ray, we investigated the hypothesis that the plasma membrane in contact with the growth medium is a target for generation of damage-inducing signals to bystander cells.

Transport of ^{3}He ions through cells was modeled with tracks simulated by PITS (*2*) and the absorption of soft X rays was simulated by XPITS, a code recently developed by Wilson. The geometry of an attached cell was modeled based on confocal microscopy data (*3*). Recognizing that cell thickness changes during attachment and that this parameter of the model is important for determining the dose to the part of the plasma membrane in contact with the growth medium, we considered two cell models, one for the fully attached cell and one for a cell 4 h after plating. In both cases, the geometry contained five compartments: nucleus, cytoplasm, nuclear membrane, plasma membrane in contact with the plate, and plasma membrane in contact with the growth medium. Along the projected beam axis, the total thickness of the model was 10 μm for a cell 4 h after seeding and 5 μm for a fully attached cell. Differences in material composition and density of different compartments were ignored; however, differences in size and geometric relationship to the beam entry point are probably the major factors determining the variations in dose to different compartments, and these factors were included in the model.

Following the normalization procedure of Prise *et al.* (*1*), we calculated the dose to the plasma membrane in contact with the growth medium subject to the constraint that the dose to the nucleus was 1 Gy. For the thick model of an anchorage-dependent cell 4 h after seeding, two ^{3}He ions deposited about 1 Gy in the nuclear compartment of the model. Four ^{3}He ions were required to give a nuclear dose of this magnitude in the thinner model of a fully attached cell. A total of 100,000 cases were run to obtain good statistics on doses to each compartment from ^{3}He-ion irradiations. Regardless of the thickness of the model, about 12,000 soft X-ray photons were required to impart a nuclear dose of 1 Gy, due to the large number of photons absorbed in the Mylar substrate and the compartment traversed before reaching the nuclear compartment. A total of 10,000 cases of 12,000 injected photons were run to accumulate good statistics on doses in all compartments.

For the thick model of an anchorage-dependent cell 4 h after seeding, ^{3}He ions delivered a dose to the plasma membrane in contact with the growth medium that was about 10% of the nuclear dose and a factor of 10 greater than the dose delivered to the plasma membrane in contact with the growth medium by soft X rays for the same nuclear dose. Similar but less dramatic results were found for the thin model of a fully attached cell. In this case the dose to the membrane is about 16% for the nuclear dose for energy deposited by ^{3}He ions and about 5% of the nuclear dose for soft X rays. When attached cells are irradiated from below the dish, ^{3}He ions clearly have greater capacity to deliver energy to the part of the plasma membrane that is in contact with the growth medium. If dose to this compartment is effective in releasing molecules that diffuse to neighboring cells, then ^{3}He ions would be expected to deliver a stronger signal of this type than soft X rays for the same dose to the nucleus of the cell.

The differences in the distribution of doses delivered to cellular compartments by ^{3}He ions and soft X rays are primarily due to differences in beam attenuation per unit of penetration. Attenuation of the soft X-ray beam is approximately exponential with penetration, while the rate of energy deposition by the ^{3}He ions is only weakly dependent on penetration. Otherwise, the spatial properties of the beams are very similar. Beam divergence is minimal, and energy deposition is concentrated near the beam axis. These properties of the beams imply that dose delivered to the plasma membrane in contact with the growth medium will be highly nonhomogeneous with very high concentrations of energy on the nanometer scale. Total membrane dose is probably a poor starting point for modeling bystander signal production, and our future work in this area will focus on specific targets within the membrane, such as lipid rafts, which are important for cellular signaling (*4*) and have been implicated in bystander effects (*5*). Nevertheless, our results thus far illustrate the heterogeneity of cellular dose that can result from different microbeam probes and may suggest new experiments to gain a better understanding of the origin of signals that influence neighboring cells.

References

1. K. M. Prise, M. Folkard and B. D. Michael, Bystander responses induced by low LET radiation. *Oncogene* **22**, 7043–7049 (2003).
2. W. E. Wilson, J. H. Miller and H. Nikjoo, PITS: A code set for positive ion truck structure, In *Computational Approaches in Molecular Radiation Biology* (M. N. Varma and A. Chatterjee, Eds), pp. 137–153. Plenum Press, New York, 1994.
3. G. Schettino, M. Folkard, K. M. Prise, B. Vojnovic, K. D. Held and B. D. Michael, Low-dose studies of bystander cell killing with targeted soft X rays. *Radiat. Res.* **160**, 505–511 (2003).
4. K. Simons and D. Toomre, Lipid rafts and signal transduction. *Nat. Rev. Mol. Cell. Biol.* **1**, 31–39 (2000).
5. H. Nagasawa, A. Cremesti, R. Kolesnick, Z. Fuks and J. B. Little, Involvement of membrane signaling in the bystander effect in irradiated cells. *Cancer Res.* **62**, 2531–2534 (2002).

Comparisons of Bystander Responses Observed in Two-Dimensional and Three-Dimensional Systems after Microbeam Irradiation

Brian Ponnaiya, Gloria Jenkins-Baker, Gerhard Randers-Pehrson and Charles R. Geard

RARAF, Center for Radiological Research, Columbia University, New York, New York

While there are considerable data documenting bystander responses after irradiation with high-LET radiation, very little is known about the mechanisms underlying the phenomenon. To better understand how irradiation of a cell can give rise to similar biological responses in neighboring nonirradiated cells, we have examined signaling pathways in both irradiated and bystander cells using the charged-particle microbeam at Columbia University. These studies have been conducted in the context

of the cellular environment to test the hypothesis that responses that arise due to communication between cells in two dimensions (cellular monolayers) may be different from those observed in cells in a three-dimensional matrix.

We have previously used the charged-particle microbeam to establish bystander responses between cells grown as monolayers. Using this approach we have shown that normal human fibroblast bystander cells have higher yields of micronuclei and increased periods of cell cycle delay (*1*). Furthermore, we have demonstrated increased levels of CDKN1A (p21/WAF1) and the enhanced phosphorylation of MAP kinase signaling molecules in bystander cells when compared to nonirradiated control cells.

Here we present data of bystander responses observed in three-dimensional artificial skin tissues (EpiDerm, MatTek, Ashland, MA) after microbeam irradiation. The tissue consists of normal, human epidermal keratinocytes that have been cultured to form a multilayered, differentiated model of the human epidermis containing about 10–12 cell layers (75–100 μm thick). It closely resembles human skin microarchitecture with *in vivo*-like morphological and growth characteristics and has been used previously to demonstrate apoptosis and micronuclei in bystander cells (*2*).

Initial studies concentrated on establishing immunohistochemical protocols to assay the induction of specific proteins and specific phosphorylation events in these tissues. Tissues were irradiated and fixed in formalin at 15, 30, 45 and 60 min postirradiation, after which they were embedded in paraffin, sectioned and placed on microscope slides. Immunohistochemical analyses were performed with specific antibodies using a biotin-free Tyramide Signal Amplification system (DAKO).

Both irradiated and bystander cells showed elevated levels of CDKN1A protein at all the times assayed. This pattern of induction was mirrored in the enhanced phosphorylation of p53 at serine 15. This specific phosphorylation event has been linked to the activation of ATM after exposure to ionizing radiation. In addition, proteins in the MAP kinase signaling pathways were found to be activated (phosphorylated) in both irradiated and bystander cells. Specifically, JNK and ATF2 were seen to be phosphorylated at higher levels in irradiated and bystander cells when compared to time-matched controls. Studies are ongoing to examine the relationship between the immunohistochemical results presented here and the induction of micronuclei and apoptosis.

References

1. B. Ponnaiya, G. Jenkins-Baker, D. J. Brenner, E. J. Hall, G. Randers-Pehrson and C. R. Geard, Biological responses in known bystander cells relative to known microbeam-irradiated cells. *Radiat. Res.* **162**, 426–432 (2004).
2. O. V. Belyakov, S. A. Mitchell, D. Parikh, G. Randers-Pehrson, S. A. Marino, S. A. Amundson, C. R. Geard and D. J. Brenner, Biological effects in unirradiated human tissue induced by radiation damage up to 1 mm away. *Proc. Natl. Acad. Sci USA* **102**, 14203–14208 (2005).

Tracking Down the Bystander Response

E. L. Pyke,[a] D. L. Stevens,[a] S. Gaillard,[b] M. Fromm[b] and M. A. Hill[a]

[a]MRC Radiation and Genome Stability Unit, Harwell, Oxfordshire OX11 0RD, United Kingdom; and [b]Laboratoire de Microanalyses Nucléaires Alain Chambaudet, UMR CEA-E4, Université de Franche-Comté 16, route de Gray, 25030 BESANCON Cedex, France

Introduction

Exposure to ionizing radiation can induce a wide variety of biological responses not only in cells traversed by radiation but also within nonexposed neighboring cells that have not received any energy deposition. These nonirradiated cells respond to ''signals'' produced by the irradiated cells that may be transmitted either by direct cell-to-cell contact (through gap junctions) or indirectly (through secreted factors). This well established phenomenon has been referred to as the bystander effect (for reviews, see *1–4*) and is particularly relevant to the low doses and dose rates associated with typical human environmental exposures, where cells in the body will rarely see more than one α-particle track or one isolated electron, with many cells receiving none, over many days to years. The biological effects of α particles are of particular interest since radon with its α-particle-emitting progeny is the dominant natural source of environmental exposure, contributing ~50% of the average effective dose to the general population.

Although microbeams provide a very useful tool for studying bystander effects, few are fully operational worldwide, the irradiation of many samples may be time-consuming, and technical and practical constraints limit protocol choices for particular biological systems. A range of non-microbeam techniques have been developed at the Medical Research Council (MRC), Harwell, which are being used to address some of the questions raised in the bystander field, using both high-LET α particles and low-LET ultrasoft X rays (M. A. Hill *et al.,* manuscript submitted for publication).

Induction of CDKN1A, a cyclin-dependent kinase inhibitor that is transcriptionally activated by TP53, is an integral part of cell growth arrest and would therefore be an effective reporter system for measuring initial DNA damage caused by radiation by its increase in induction. It also provides a means of visualizing whether the ATM/TP53 pathway and therefore downstream genes are up-regulated in bystander cells in response to signals from damaged cells. To examine the signal-induced changes in CDKN1A levels, we employed a cell coculture irradiation system and also partially irradiated a confluent monolayer through a half-shield with a fixed blade providing a well-defined edge to allow close monitoring of the distance over which any signal may induce changes in unirradiated neighbor cells. Further characterization of the distance response was achieved by using a CR39 nuclear track etch detector to determine the precise location of each α-particle track traversal.

Methodology

Cells were exposed to an essentially monoenergetic beam (3.26 ± 0.22 MeV; LET 121 keV μm^{-1}) using the MRC ^{238}Pu irradiator (*5*). The coculture system and partially shielded irradiations were as described in Hill *et al.* (*6*). To produce a distinct edge in the partially shielded dishes, a razor blade was attached to the base of the dish to determine the response with distance from the irradiated area. More precise measurements are currently being made by using dishes on which a 10-μm layer of CR39 has been polymerized onto a 2.5-μm PET base (*7*). Subsequent etching of the CR39 with 10 *M* KOH at 37°C reveals pits at the site of α-particle traversal.

Cell Culture and Immunohistochemistry

The cell culture and immunohistochemical staining were performed essentially as by Azzam *et al.* (*8*) but with modifications for use with the Hostaphan-based irradiation dishes as described above. Cells were fixed 3 h postirradiation prior to staining for CDKN1A expression and/or etching. The antifade agent Vectashield containing propidium iodide (Vector, UK) was used in mounting the samples prior to confocal microscopy. The propidium iodide (PI)-stained nuclei and the nuclear CDKN1A-FITC signals were obtained independently and merged for a number of fields of view, enabling both total cells present and the proportion that were found to express elevated levels of CDKN1A to be counted. With the CR39-based dishes, images of the pits were taken by reflective confocal microscopy and merged with the relevant fluorescent image to produce a composite picture, allowing track traversal to be related precisely to responding cells and a distance over which a bystander signal may exert an influence.

Results and Conclusions

Results obtained for the coculture experiments showed an increase in the CDKN1A levels of the nonirradiated cells grown on the insert over

a range of doses from 0.005 to 1 Gy. Increased CDKN1A levels were also observed in the unirradiated side of a half-shielded dish. Closer examination with the blade experiments has indicated that for standard dishes there is a distance-related bystander response particularly at 0.5 Gy up to a distance of 200 μm and that the response at greater distances remains relatively constant (but is still elevated compared to control levels). However, initial studies after 0.125 Gy have not shown any noticeable decrease with distance. These responses are currently being characterized in a more precise fashion using the CR39-based dishes to clearly define which individual cells have been irradiated. The current results indicate that direct cell-cell signaling does play a role in the bystander response with an additional component from medium-borne factors.

References

1. C. Mothersill and C. B. Seymour, Radiation-induced bystander effects: Past history and future directions. *Radiat. Res.* **155**, 759–767 (2001).
2. E. J. Hall, The bystander effect. *Health Phys.* **85**, 31–35 (2003).
3. W. F. Morgan, Non-targeted and delayed effects of exposure to ionizing radiation: I. Radiation-induced genomic instability and bystander effects *in vitro*. *Radiat. Res.* **159**, 567–580 (2003).
4. E. I. Azzam and J. B. Little, The radiation induced bystander effect: Evidence and significance. *Hum. Exp. Toxicol.* **23**, 61–65 (2004).
5. D. T. Goodhead, D. A. Bance, A. Stretch and R. E. Wilkinson, A versatile plutonium-238 irradiator for radiobiological studies with alpha particles. *Int. J. Radiat. Biol.* **59**, 195–210 (1991).
6. M. A. Hill, J. R. Ford, P. Clapham, S. J. Marsden, D. L. Stevens, K. M. S. Townsend and D. T. Goodhead, Bound PCNA in nuclei of primary rat tracheal epithelial cells after exposure to very low doses of plutonium-238 alpha particles. *Radiat. Res.* **163**, 36–44 (2005).
7. S. Gaillard, V. Armbruster, M. A. Hill, T. Gharbi and M. Fromm, Production and validation for alpha-particle radiobiological experiments. *Radiat. Res.* **163**, 343–350 (2005).
8. E. I. Azzam, S. M. Toledo, T. Gooding and J. B. Little, Intercellular communication is involved in the bystander regulation of gene expression in human cells exposed to very low fluences of alpha particles *Radiat. Res.* **150**, 497–504 (1998).

Long-term Biological Bystander Effects of Microbeam Irradiation in 3D Human Tissue Models

O. A. Sedelnikova,[a] A. Nakamura,[a] O. Kovalchuk,[b] I. Koturbash,[b] S. A. Mitchell,[c] S. A. Marino,[c] D. J. Brenner[c] and W. M. Bonner[a]

[a]Laboratory of Molecular Pharmacology, Center for Cancer Research, National Cancer Institute, NIH, Bethesda, Maryland; [b]Department of Biological Sciences, University of Lethbridge, Lethbridge, Alberta, Canada; and [c]Radiation Accelerator Research Facility, Center for Radiological Research, Columbia University, New York, New York

Irradiated cells can induce genomic instability in unirradiated neighboring cells *in vitro*. This phenomenon, the radiation-induced bystander effect, has important implications for radiotherapy and diagnostic radiology and for low-dose radiation protection as well as for human health.

Recently we have shown that DNA DSBs are involved in the cellular bystander response. Using γ-H2AX focus formation as an indicator of DNA DSBs (*1, 2*), we have detected an increase in the incidence of γ-H2AX foci in bystander cell populations cultured in medium conditioned on γ-irradiated cells or cocultured with cells that had been irradiated with an α-particle microbeam or a γ irradiator (*3*). In the α-particle experiments, we have been able to distinguish γ-H2AX focus formation in irradiated and bystander cells by using a vital stain to mark one population. Directly irradiated cells exhibited the expected early and linear dose-dependent γ-H2AX focus formation, and most of the foci were repaired by 18 h postexposure. In contrast, bystander cells exhibited a slower increase in γ-H2AX foci, and the levels remained elevated up to 48 h postirradiation. The bystander response has been found to be independent on the dose of radiation. The DNA DSB nature of γ-H2AX foci was confirmed by their colocalization with DSB repair proteins. Thus we concluded that DSB formation is an early step in the bystander effect and that these DSBs may be responsible for its downstream manifestations.

Until now, most of the bystander effect studies have been performed on conventional 2D cell cultures that lack the geometric arrangement and cell-cell communication present in tissues. Use of artificial 3D tissues is a means to overcome the deficiencies of cultured cell studies and obtain important information relevant to the bystander effects *in vivo*. Recently Belyakov *et al.* (*4*) have reported induction of micronuclei and apoptosis in unirradiated cells located up to 1 mm away from irradiated cells in a reconstructed human skin.

To find out how the bystander cells deal with the increased level of DNA DSBs, we examined two human tissue models, airway (Air-100) and full-thickness skin (EFT-300) (MatTek, Ashland, MA). The airway tissue model contains epithelial cells, while the skin tissue model contains epidermal keratinocytes and dermal fibroblasts maintaining the 3D geometry and intercellular communication present *in vivo*.

After cells located in a thin plane through the tissue were microbeam-irradiated, several biological end points were measured in distal bystander cells (up to 2.5 mm away from the irradiation plane) as a function of time postexposure (0 h–7 days). Here we report an extensive increase in the incidence of DNA DSBs involving 40–60% of the distal bystander cells at 1–2 days postirradiation. The levels remained elevated for several days. These increases in DSB formation were followed by increased amounts of apoptosis and micronucleus formation, by loss of nuclear DNA methylation, and eventually by increased fraction of cells exhibiting characteristics of senescence.

These findings demonstrate for the first time the widespread nature of the bystander response in tissue models. We suggest that the radiation-induced bystander effect is a complex response initiated by DSB formation and involves multiple pathways. The long-term involvement of tissues surrounding the exposure sites may serve as a protective response in the whole organism to potentially carcinogenic DNA damage. The study points to the importance of indirect delayed biological effects of radiation in the development of cancer risk models.

Acknowledgments

We thank RARAF staff, Columbia University, for help with tissue irradiation. We are grateful to Lubomir Smilenov, Columbia University, for his continuous support and critical comments and to Robert Statz and Jordan Zaner, NIH, for their help with data entry and statistical analysis. This work was supported by the Intramural Research Program of the National Cancer Institute, Center for Cancer Research, NIH, and by the U.S. Department of Energy Low Dose Radiation Program through grants DE-FG02-03ER63632 and DE-FG02-01ER63226, and by Grants P41 EB002033-09 and P01 CA-49062 from the NIH.

References

1. E. P. Rogakou, C. Boon, C. Redon and W. M. Bonner, Megabase chromatin domains involved in DNA double-strand breaks *in vivo*. *J. Cell Biol.* **146**, 905–915 (1999).
2. O. A. Sedelnikova, E. P. Rogakou, I. G. Panyutin and W. M. Bonner, Quantitative detection of ^{125}IdU-induced DNA double-strand breaks with γ-H2AX antibody. *Radiat. Res.* **158**, 493–504 (2002).
3. M. V. Sokolov, L. B. Smilienov, E. J. Hall, I. G. Panyutin, W. M. Bonner and O. A. Sedelnikova, Radiation induces DNA double-strand breaks in unirradiated primary human fibroblasts. *Oncogene* **24**, 7257–7265 (2005).
4. O. V. Belyakov, S. A. Mitchell, D. Parikh, G. Randers-Pehrson, S. A. Marino, S. A. Amundson, C. R. Geard and D. J. Brenner, Biological effects in unirradiated human tissue induced by radiation damage up to 1 mm away. *Proc. Soc. Natl. Acad. Sci. USA* **102**, 14203–14208 (2005).

Low-LET Bystander Responses in Gap Junction Null Human Colon Carcinoma Cells (RKO36)

M. B. Sowa,[a] W. Goetz,[b] J. E. Baulch[b] and W. F. Morgan[b]

[a]Chemical Structure and Dynamics, Pacific Northwest National Laboratory, Richland, Washington 99352; and [b]Radiation Oncology Research Laboratory and Greenebaum Cancer Center, University of Maryland, Baltimore, Maryland

Introduction

Combined with sensitive molecular techniques, the microbeam has proven extremely useful in studying radiation biology (*1–3*). This technology allows individual cells or selected groups of cells to be irradiated at specific doses and dose rates. Such capabilities lend themselves well to studies of low-dose responses, delayed and nontargeted bystander effects of radiation. High- LET microbeams mimic heavy energetic particles such as the α particles associated with radon exposure and have been used in numerous biological studies (reviewed in refs. *2, 4*). Several low-LET microbeams have also been developed (reviewed in ref. *1*). One such low-LET microbeam, developed at the Pacific Northwest National Laboratory and currently located at the University of Maryland Radiation Oncology Research Laboratory, uses a variable energy electron source to mimic low-LET radiation and allows observation of how X rays and γ rays affect mammalian cells.

Methods and Materials

Cell culture. RKO36 cells from the RKO human colon carcinoma line were used in this study (*5*). Cells were grown in Dulbecco's modified Eagle's medium supplemented with 10% dialyzed fetal bovine serum, 2 m*M* L-glutamine and 1 mg/ml G418 (Research Products International). Cells were plated at 95–100% confluence on a 1.5-μm Mylar® growth substrate in 1″-diameter custom-fabricated medical grade stainless steel culture dishes (*6, 7*) and then held in humidified incubators at 37°C and 95% air/5% CO_2 for approximately 12 h prior to irradiation. For clonogenic studies, cells were trypsinized immediately after irradiation and plated at densities appropriate for resulting in 100 surviving colonies on a 100-mm culture plate. Each irradiated dish was plated into culture dishes. At 10 to 12 days postirradiation, colonies were fixed, stained with crystal violet and scored.

Irradiation procedure. The details of the electron microbeam and the standard irradiation protocol have been described in detail previously (*6, 7*), and only a summary will be given here. These experiments use the broad-beam mode of microbeam operation, which involves irradiating multiple locations with sufficient overlap of the Gaussian beam profile to provide uniform exposure at the Mylar® surface. The broad-beam capabilities are achieved using a gap between the collimation aperture and the cell substrate. The scattering characteristics of the electron beam in air have been described in ref. (*7*). Using a 5-mm air gap, the stage was stepped every 700 μm across the Mylar® dish to achieve a uniform dose distribution for a beam energy of 50 keV. Irradiations were performed at 37°C exposing 10% or 100% of the Mylar surface. Using a Pantak Xrad-320 operated at 250 keV and 13mA, identical dishes were irradiated with X rays to provide positive controls. Additional nonirradiated dishes were used as negative controls.

γ-H2AX focus assay. After irradiation, cells were first washed with PBS and then fixed for 10 minutes in a paraformaldehyde solution, followed by two more washes in PBS. A 0.5% Triton X-100 solution was used to permeabilize the cells, this was followed by another wash in PBS. Mylar dishes were then blocked in a humidified incubator at 37°C for 1 h in a 10% solution of FFBS (FCS) in PBS. Next, three more PBS washes were completed for 5 min each. The cells were incubated for 1 h with the primary antibody, a 1:100 solution of mouse anti-human γ-H2AX antibody (Upstate) and 1% BSA in PBS. Another triplet of 5-min PBS washes was done followed by incubation with the second antibody, AlexaFluo 488 goat anti-mouse (KPL) in a 1:200 dilution with 1% BSA in PBS. Dishes were washed twice more for 5 min in PBS and then for an additional 5 min in PBS with 0.1 μg/ml of DAPI to counterstain. One final 5-min wash with PBS was followed by mounting with VECTASHIELD® HardSet™ Mounting Medium for fluorescence H-1400 (Vector Laboratories). γ-H2AX foci were observed using a Nikon Eclipse E600 microscope.

Results and Discussion

Accurate dosimetry is of primary importance in such studies. GafChromic® HD-810 dosimetry film has proven to be a reliable tool for calibrating dose when used in conjunction with a sensitive photodiode, as reported previously (*7*). These films are suitable for beam profiling and dose mapping over a wide range of absorbed dose (*8*). Electron-irradiated films are placed in a 35-mm slide holder and scanned with a Polaroid SprintScan35 (Model no. CS-2700). The use of the optical scanner provides a rapid method to reconfirm our dosimetry before each set of exposures and has been demonstrated to provide good agreement with microdensitometer measurements (*9*). Calibration films made using a Pantak Xrad-320 are scanned in the same manner. The film orientation with respect to the active surface during scanning did not make any significant difference in the measure intensity. Prior to the relocation of the microbeam, GafChromic® calibrations were routinely done at the 300–500-Gy region, where we had good film response; however, the film intensity measurements were not found to be linear over a significant dose range, and lower-dose regions (>100 Gy) were below the sensitivity of our procedure. The current method of scanning the radiochromic film has proven much more sensitive than those employed previously (*6, 7*). The relationship between dose and intensity was found to be linear over the dose range examined. Comparing the intensity at 15 and 90 min after irradiation showed that film growth (i.e., increasing intensity over time) is insignificant over this period. For 50 keV electron irradiation, a linear relationship was found between dose and exposure time as well as dose and current. All GafChromic® measurements are cross calibrated with a calibrated photodiode (*7, 10*).

DNA double-strand breaks have long been considered the most relevant in causing the detrimental effects observed after radiation exposure (*11–13*). Visualizing γ-H2AX focus production in RKO36 cells, we have demonstrated electrons are capable of producing double-strand breaks. By shielding the beam so that only 10% of the cell population is exposed to radiation, we have examined the spatial extent of focus production.

Acknowledgment

This work was supported by the Biological and Environmental Research Program (BER), U.S. Department of Energy, Grant No. DE-FG02-05ER64082.

References

1. M. B. Sowa Resat and W. F. Morgan, Microbeam developments and applications: A low-linear energy transfer perspective. *Cancer Metastasis Rev.* **23**, 323–331 (2004).
2. M. Folkard, K. M. Prise, B. Vojnovic, S. Gilchrist, G. Schettino, O. V. Belyakov, A. Ozols and B. D. Michael, The impact of microbeams in radiation biology. *Nucl. Instrum. Methods Phys. Res. B* **181**, 426–430 (2001).
3. M. Folkard, B. Vojnovic, K. M. Prise and B. D. Michael, The application of charged-particle microbeams in radiobiology. *Nucl. Instrum. Methods Phys. Res. B* **188**, 49–54 (2002).
4. E. J. Hall and T. K. Hei, Genomic instability and bystander effects induced by high-LET radiation. *Oncogene* **22**, 7034–7042 (2003).
5. L. Huang, S. Grim, L. E. Smith, P. N. Kim, J. A. Nickoloff, O. G. Goloubeva and W. F. Morgan, Ionizing radiation induces delayed hyperrecombination in mammalian cells. *Mol. Cell. Biol.* **24**, 5060–5068 (2004).
6. M. B. Sowa, L. E. Kathmann, B. A. Holben, B. D. Thrall and G. A. Kimmel, Low-LET microbeam investigation of the track end dependence of electron induced damage in normal human diploid fibroblasts. *Radiat. Res.* **164**, 677–679 (2005).

7. M. B. Sowa, M. K. Murphy, J. H. Miller, J. C. McDonald, D. J. Strom and G. A. Kimmel, A variable energy elctron microbeam: A unique modality for targeted low-LET radiation. *Radiat. Res.* **164**, 695–700 (2005).
8. A. Niroomand-Rad, C. R. Blackwell, B. M. Coursey, K. P. Gall, J. M. Galvin, W. L. McLaughlin, A. S. Meigooni, R. Nath, J. E. Rodgers and C. G. Soares, Radiochromic film dosimetry: Recommendations of AAPM Radiation Therapy Committee Task Group 55. *Med. Phys.* **25**, 2093–2115 (1998).
9. A. S. Aydarous, P. J. Darley and M. W. Charles, A wide dynamic range, high-spatial-resolution scanning system for radiochromic dye films. *Phys. Med. Biol.* **46**, 1379–1389 (2001).
10. R. Korde and J. Geist, Quantum efficiency stability of silicon photodiodes. *Appl. Optics* **26**, 5284–5290 (1987).
11. J. F. Ward, DNA damage produced by ionizing radiation in mammalian cells: Identities, mechanisms of formation, and reparability. *Prog. Nucleic Acid Res. Mol. Biol.* **35**, 95–125 (1988).
12. J. H. J. Hoeijmakers, Genome maintenance mechanisms for preventing cancer. *Nature* **411**, 366–374 (2001).
13. D. C. van Gent, J. H. J. Hoeijmakers and R. Kanaar, Chromosomal stability and the DNA double-stranded break connection. *Nat. Rev. Genet.* **2**, 196–206 (2001).

Cytoplasmic Radiation-Induced Bystander Mutagenesis

Hongning Zhou,[a] Masao Suzuki,[b] Joseph Gillispie,[a] Gerhard Randers-Pehrson[a] and Tom K. Hei[a]

[a]Center for Radiological Research, College of Physicians and Surgeons, Columbia University Medical Center, New York, New York 10032; and [b]International Space Radiation Laboratory, National Institute of Radiological Science. 4-9-1 Anagawa, Inage-Ku, Chiba-Shi, Chiba 263-8555, Japan

In the past decade, increasing evidence has indicated that direct nuclear irradiation is not essential to induce the genotoxic responses such as chromosome damage and mutation. For example, irradiation of just the cellular cytoplasm could induce mutation in the nucleus of the target cells by a process involving oxyradicals. In addition, very low doses of α particles could induce bystander response in nonirradiated bystander cells using different end points and various types of cells. More recently, researchers from Gray Cancer Institute showed that cytoplasmic irradiation could induce bystander responses using micronuclei as the end point.

Using the Columbia University charged-particle microbeam, we targeted only the cytoplasm of each A_L cell and irradiated each cell with an exact number of α particles. After irradiation, cells were maintained in the same microbeam dish overnight before detachment for further analysis. When 10% of the cells were irradiated with eight α particles through the cytoplasm, the induced mutant yield was significantly higher than that of assuming there was no crosstalk between the irradiated and nonirradiated cells, and the mutant yield was almost the same as that when all the cells were irradiated. Addition of a scavenger of reactive nitrogen species and a gap junction inhibitor would reduce cytoplasmic radiation-induced bystander mutagenesis.

To further demonstrate the genotoxic bystander effect observed in the A_L cells, normal human bronchial epithelial cells were also used in this study. Using a Calyculin A-induced G_2 premature chromosome condensation assay, the preliminary data show that the incidence of chromatid-type breaks in cells where eight α particles were delivered to the cytoplasm in 10% of cells was significantly increased compared with those assuming no bystander effect, and the profile of chromatid breaks was very different from that in a cell population in which 100% of the cells were hit. These data could have a high impact on radiation risk estimation, since it is more likely for the bronchial or lung cells to get an α-particle traversal through the cytoplasm than the nuclei during environmental exposures.